CZECH TECHNICAL UNIVERSITY IN PRAGUE
ČESKÉ VYSOKÉ UČENÍ TECHNICKÉ V PRAZE

FACULTY OF ELECTRICAL ENGINEERING
DEPARTMENT OF MICROELECTRONICS

FAKULTA ELEKTROTECHNICKÁ
KATEDRA MIKROELEKTRONIKY

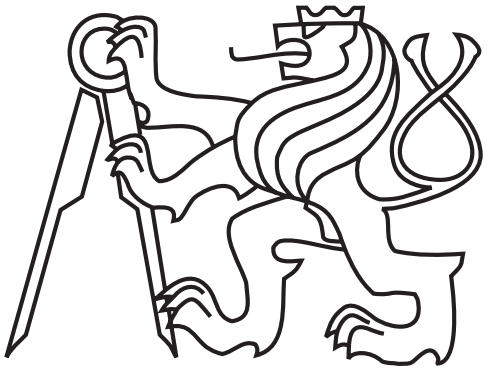

MEASUREMENT OF EVAPORATION AND EVALUATION OF CHANGES OF THE MECHANICAL PROPERTIES OF CARBON COMPOSITE ON NANOSATELLITE MINICUBE MISSION QB50

MASTER'S THESIS
DIPLOMOVÁ PRÁCE

2015 Bc. MARTIN URBAN

CZECH TECHNICAL UNIVERSITY
IN PRAGUE
ČESKÉ VYSOKÉ UČENÍ TECHNICKÉ V PRAZE

FACULTY OF ELECTRICAL ENGINEERING
DEPARTMENT OF MICROELECTRONICS

FAKULTA ELEKTROTECHNICKÁ
KATEDRA MIKROELEKTRONIKY

MEASUREMENT OF EVAPORATION AND EVALUATION OF CHANGES OF THE MECHANICAL PROPERTIES OF CARBON COMPOSITE ON NANOSATELLITE MINICUBE MISSION QB50

MĚŘENÍ EVAPORACE A VYHODNOCENÍ ZMĚN MECHANICKÝCH VLASTNOSTÍ UHLÍKOVÉHO KOMPOZITU NA NANOSATELITU MINICUBE MISE QB50

MASTER'S THESIS
DIPLOMOVÁ PRÁCE

AUTHOR — Bc. MARTIN URBAN
AUTOR PRÁCE

SUPERVISOR — Ing. LADISLAV SIEGER, CSc.
VEDOUCÍ PRÁCE

Prague 2015

České vysoké učení technické v Praze
Fakulta elektrotechnická

katedra mikroelektroniky

ZADÁNÍ DIPLOMOVÉ PRÁCE

Student: **Bc. U R B A N Martin**

Studijní program: Komunikace, multimédia a elektronika
Obor: Elektronika

Název tématu: **Měření evaporace a vyhodnocení změn mechanických vlastností uhlíkového kompozitu na nanosatelitu miniCube mise QB50**

Pokyny pro vypracování:

1) Prostudujte problematiku vyhodnocení spektrálních vlastností pomocí FFT exponenciálně tlumeného signálu vznikajícího kmitáním uhlíkového kompozitu.
2) Navrhněte algoritmus vyhodnoceni spektrálních vlastností reálně měřeného signálu.
3) Prostudujte vlastnosti použitých čidel a senzorů vlkosti HYT 271, HYT 939 a HAL2.
4) Navrhněte Payload pro použití čidel a senzorů z 3) pro nanosatelit miniCube mise QB50.
5) Proveďte kalibraci a změření teplotní závislosti čidel a senzorů z 3) pro použití ve vesmíru.
6) Navrhněte komunikační protokol pro komunikaci mezi čidly a hlavním počítačem nanosatelitu.
7) Zhodnoťte vhodnost použitých postupů, poznatky a jejich možnosti dalšího využití.

Seznam odborné literatury:

[1] JAN, J. Číslicová filtrace, analýza a restaurace signálů. 2nd ed. Brno: VUTIUM, 2002. 427 p. ISBN 80-214-2911-9
[2] TŮMA, J. Zpracování signálů získaných z mechanických systémů užitím FFT. Praha: Sdělovací technika, 2000. 168 p. ISBN 80-901936-1-7
[3] HANA, P., INNEMAN, A., DANIEL, V., et al. Mechanical properties of Carbon Fibe Composites for applications in space. Proc. SPIE 9442, Optics and Measurement Conference 2014, 2015, , no. 1, DOI: 10.1117/12.2175925
[4] Bell, S. Guide to the Measurement of Humidity. http://www.npl.co.uk/publications/guide-to-the-measurement-of-humidity

Vedoucí: **Ing. Ladislav Sieger, CSc.**

Platnost zadání: 31. 8. 2016

L.S.

prof. Ing. Miroslav Husák, CSc.
vedoucí katedry

prof. Ing. Pavel Ripka, CSc.
děkan

V Praze dne 16. 2. 2015

ABSTRACT

The content of this master's work is an introduction to the problematics of CubeSat nanosatellites and the construction of a mesurement tasks to use in space, as a part of nanosatellite VZLUsat-1. This work deals in more detail with testing of suitability of newly developed carbon composite for the space use, mainly from the point of mechanical aging and evaporation. The first part of this thesis deals with choosing a proper procedure for evaluation of mechanical changes of the composite using Fast Fourier Transform. The goal is to use suitable digital signal processing and with the most accuracy to evaluate the changes in structure of the carbon composite. The second part deals with the issue of evaporation of previously mentioned material. This part describes the process of constructing the measurement, sensor calibration and evaluation of measured data. VZLUsat-1 probe will be launched is 2016 during QB50 mission.

KEYWORDS

Calibration, CubeSat, DSP, Digital Signal Processing, Evaporation, Fast Fourier Transform, FFT, HAL2, Humidity, Mission QB50, Nanosatellite, Research, Space, VZLUsat-1

ANOTACE

Obsah této diplomové práce je seznámení se s problematikou nanosatelitů CubeSat a konstrukce měřicích úloh vhodných pro použití ve vesmíru na satelitu VZLUSat-1. Tato práce se konkrétněji zabývá testováním vhodnosti nově vyvinutého karbonového kompozitu pro vesmírné účely, především z hlediska mechanického stárnutí a evaporace. První část práce se věnuje výběru vhodného postupu vyhodnocení mechanických změn materiálu, a to za použití Rychlé Fourierovy Transformace. Cílem je vypočítat s co nejvyšší přesností změny ve struktuře uhlíkového kompozitu vzniklé dlouhodobým pobytem v orbitálním vakuu pomocí vhodného způsobu číslicového zpracování signálu. Ve druhé části práce je rozebírána problematika uvolňování plynů ze zmiňovaného uhlíkového kompozitu. Tato část popisuje celý proces získávání dat, od konstrukce meřicího přípravku, přes kalibraci senzorů po vyhodnocení výsledků. Družice VZLUSat-1 bude vypuštěna v roce 2016 společně s dalšími satelity mise QB50.

KLÍČOVÁ SLOVA

CubeSat, CZS, Číslicové zpracování signálu, Evaporace, FFT, HAL2, Kalibrace, Mise QB50, Nanosatelit, Rychlá Fourierova Transformace, Vesmír, Vlhkost, Výzkum, VZLUsat-1

URBAN, Martin. *Measurement of evaporation and evaluation of changes of the mechanical properties of carbon composite on nanosatellite miniCube mission QB50*: master's thesis. Prague: Czech Technical University in Prague, Faculty of Electrical Engineering, Department of Microelectronics, 2015. 107 p. Supervised by Ing. Ladislav Sieger, CSc.

ACKNOWLEDGEMENT

I would like to thank my mentor Ing. Ladislav Sieger, CSc. for many advices and useful comments during work on this thesis.
Also I would like to express thanks Ing. Lenka Mikuličková for advices and patience during testing and calibrations of sensors.
Last but not least I would like to express many thanks and my gratitude to professor Kazuo Yana, Ph.D, from Hosei University in Tokyo, Japan. Who helped me during summer internship in 2014 in Japan not only with signal processing.

DECLARATION

I declare that I have written my master's thesis on the theme of "Measurement of evaporation and evaluation of changes of the mechanical properties of carbon composite on nanosatellite miniCube mission QB50" independently, under the guidance of the master's thesis supervisor and using the technical literature and other sources of information which are all quoted in the thesis and detailed in the list of literature at the end of the thesis.

As the author of the master's thesis I furthermore declare that, as regards the creation of this master's thesis, I have not infringed any copyright. In particular, I have not unlawfully encroached on anyone's personal and/or ownership rights and I am fully aware of the consequences in the case of breaking Regulation § 11 and the following of the Copyright Act No 121/2000 Sb., and of the rights related to intellectual property right and changes in some Acts (Intellectual Property Act) and formulated in later regulations, inclusive of the possible consequences resulting from the provisions of Criminal Act No 40/2009 Sb., Section 2, Head VI, Part 4.

In Prague, July 31, 2015

.....
author's signature

Contents

List of Figures

List of Tables

List of Codes

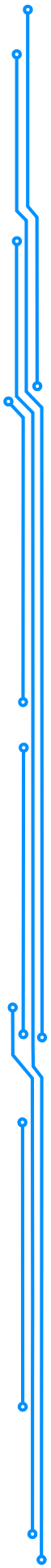

List of Acronyms

ACK
Acknowledge

ADC
Analog to Digital Converter

Al_2O_3
Aluminium oxide

AO
Atomic oxygen

approx.
approximately

ARM
Advanced RISC Machine

CDC
Capacitance to digital converter

CdTe
Cadmium-Telluride

CERN
European Organization for Nuclear Research

CMOS
Complementary Metal–Oxide Semiconductor

CubeSat
Small standard nanosatellite of dimensions $10 \times 10 \times 10$ cm per unit

DF
Data Fetch

DFT
Discrete Fourier Transform

DiF
Decimation-in-Frequency

DiT
Decimation-in-Time

DSP
Digital Signal Processing

e.g.
for example

EMC
Electromagnetic Compatibility

EPS
Electrical Power System

EQM
Engineering qualification model

FEM
Finite element method

FFT
Fast Fourier Transform

FIPEX
Flux-Φ-Probe Experiment

FIR filter
Finite impulse response filter

FLASH
Type of non-volatiles memory

HM
Heath monitor

HW
Hardware

I/O
Input/Output

I^2C
Inter-Integrated Circuit

INMS
Ion-Neutral Mass Spectrometer

IR
Infra-red

IST s.r.o.
Innovative Sensor Technology

LP filter
Low-pass filter

m-NLP
multi-Needle Langmuir Probe

MCU
Microcontroller

MEMS
Micro-electro-mechanical system

MR
Measurement request

MSB
Most significant bit

N_2
Nitrogen

NACK
No-Acknowledge

NO
Nitric oxide

O_2
Molecular oxygen

OBC
On Board Computer

PCB
Printed circuit board

PIN
P-type, Intrinsic, N-type semiconductor

QB50
Mission of nanosatellites of CubeSat category

RAM
Random Access Memory, type of volatiles memory

RDC
Resistance to digital converter

Rigaku s.r.o.
Rigaku Innovative Technologies Europe

RISC
Reduced instruction set computing

SCL
Serial clock

SDA
Serial data

SPI
Serial peripheral interface

SRAM
Static Random Access Memory, type of volatiles memory

SW
Software

TDC
Time to digital converter

TTS s.r.o.
Thin-film Technology Service

U
Standardized Unit

USB
Universal Serial Bus

UV
Ultraviolet

VZLUSat–1
Nanosatellite from VZLÚ a.s.

VZLÚ a.s.
Výzkumný a Zkušební Letecký Ústav – Aerospace Research and Test Establishment

XRB
X-Ray Background

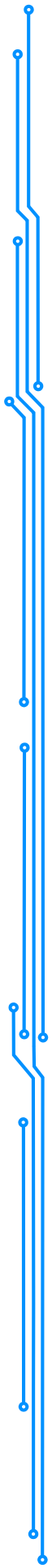

List of Symbols

A	Cross sectional area $\left(\mathrm{m}^2\right)$
B	Frequency resolution (Hz)
C_p	Parasitic capacity (F)
D	Decimation factor $(-)$
DP	Dew point (°C)
E	Elastic Modulus (Pa)
F_d	Damping force (N)
F_i	Inertial force (N)
F_r	Reverse force (N)
H	Height of PCB (m)
I_n	Noisy current (A)
J	Quadratic torque-section $\left(\mathrm{m}^4\right)$
L	Cantilever length (m)
N	Number points of signal $(-)$
N	Length of signal (Samples)
P	Pressure (Pa)
PP	LENKO! (netušim)
P_sv	Saturation vapour pressure (Pa)
P_v	Actual vapour pressure (Pa)
Q	Length of zeros (Samples)
RH	Relative humidity (%rh)
R_PU	Pull-up resistor (Ω)
S	Dimension of capacitor boards $\left(\mathrm{m}^2\right)$
T	Temperature (°C)
T_0	Length of signal (s)
W	Cantilever width (m)
Y_k	Discrete spectrum
Δf	Frequency step (Hz)
β_n	Own root of frequency equation

δ	Attenuation of system $\left(\mathrm{s}^{-1}\right)$
λ	Wavelenght (m)
ω	Angular frequency of oscillations $\left(\mathrm{rad} \cdot \mathrm{s}^{-1}\right)$
ω_0	Angular frequency of natural oscillations $\left(\mathrm{rad} \cdot \mathrm{s}^{-1}\right)$
ω_n	Angular frequencies of natural oscillations $\left(\mathrm{rad} \cdot \mathrm{s}^{-1}\right)$
ρ	Material Density $\left(\mathrm{kg} \cdot \mathrm{m}^{-3}\right)$
ε_0	Permittivity of vacuum $8,852.10^{-12}\left(\mathrm{F} \cdot \mathrm{m}^{-1}\right)$
ε_r	Relative permittivity $(-)$
b	Damping constant $\left(\mathrm{kg} \cdot \mathrm{s}^{-1}\right)$
c	Window constant $(-)$
c_0	Velocity of longitudinal waves $\left(\mathrm{m} \cdot \mathrm{s}^{-1}\right)$
f	Frequency of oscillations (Hz)
f_s'	Decimated sample frequency (Hz)
f_1	First example of harmonic signal (Hz)
f_2	Second example of harmonic signal (Hz)
f_m	Maximum contained frequency (Hz)
f_res	Resonant frequency (Hz)
f_s	Sampling frequency (Hz)
h	Cantilever height (m)
j	Quadratic sectional radius (m)
k	Number points of moving averages $(-)$
k	Spring constant $\left(\mathrm{N} \cdot \mathrm{m}^{-1}\right)$
k	Discrete frequency (Hz)
l	Distance of capacitor boards (m)
m	Weight of the Mass (kg)
r	Discrete sample point $(-)$
v	Velocity of propagation $\left(\mathrm{m} \cdot \mathrm{s}^{-1}\right)$
x	Point of signal (mV)
x	Deviation (m)

y_{r}	Discrete signal
y_r^e	Even-order samples
y_r^o	Odd-order samples

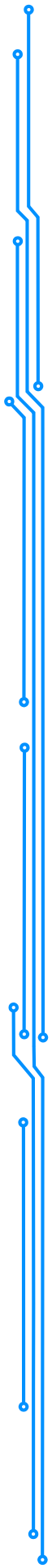

1 Introduction

The measurement environment in space is different from the standard measurements performed on the ground in laboratory. The system design specification has a large constraint in size, weight and power consumption by the limits of space probes. Each task has to work automatically and without operator intervention. [2]

This master's thesis describes problematic of the Small standard nanosatellite of dimensions $10 \times 10 \times 10$ cm per unit (CubeSat). Main part of this thesis is about measurement of evaporation and evaluation of mechanical changes. These tasks are part of tasks which are contained in Nanosatellite from VZLÚ a.s. (VZLUSat–1).

One of the main goals for VZLUSat–1 is testing and verifying carbon fiber material which could be used as new construction material for space satellite in future and replaced heavy wolfram shielding. Some sensors and devices are also tested for space use and changes of their properties are analyzed during the time.

Evaporation from carbon fiber material is evaluated throught analog capacitance HAL2 humidity sensors from company Thin-film Technology Service (TTS s.r.o.) and digital humidity sensors HYT from company Innovative Sensor Technology (IST s.r.o.). Each digital sensor has integrated thermometer. Information from analog HAL2 sensors is evaluated by small board with microprocessor PicoCap2.

Evaluation of changes of the mechanical properties of carbon composite is using Fast Fourier Transform. There is a carbon fiber cantilever for testing purposes, which is reguraly excitated by a coil. These mechanical damped vibrations are sensed by piezo-element and changed to electric signal. Evaluation process of mechanical changes consists of Digital Signal Processing using Fast Fourier Transform and attenuation of the signal.

More details about sensing of mechanical vibrations, evaluation of signal attenuation and program implementation to the chip are included in the thesis *Measurement of changing mechanical properties of carbon composite on nanosatellite miniCube mission QB50* [1], author Bc. Ondřej Nentvich with whom I cooperated.

Nanosatellite has also payload, which deals with the measurement of radiation resistance of the composite. This issue is described in the Bc. Veronika Stehlíková's thesis *Radiation resistance measurement on nanosatellite miniCube mission QB50* [3].

Most measurements were performed in company Rigaku Innovative Technologies Europe (Rigaku s.r.o.).

2 Mission QB50

The Mission of nanosatellites of CubeSat category (QB50) will demonstrate the possibility of launching 50 CubeSats built and designed by Universities Teams as student's projects and by companies for commercial purpose all over the world, as nanosatellite with low-cost launch, to perform first-class science in the largely unexplored lower thermosphere.

Due to the low orbit of the satellites, their orbital lifetime is limited.. With respect to this property, space agencies are not supporting a satellite network from industrial standard satellites for in-situ measurement in the lower thermosphere, because the cost of a network of 50 satellites would be extremely high.

Extremly high cost and limited lifetime are reasons why no in-situ measurements has been carried out. This should be justifiable and realised by using low-cost satellites, one of the options are CubeSat class satellites.

Fig. 2.1: QB50 Mission Objectives [4]

2.1 CubeSat

CubeSat is a miniaturised satellite, consisting of one or more Standardized Unit (U). This Standardized Unit has precisely defined a dimensions and weight (Tab. 2.1). These units can be assembled to larger satellite, but only in integral multiples of U. You can start with 1U and put together 2U, 3U or 6 U which will provide more interior space and flexibility for the used measurement.

CubeSat offers all functions of standard satellite such as telecommunications, measurement, power subsystem from battery or solar panel and attitude determination and control. One of the advantages of CubeSat are existing standardized Hardware (HW) boards, for example (e.g.) On Board Computer (OBC), Radio Board, Electrical Power System (EPS) with battery pack and solar board. [5]

The cost of HW for CubeSat is usually in range of 50 – 100 thousands Euro, but it also can be more expensive, up to 500 thousands Euro. [4]

Tab. 2.1: Standardized Unit Properties [6]

Property	Value
Dimensions	$4 \times 4 \times 4$ inch $\rightarrow$ approx. $10 \times 10 \times 10$ cm per unit
Weight	up to 3 lbs $\rightarrow$ 1.3 kg per unit
Units	in this mission up to 3 Units in a row ($30 \times 10 \times 10$ cm)

One of the goals of QB50 CubeSat is to realize atmospheric research in the lower thermosphere with altitude between approximately (approx.) 200 – 380 km. It is the least explored part of the atmosphere. Sounding rocket provide only short time in-situ measurements. Time spent on the in-situ measurement in lower layers of thermosphere is only several minutes.

Another way is measurement by methods for remote sensing, which are very powerfull and they are using the reflected signal from atmospheric discontinuities. These methods can't be used, because atmosphere is so sparse and returned reflected signal is weak from lower thermosphere. The same property is true for measurements from Earth observation satellites in higher orbits and from the Earth's surface radars.

QB50 nanosatelites bring oportunity to create relatively cheap multi-point in-situ measurements network. This network of CubeSats can carry out more accurate in-situ measurement than one-point measurement using rockets. [4]

Each of the QB50 nanosatellites carries one of the three different types of science sensors, which is compulsory part of a start set. All types of science sensors are equipped with a thermometer such as Thermistor, Thermocouple, ...

Tab. 2.2: Science sensors

Label	Designation
INMS	Ion-Neutral Mass Spectrometer
FIPEX	Flux-Φ-Probe Experiment
m-NLP	multi-Needle Langmuir Probe

Ion-Neutral Mass Spectrometer (INMS) is a miniaturised analyser designed for sampling of low mass ionised and neutral particles in the spacecraft ram direction with the instrument resolutions optimised for resolving the major constituents in the lower thermosphere, it is, Atomic oxygen (AO), Molecular oxygen (O_2), Nitric oxide (NO) and Nitrogen (N_2).

The key sensor components consist of a collimator/ion filter, an ioniser and a charged particle spectrometer. When is this instrument active can generate high voltages up to 2500 V. [19]

Flux-Φ-Probe Experiment (FIPEX) is able to distinguish and measure the time resolved behavior of atomic oxygen as a key parameter of the lower thermosphere.

Atomic oxygen is the dominant species in these regions and therefore its measurement is crucial in the correlation and validation of atmosphere models. Moreover, erosion of spacecraft surfaces due to interaction with atomic oxygen is a serious concern and merits in-situ study in its own right.

The measurement is based on solid oxide electrolyte micro-sensors. For oxygen conducting solid state electrolytes, e.g. yttrium-doped zirconia, the conductivity starts at high temperatures and so the sensor operates at an elevated temperature of 600 – 700 °C, heated by an electrical resistance. Oxygen is "pumped" from one electrode to the other by an applied direct voltage and in accordance with Faradays' law; the measured current is proportional to the mass flux by electrolysis. To distinguish between Atomic oxygen (AO) and Molecular oxygen (O_2) sensor elements with different cathode materials are used. [18]

multi-Needle Langmuir Probe (m-NLP) works by measuring the current collected individually from four needle probes, placed in front of the satellite's shock front. The collected current is converted to voltage, filtered, digitalized and then sent to the central telemetry system. By using data from four fixed-bias Langmuir needle probes, sampled at the same time, the plasma electron density can be derived with high time resolution without the need to know the electron temperature and the spacecraft potential. With the selected needle probe design and the estimated electron densities, the instrument is to be capable of measuring currents ranging from 1 nA to 2 µA. [20]

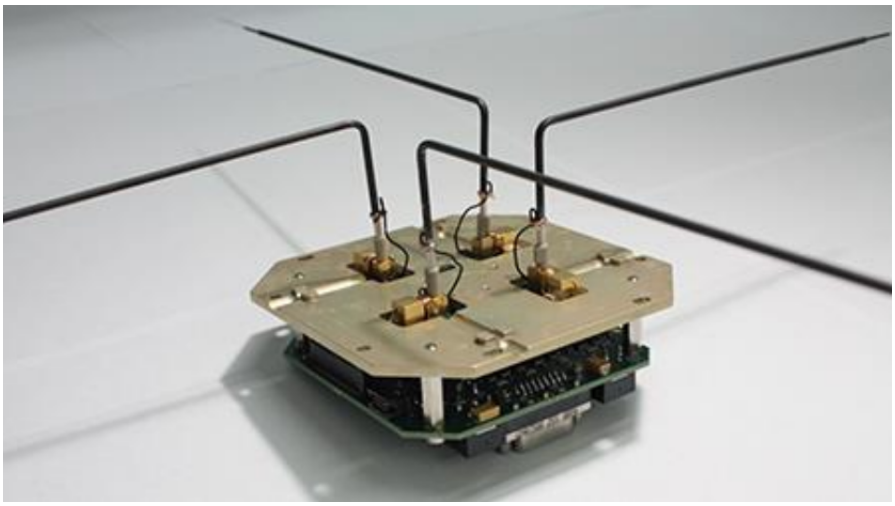

Fig. 2.2: m-NLP deployed instrument [20]

Next of many goals is another type of payload. These are new technologies, sensors and materials which should be tested and qualified in space. Because normal big satellites are too expensive, they have to have verified and reliable components and materials. There is no place for mistakes and experiments e.g. with new shielding material, which could endanger the whole mission and satellite in the price of millions.

3 CubeSat VZLUSat–1

The probe belongs to the family of nanosatellites called CubeSat. This project is a joint work of several companies and universities from Czech Republic. Its goals are to get an experience with this type of device, try to operate and communicate with it and if the mission proves successful, to get the data about new materials as well. Main part of construction and testing takes place in VZLÚ a.s., but we were also using a lot of other specialised workplaces. There are about 40 people from different branches connected to this project, who are working on universal tasks like Software (SW) or on single measurements and sensors. Results of this experiment should be used in the next generation of VZLUSat–1, which is possible to come in case of VZLUSat–1's success.

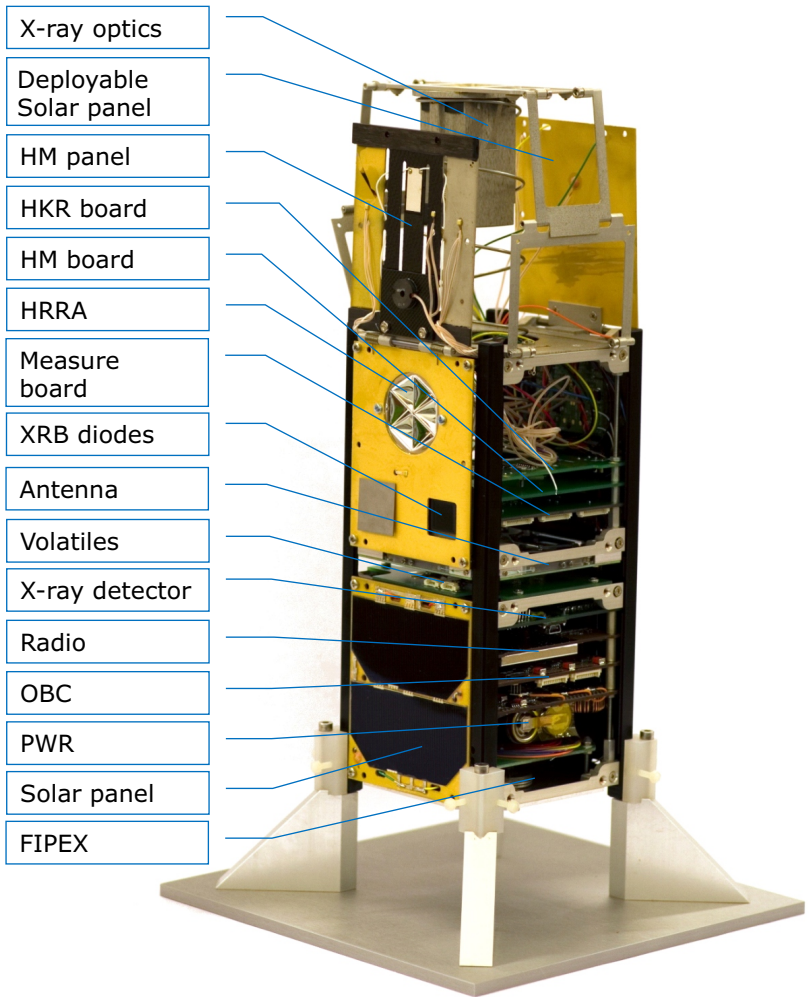

Fig. 3.1: CubeSat VZLUSat-1

3.1 Parameters

There are several restrictions, resulting from the character of QB50 mission. The main problem for all the space missions is the weight, which can be carried to the orbit. QB50 is only a next part of classical mission, so the weight was limited to 1 kg per U. Our satellite consists of two units, so the final possible weight is 2 kg. This restriction determines an application of lightweight materials, reduction of superfluous construction parts and, unfortunately, also the lower quality of radiation shielding, which is usually made from heavy metals. Rules for Mission of nanosatellites of CubeSat category do not allow using a reaction engine for solid, liquid or gaseous fuels as well, this problem is solved by the possibility of interaction between stabilising coils and the Earth's magnetosphere. Another limitation applies to power per a unit, which makes 1 W. Because of that, our two watt satellite will switch between tasks to manage power consumption over time.

Tab. 3.1: VZLUSat–1 Properties

Property	Value
Dimensions	2 U → approx. $20 \times 10 \times 10\,cm$ as folded
	3 U → approx. $30 \times 10 \times 10\,cm$ (almost) when expand
Weight	total up to $2\,kg$
Power	total up to $2\,W$

3.2 Experiments

This section describes individual tasks and board, which VZLUSat–1 is carrying. They are stacked one above the other inside the probe, interconnected by standardized connectors dedicated for CubeSats.

3.2.1 X-Ray Optics and Medipix

On the top of the satellite is an extendible part carrying X-Ray optics. This optics creates a picture by reflecting on narrow walls, not by refraction. It has focal length of approx. 20 cm and it focuses X-Rays on Medipix, a special Complementary Metal–Oxide Semiconductor (CMOS) silicone detector for low-energy Roentgen radiation. As the name suggests, this device, originally developed for European Organization for Nuclear Research (CERN), is today used as a medical equipment as well. Orientation of this system to the Sun will be tested by Infra-red (IR) and two Ultraviolet (UV) diodes. Main reason why the probe has two UV diodes is that one is sensitive in maximum radius of approx. 80°, second one has sensitive radius reduced to approx. 15° by a small tube. The first one is looking for sources in wide angle and the second one has narrower angle for more precise designation of their position. If both sensors have strong UV signal then Medipix will start up and take a picture.

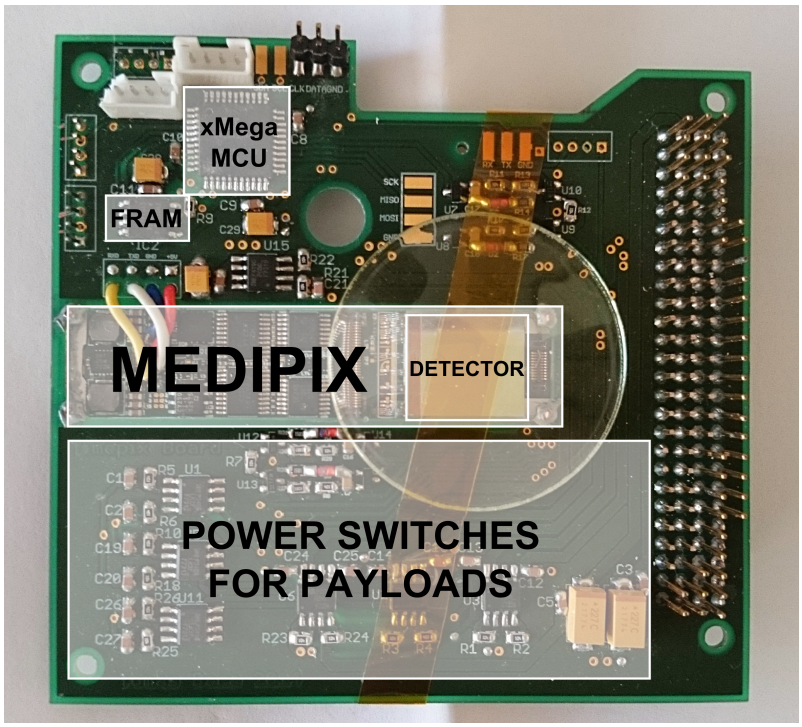

Fig. 3.2: Medipix board with labels

3.2.2 HM system

Heath monitor system is used for testing mechanical properties of a carbon-fibre composite. This system has two parts, one is tilting panel located at the top of the probe. It is made of the mentioned material with milled cantilever. It has glued permalloy on its open end. There is coil for excitation of the cantilever located above the permalloy. The beam produces damped oscillations which are measured by a piezo.

The Coil and the piezo are connected to the HM board, where MCU is located. It processes all measurements and communication with other boards.

Results of this experiment are natural frequencies of cantilever gained by the FFT. From these values Young's modulus of elasticity is computed and it determines the quality of the carbon-fibre composite over time. The main reason for testing the quality is the radiation influence in space.

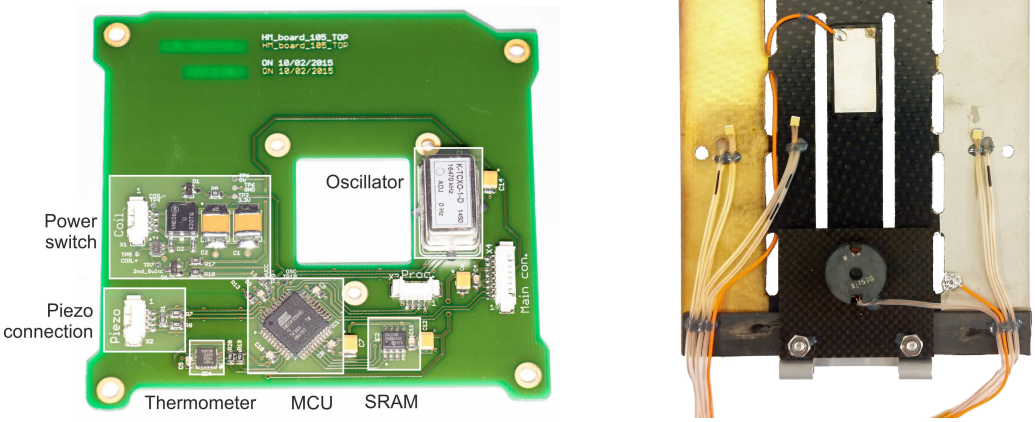

(a) Heath monitor board with descriptions (b) HM panel

Fig. 3.3: Heath monitor system

3.2.3 Measurement of Radiation Resistance

The Measurement of radiation resistance consists of two boards, measure board and X-Ray Background (XRB) board. These boards are a pair of plates, which will test the effect of irradiation on parts and materials and also the shielding quality of the new carbon-fibre material.

Measure board carries a row of thermosensors, which should serve for several other measurements, a microprocessor unit and CdTe detector. This detector is, compared to Medipix and XRB diodes, more sensitive to high-energy particles, and it needs 200 V power supply. CdTe is quite a new type of material for detecting radiation, because for a long time, it was too difficult to made large sensors from this material in sufficient quality.

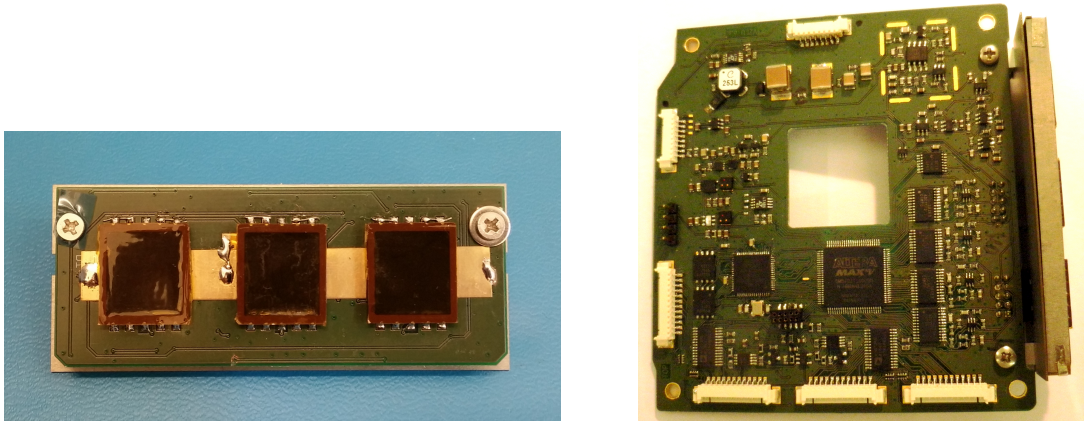

(a) Board with XRB diodes

(b) Measure board

Fig. 3.4: Measurement of radiation resistance

Attached to the Measure board is the XRB board, where are three PIN diodes. Each of them has different radiation shielding, one has none, one is hidden behind a Tungsten sheet and the middle one will be protected by the tested carbon-fibre. The results from single channels will be compared and the efficiency of shielding studied. Design of low-noise amplifiers on XRB board and testing of this system was as a part of work of my colleague Veronika Stehlíková [3].

3.2.4 HKR Board

This board is the last version of simple technical system for releasing the folding part of the spacecraft. This system burns off on orbit and it unlocks the antennas, a part of solar panels, HM panel and X-Ray optics as well.

3.2.5 Hollow Retro Reflector Array

This panel helps to identify the position of the satellite. There are six corner reflectors made of glass with thin metal layer situated on the probe. The main attribute of mirrors in such a spatial arrangement is, that incident ray reflects ever

right to its source, no matter how the reflector is oriented.

3.2.6 On Board Computer

This board operates all the other measurements, sets the order of single tasks and drives the power supply. Because the energy for the whole satellite is only 2 W, it is necessary to switch among tasks and to combine them appropriately. OBC will also communicate with the Pilsen radio station through the Radio board.

3.2.7 Radio

The radio board is a product of the University of Western Bohemia in Pilsen and it will provide a communication with the probe on radio-amateur free frequency of 436 MHz. In Pilsen, they will download the results from the probe during a short connections (approximately 10 minutes every 12 hours) and it will be possible to set new configurations of measurements as well.

3.2.8 Electronic Power System

Power supply is limited by QB50 project prescription, that is only 1 W per an unit. VZLUSat–1 will be powered by three-layer solar panels, which can use a wider part of spectre than the usual solar cells to generate energy. Each od them can produce up to 2.4 V and 500 mA in loaded and 2.7 V in open-circuit case or 520 mA as short-circuit. These panels have the efficiency of approx. 30 % for power density 1367 W/m^2. There will be Lithium accumulators for storing energy during the flight and on the dark side of orbit as well. Power board serves to control the energy consumption on the whole satellite, when a reserve in accumulators drops under a critical value, this board has to cut all the others safely and when the energy supply is restored, restart them.

3.2.9 Volatiles board

Volatiles board consists of the humidity sensors which are looking for residual humidity or evaporation from the whole probe, mainly from the tested carbon-fibre materials. There are three types of sensors. Two types of them are digital sensors and third is analog. Analog sensors are connected to the board with a driver called PCap02A. All HYT and PCap02A sensors communicate via I^2C bus connected directly to the OBC. Problematic about humidity sensors and measurement is described in this thesis.

3.2.10 Fipex

Each of the CubeSats in project QB50 should have one of the science experiments shown in Tab. 2.2 on board. This set of experiments study the lower thermosphere and the results will help to improve the atmospheric models, which are important for meteorology and other branches all around the world. For VZLUSat–1 the FIPEX was chosen, a device that studies atomic oxygen, dominant element in this layer of atmosphere. The device is based on solid oxide electrolyte micro-detector.

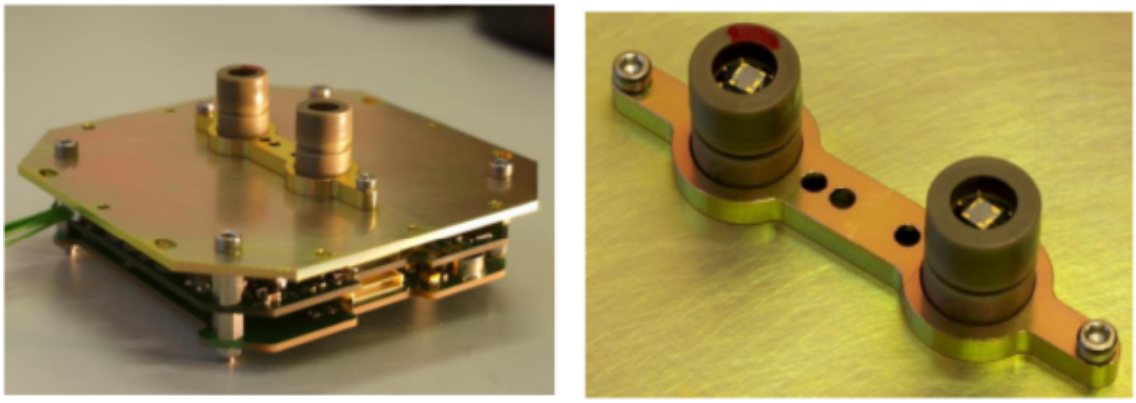

(a) FIPEX board (b) Detail of sensors

Fig. 3.5: Flux-Φ-Probe Experiment [18]

4 Evaluation of Mechanical Changes

One of the tasks placed on the board will be responsible for measuring mechanical changes during space mission of Nanosatellite from VZLÚ a.s. (VZLUSat–1).

There are many different approaches to evaluate mechanical changes of the material. One of them is the evaluation using exact model of the vibrating beam. This model is described by Finite element method (FEM). As input variables for this model of composite cantilever are, in addition, the beam dimensions and material constants of the used material also the resonant and natural frequency and attenuation coefficient of the vibrating beam. On the following pages a topic about damped oscillations id outlined, elementary calculation example for string and simple model of cantilever with one fixed side.

4.1 Damped Oscillations

In Fig. 4.1 is an illustration of damped oscillations system with spring. Oscillating mass is represented as hanged Weight of the Mass (m). This mass oscillates on a spring with k as Spring constant. Deviation of the entire system is referred to as x.

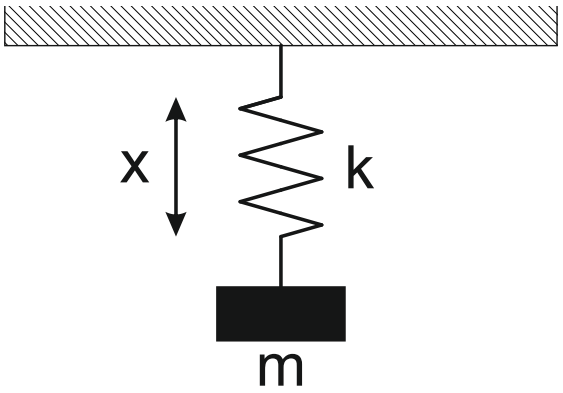

Fig. 4.1: Picture of basic damped oscillations

There is a basic equation for description of this oscillations (4.1).

$$F_{\mathrm{i}} + F_{\mathrm{d}} + F_{\mathrm{r}} = 0 \tag{4.1}$$

The forces mentioned in the equation (4.1) are Inertial force (F_i), Damping force (F_d) and Reverse force (F_r). Each of these forces can be calculated as:

$$F_\mathrm{i} = m\frac{\mathrm{d}^2x}{\mathrm{d}t^2} \tag{4.2}$$

$$F_\mathrm{d} = b\frac{\mathrm{d}x}{\mathrm{d}t} \tag{4.3}$$

$$F_\mathrm{r} = kx \tag{4.4}$$

When equations (4.2 – 4.4) are put into equation (4.1), it gets differential second order equation (4.5).

$$m\frac{\mathrm{d}^2x}{\mathrm{d}t^2} + b\frac{\mathrm{d}x}{\mathrm{d}t} + kx = 0 \tag{4.5}$$

Where b is Damping constant. This formula has constant coefficients and zero right side. It means that, the oscillation system does not have periodic excitation and thus is damped.

After modifying to the general mathematical form

$$\frac{\mathrm{d}^2x}{\mathrm{d}t^2} + 2\delta\frac{\mathrm{d}x}{\mathrm{d}t} + \omega_0^2x = 0 \Longleftrightarrow x(\mathrm{t}) = x_0e^{-\delta t}\sin\left(t\sqrt{\omega_0^2 - \delta^2}\right) \tag{4.6}$$

and substitution of ω for $\sqrt{\omega_0^2 - \delta^2}$. It gets prescription for damped sine oscillations

$$x(\mathrm{t}) = x_0e^{-\delta t}\sin(\omega t) \tag{4.7}$$

In these equations δ is Attenuation of system, ω_0 is Angular frequency of natural oscillations and ω is Angular frequency of oscillations.

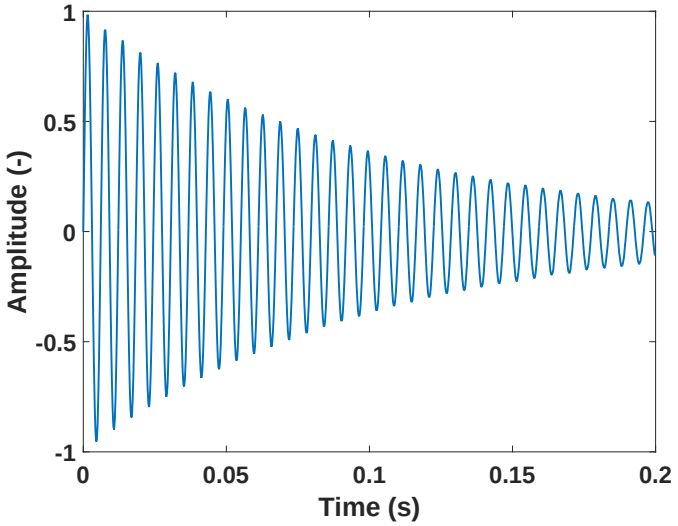

Fig. 4.2: Simulated damped signal

4.2 Elementary Oscillator

Elementary oscillator could be described on simplified example as a string. For this case can be applied following equation (4.8) for examination Young's modulus of elasticity.

$$v = \sqrt{\frac{E}{\rho}} \tag{4.8}$$

Elastic Modulus is designated as E, Velocity of propagation as v and ρ is Material Density. Velocity of propagation is defined as

$$v = \lambda f \tag{4.9}$$

where λ is Wavelenght and f is Frequency of oscillations, which is obtained using of Angular frequency of oscillations (ω) from equation

$$f = \frac{\omega}{2\pi} \tag{4.10}$$

In this case it is possible to determine that $\lambda = 4L$, where L is length of string illustrated in Fig. 4.3.

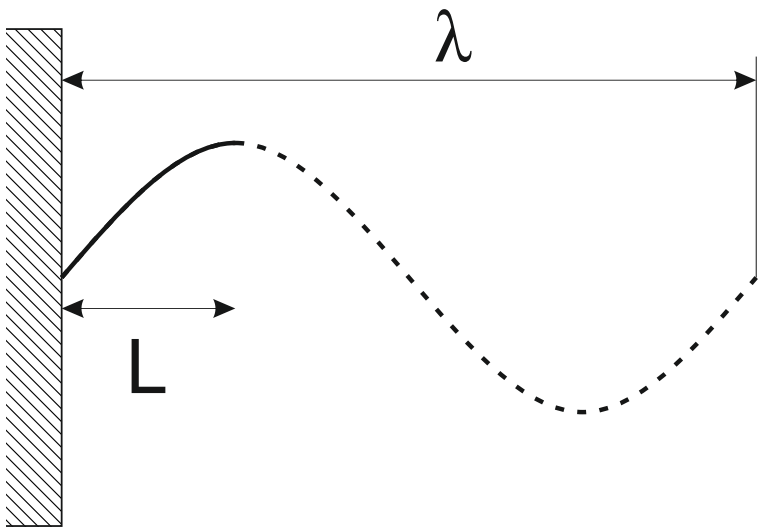

Fig. 4.3: Length of string L vs. wavelength λ

4.3 Cantilever Oscillations

A more precise approach to real situation is in our case a simple cantilever with one fixed side and one freely hanged as is in the Fig. 4.4.

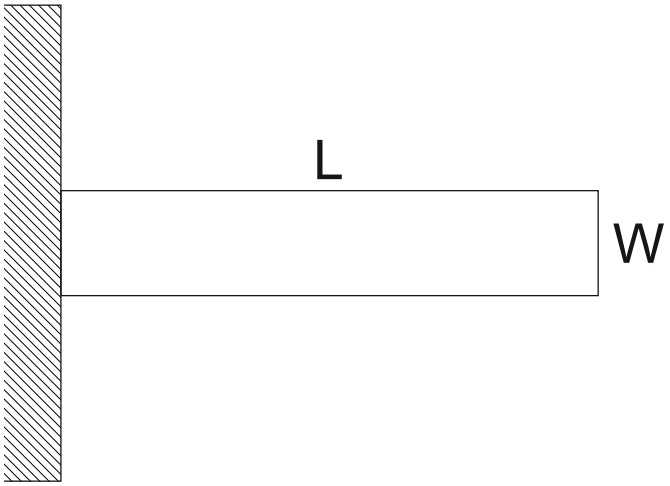

Fig. 4.4: Picture of Cantilever

The oscillating cantilever could be described by a few equations. At first it is necessary to find out own roots of frequency equation (4.11), next is computing natural frequencies.

$$\cosh(\beta_n L) \cdot \cos(\beta_n L) + 1 = 0 \tag{4.11}$$

where β_n is Own root of frequency equation, L is Cantilever length [27].

The solution for this formula is possible only by a numeric method. Computing natural frequencies ω_n of cantilever shows the following equation

$$\omega_{\mathrm{n}} = \frac{(\beta_{\mathrm{n}} L)^2}{L^2} c_0 j \tag{4.12}$$

For this equation it is required to know computed roots and some other parameters. These parameters are in Tab. 4.1 and when they are inserted into equation (4.14).

$$\omega_{\mathrm{n}} = \frac{(\beta_{\mathrm{n}} L)^2}{L^2}\sqrt{\frac{E}{\rho}}\sqrt{\frac{J}{A}} = \tag{4.13}$$

$$= \frac{(\beta_{\mathrm{n}} L)^2}{L^2}\sqrt{\frac{E}{\rho}}\sqrt{\frac{h^2}{12}} \tag{4.14}$$

where j is Quadratic sectional radius, c_0 is Velocity of longitudinal waves, J is Quadratic torque-section and A is Cross sectional area.

Tab. 4.1: Cantilever parameters

Description	Symbol	Value
Cantilever length	L	13.2 mm
Cantilever width	W	64.4 mm
Cantilever height	h	1.2 mm
Elastic Modulus	E	$3.8 \cdot 10^{10}$ Pa
Material Density	ρ	2300 kg $\cdot m^{-3}$

For creating the FEM model and its detailed description, cooperation with RNDr. Petr Hána from Technical University of Liberec have been established, results of this method were almost the same as when using equation (4.14) [8, 12, 27, 28].

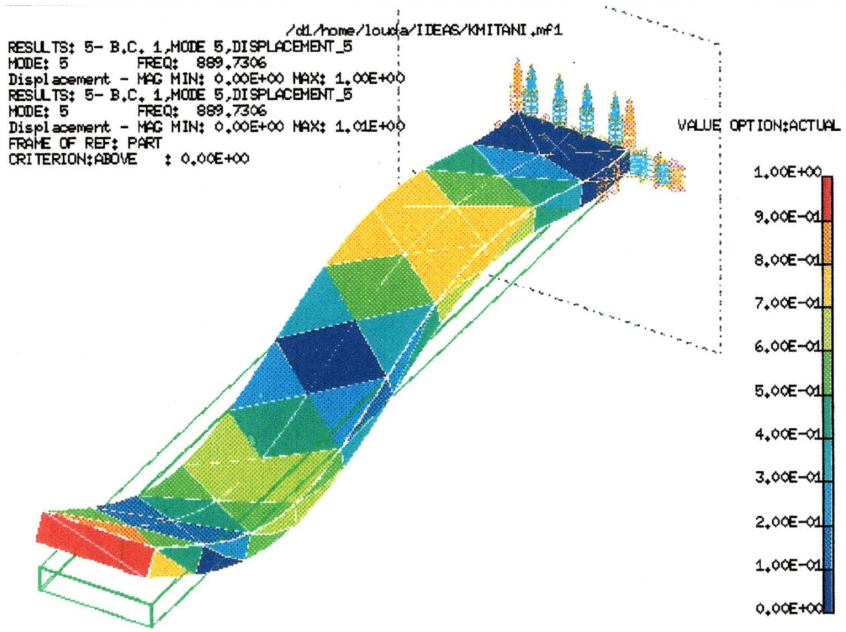

Fig. 4.5: Example of cantilever simulated by FEM [8]

From the equation (4.14) with parameters from Tab. 4.1 natural frequencies are obtained. These first three frequencies are listed in the following Tab. 4.2.

Tab. 4.2: Natural frequencies

Natural resonace	Value
First natural frequency	171.6 Hz
Second natural frequency	1075 Hz
Third natural frequency	3011 Hz

4.4 Young's Modulus of Elasticity

Young's modulus is a synonym for elastic modulus E. It is a material property, that describes its stiffness and is therefore one of the most important properties of solid materials. Modulus is characterized as ratio of stress to strain. From measured frequencies it is possible to get back Young's modulus and that would measure quality of the material.

5 Construction of Material Ageing Measurement

During space mission, material aging measurement is provided by payload HM which contains HM board with HM panel. This panel is testing and measuring the changes of carbon composite beam properties. The tested material is exposed to free space and cosmic radiation which can change material properties.

Mechanical properties of the material are checked by Resonant frequency (f_{res}) and vibration attenutation δ of the carbon fiber cantilever. From these values can be recursively calculated elastic modules and other properties.

This thesis describes the procedure and Digital Signal Processing needed to get better resolution in frequency f_{res} with respect to the computational complexity, Hardware (HW) and Software (SW) requirements.

Details about mechanical vibrations sensing, evaluation of signal attenuation and implementation of program to microcontroller describes thesis *Measurement of changing mechanical properties of carbon composite on nanosatellite miniCube mission QB50* [1].

5.1 Construction of HM Panel

Mechanical properties are tested on HM panel which is made from carbon composite material. Within this carbon-fiber material is formed to cantilever, on which property changes are tested by a composite health monitoring system. Drawing of this panel is in Fig. 5.1.

HM panel is mounted as a hinged panel. It is folded to the wall of the satellite when VZLUSat–1 is in the shuttle and when it is launching. In free space it will be unlocked and it will pop up to Space where the material will be tested. Unfolded state of satellite is shown in Fig. 3.1.

Panel consists of several parts like glued permalloy magnet on the free end of tested beam. By using this tiny permalloy strip oscillation of the cantilever are excited. Oscillations are caused by an electric pulse to the small coil, located above the strip.

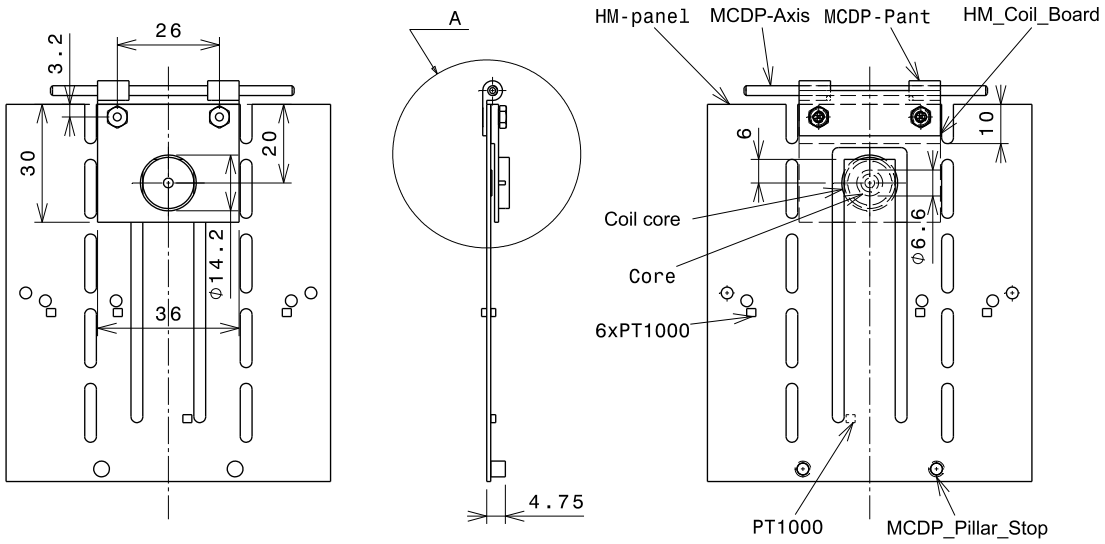

Fig. 5.1: Drawing of HM panel

Surface of each side part is covered by a thin layer of reflective materials. There is golden a compound on one side and on the other side is compound of nickel. These materials should reflect thermal radiation for example from the Sun. This reflectivity is studying through platinum thermometers.

Temperature is measured on HM panel as well. There is a measuring network consisting of many platinum temperature sensors PT1000. We need to have information about temperature on carbon composite cantilever, because with the change in temperature, there can also be a change in properties of the beam and in results of measurement as well.

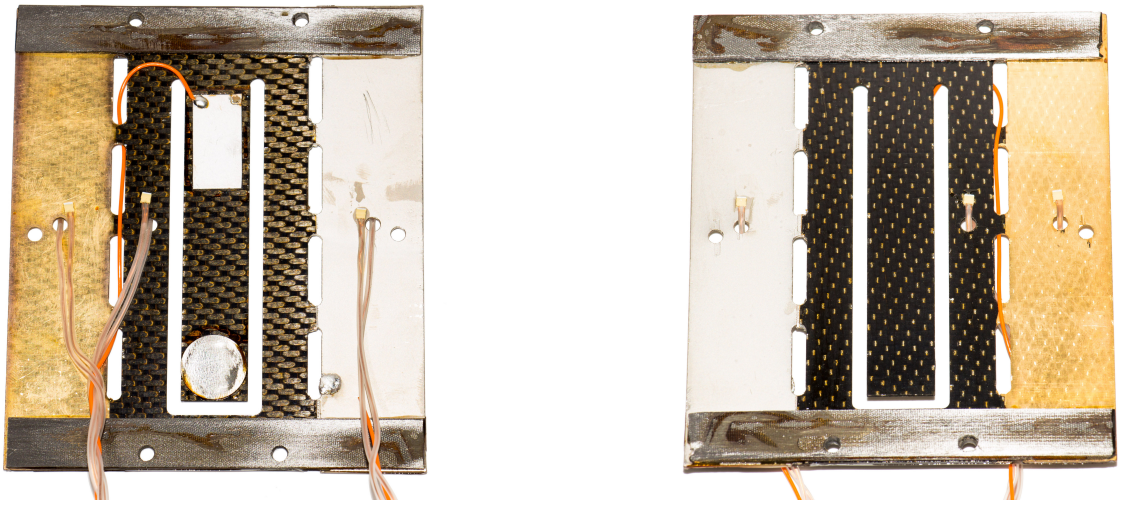

(a) Front side

(b) Back side

Fig. 5.2: Photo of HM panel

5.2 Sensed Signal

For verifying natural frequencies and hence also Elastic Modulus (E), it is needed to get oscillating signal from the beam. The basic principle is to use a converter from mechanical quantity into electrical quantity. There are two methods how this can be performed. One is through acceleration by accelerometer and the second one is through deformation by a piezoelectric plate. [12]

5.2.1 Sensing through Accelerometer

Accelerometer must be situated into the place with the highest acceleration. In this place is thus the highest signal variation. Unfortunately, this position is at the end of cantilever. Although, accelerometers are usually small and lightweight components, weight of accelerometer and his wires caused hight signal distortion on a lightweight beam [12].

5.2.2 Sensing through Piezo Element

Another method how to measure oscillations is based on Piezoelectricity. It is an effect when certain solid material can generate electric signal in response to applied mechanical stress.

From principle, the location where the piezo-element should be placed is clear. Required position for better sensing is the place with the mechanical stress of the measured material [12].

This position is at the fixed end of the cantilever which means, that the piezo element is glued on opposite side of the composite beam than the excited coil. When piezo is stressed, it produces electrical voltage which is measured and it corresponds to mechanical oscillations.

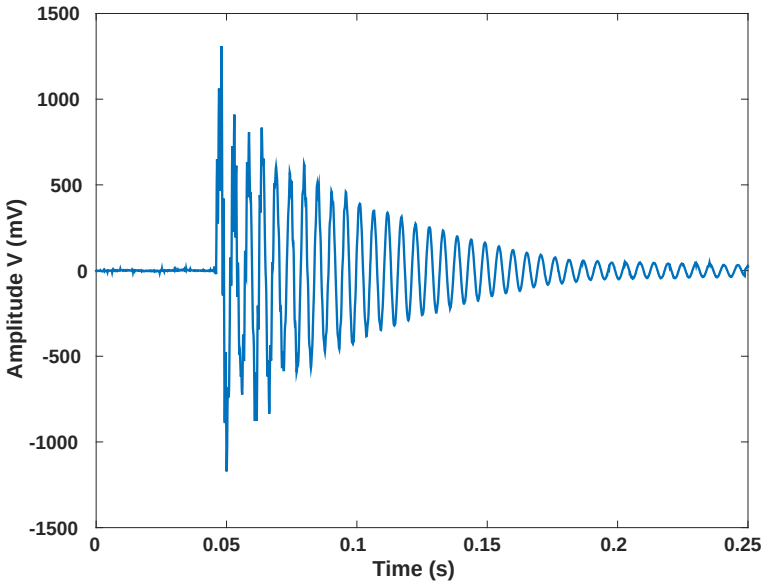

Fig. 5.3: Signal waveform in time domain with f_s= 8 kHz

Measured signal sensed by the piezoelectric sensors glued on beam is shown in Fig. 5.3. This signal is connected to HM board where is converted to digital form by Microcontroller (MCU). Converting an analog signal to digital is done through the Analog to Digital Converter (ADC) with Sampling frequency (f_s) 8 kHz.

6 Fast Fourier Transform

To find the f_{res} Fast Fourier Transform (FFT) will be used. The FFT is a method used to obtain the frequency spectrum of signal. The spectrum is representation of the signal in the frequency domain. This chart does not show time change of signal amplitude, as it is in time domain, but the amplitude and the phase of the signal for each occupied frequencies.

From the sampled discrete-time signal, the spectrum can be obtained by two ways: Discrete Fourier Transform (DFT) or Fast Fourier Transform (FFT). Examples of basic signals and their two-sided spectra can be seen in the Fig. 6.1

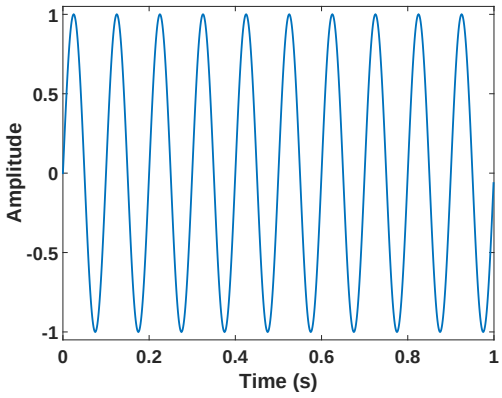

(a) The Sinusoidal waveform

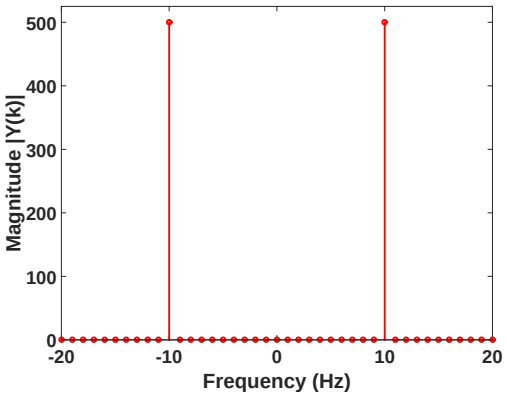

(b) Spectrum of a sinusoidal signal

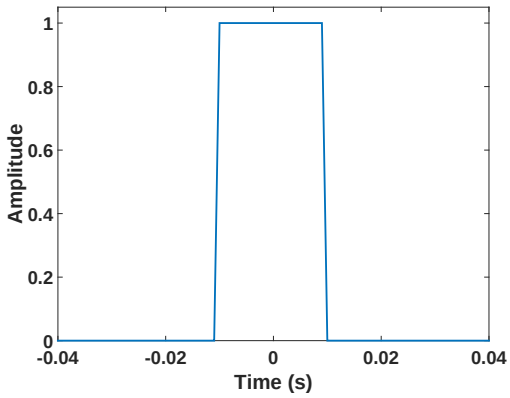

(c) Rectangle in time domain

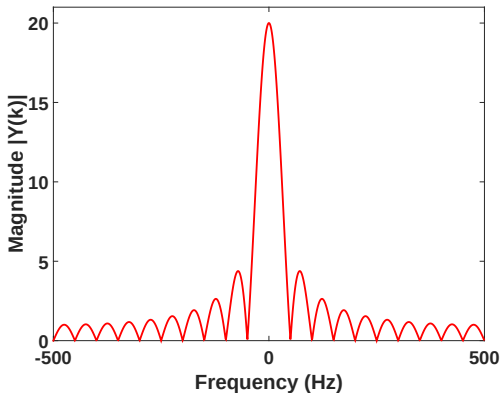

(d) Rectangle in spectral domain

Fig. 6.1: Examples of the waveform and its two-sided spectrum

6.1 Comparison of DFT and FFT

For numerical computations of spectrum from digital signal discrete version of the Fourier transform is used, it is Discrete Fourier Transform (DFT) (6.1).

$$Y_k = \frac{1}{N}\sum_{r=0}^{N-1} y_r \left[\cos\left(\frac{2\pi rk}{N}\right) - i\sin\left(\frac{2\pi rk}{N}\right)\right] \tag{6.1}$$

$$e^{ix} = \cos(x) + i\sin(x) \tag{6.2}$$

After substituting the equation (6.2) into (6.1) we get shorter form:

$$Y_k = \frac{1}{N}\sum_{r=0}^{N-1} y_r e^{\frac{-i2\pi rk}{N}} \tag{6.3}$$

$$= \frac{1}{N}\sum_{r=0}^{N-1} y_r e^{-i\left(\frac{2\pi rk}{N}\right)} \tag{6.4}$$

Where y_r is Discrete signal, r is Discrete sample point, Y_k is Discrete spectrum and k is Discrete frequency [13, 16].

This calculation method of spectrum by DFT requires 2^M complex multiplications.

Fast Fourier Transform algorithm is based on principle of decimation. *Decimation-in-Time* (DiT) where the input sequence is decimated or *Decimation-in-Frequency* (DiF) where the output sequence is decimated . This decimation involves decomposition of original time (frequency) sequence into smaller parts. As shown in equation (6.5), a DFT of Length of signal (N) can be rewritten as sum of two similar DFTs (6.6). Each of these Discrete Fourier Transforms has length $N/2$. One calculates with the odd-indexed points from N of the original signal and the other with even-indexed points (6.7). In order to maintain symmetry, required original signal length must be $N = 2^M$, as is shown in Fig. 6.2.

FFT method for calculation of the spectrum requires $N\log_2 N$ number of operations.

$$Y_k = \frac{1}{N}\sum_{r=0}^{N-1} y_r e^{-i\left(\frac{2\pi rk}{N}\right)} \tag{6.5}$$

$$= \frac{1}{N}\left\{\sum_{r=0}^{(N/2)-1} y_{2r} e^{-i\left[\frac{2\pi(2r)k}{N}\right]} + \sum_{r=0}^{(N/2)-1} y_{2r+1} e^{-i\left[\frac{2\pi(2r+1)k}{N}\right]}\right\} \tag{6.6}$$

$$= \frac{1}{N}\left\{\sum_{r=0}^{(N/2)-1} y_{2r} e^{-i\left[\frac{2\pi rk}{(N/2)}\right]} + e^{-i\left(\frac{2\pi k}{N}\right)}\sum_{r=0}^{(N/2)-1} y_{2r+1} e^{-i\left[\frac{2\pi rk}{(N/2)}\right]}\right\} \tag{6.7}$$

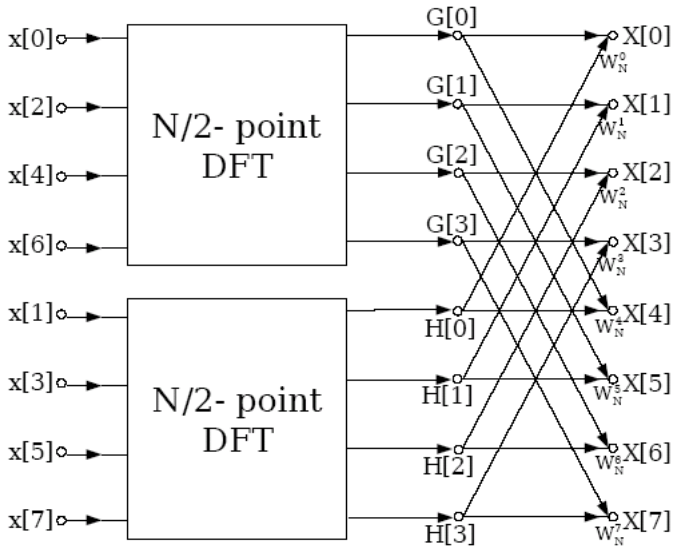

Fig. 6.2: Decimation in time of a length-N DFT into two length-N/2 DFTs [17]

If is defined W_N as

$$W_N = e^{-i\left(\frac{2\pi}{N}\right)} \tag{6.8}$$

the equation (6.4) for DFT can be rewriten as

$$Y_k = \frac{1}{N}\sum_{r=0}^{N-1} y_r W_N^{kr} \qquad k = 0, 1, 2, \cdots N-1 \tag{6.9}$$

and equation (6.7) for FFT

$$Y_k = \frac{1}{N}\sum_{r=0}^{(N/2)-1} y_r^e W_{N/2}^{kr} + \frac{1}{N} W_N^k \sum_{r=0}^{(N/2)-1} y_r^o W_{N/2}^{kr} \qquad k = 0, 1, 2, \cdots N-1 \tag{6.10}$$

where y_r^e and y_r^o represent even and odd order samples of y_r.

The computational efficiency is usually expressed by the number of complex multiplications and additions, or simply, by the number of operations [11]. A simple representation of the computational cost of DFT compared with the FFT is shown in Fig. 6.3. From this figure is obvious that when comparing the number of the operations and therefore the processing time, is FFT more advantageous than the DFT.

$$N^2 > \left(\frac{N}{2}\right)^2 + \left(\frac{N}{2}\right)^2 + N \tag{6.11}$$

$$N^2 > \frac{N^2}{2} + N \tag{6.12}$$

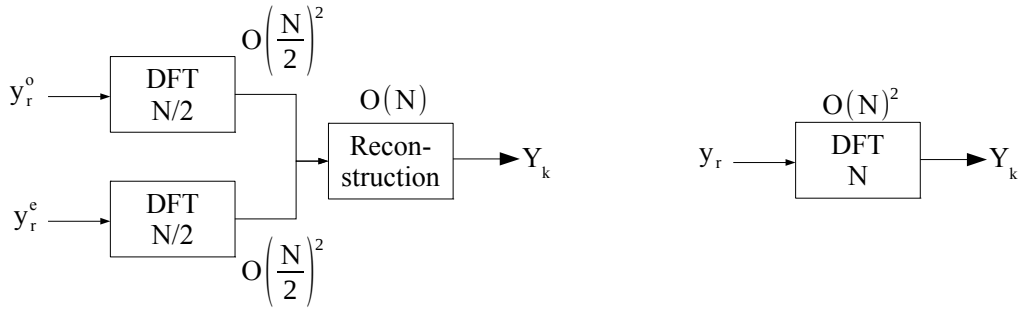

(a) FFT (b) DFT

Fig. 6.3: Number of operations

For more iterations of decomposition, the total number of necessary operations declines and thus the computational complexity will also decrease. The whole process of FFT calculation is faster in comparison with DFT and is even quicker with an increasing number of iterative decompositions for each FFT.

This is illustrated in Fig. 6.4 and by the derivation of the equations (6.13) to (6.16).

$$1: \quad N/2 \Longrightarrow \quad 2\left(\frac{N}{2}\right)^2 + N = \frac{N^2}{2} + N \tag{6.13}$$

$$2: \quad N/4 \Longrightarrow \quad 2\left[2\left(\frac{N}{4}\right)^2 + \frac{N}{2}\right] + N = \frac{N^2}{4} + 2N \tag{6.14}$$

$$3: \quad N/8 \Longrightarrow \quad 2\left\{2\left[2\left(\frac{N}{8}\right)^2 + \frac{N}{4}\right] + \frac{N}{2}\right\} + N = \frac{N^2}{8} + 3N \tag{6.15}$$

$$\vdots \qquad \vdots \qquad \qquad \vdots$$

$$M: \quad N/2^M \Longrightarrow \quad \frac{N^2}{2^M} + MN = \frac{N^2}{N} + N\log_2 N \tag{6.16}$$

where $N/2^M = 1$.

In equation (6.16) dominates final term therefore, generally the computational complexity of FFT is cited in simplified form as:

$$N\log_2 N \tag{6.17}$$

for comparison of computional acceleration, Efficiency gain [11] s defined as:

$$\text{Efficiency gain} = \frac{N^2}{N\log_2 N} \tag{6.18}$$

For $N = 1024$ efficiency gain is approx. 100 and for $N = 8196$ Fast Fourier Transform is more than 600 times faster.

Fig. 6.4: FFT sequence for $N = 8$

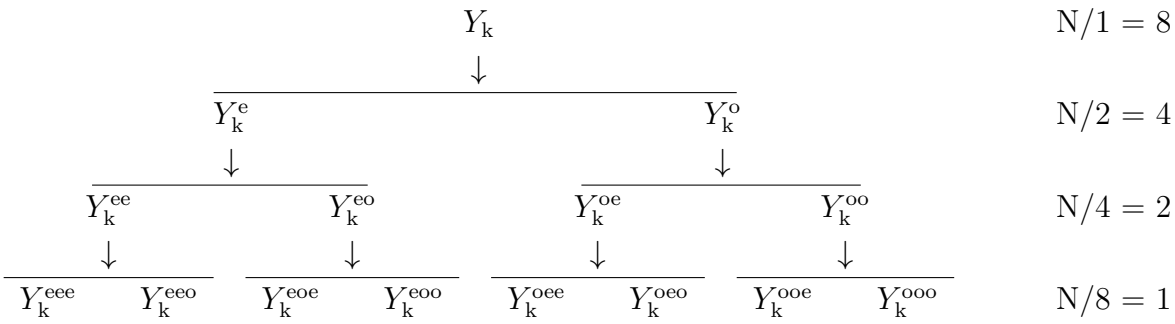

For previously mentioned reasons, the calculation of the resonant frequency by FFT is used .

The following Matlab code (Code 6.1) shows the simplest example of Digital Signal Processing using `fft` function in MATLAB R2014b environment.

Waveform sensed by piezo element is used as a source of signal and shown in Fig. 5.3 on page 24. This signal was sensed as one of the first on the development board with HM panel. Waveform signal was converted by Analog to Digital Converter with Sampling frequency $f_s = 8$ kHz. The original idea was that the signal is converted as accurately as possible, due to the processing of its envelope to determine the attenuation. Sampling frequency was limited by the capacity of SRAM memory and the processor time required for Digital Signal Processing (DSP).

Result of this process is half of two-sided amplitude spectrum in figure Fig. 6.5.

However, when you use this simple method, the resulting spectrum has only a low resolution. The distance of each spectral lines, which is defined as Frequency step (Δf), is approx. 3.9 Hz, because the signal length is only $N = 2048$ samples.

$$\Delta f = \frac{f_s}{N} \tag{6.19}$$

Code 6.1: Example of simple FFT

```
clear all
close all
clc

%% Input signal
[FileName,pathname]=uigetfile('*.csv');
fid=fopen(fullfile(pathname,FileName));
Data=textscan(fid,'%f','HeaderLines', 1);
fclose(fid);

sig = Data{1}(:,1);       % Data in 1 column
sig = sig-mean(sig);      % Elimination DC offset

fs  = 8000;               % Sample frequency
ff  = 0:fs/length(sig):fs-fs/length(sig);% Frequency axis

FFT = abs(fft(sig));     % FFT calculation

figure()
plot(ff(1:length(ff)/2),20*log10(FFT(1:length(FFT)/2)))
xlabel('Frequency (Hz)');
ylabel('Magnitude 20 log_{10}|Y(k)|');
```

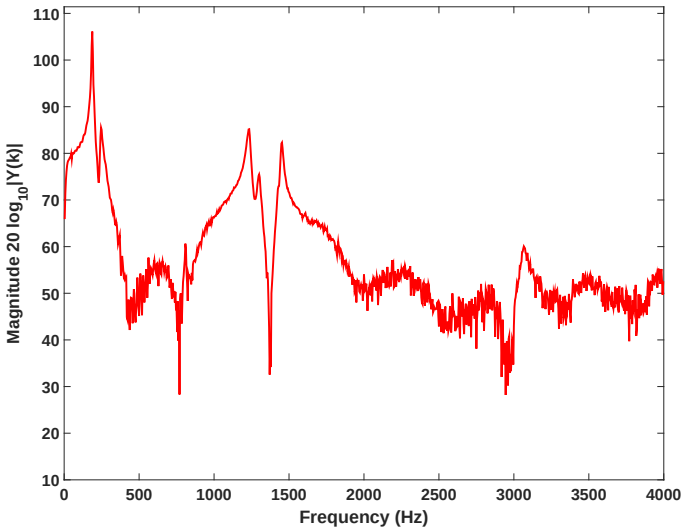

Fig. 6.5: Two-sided spectrum of the real signal in Fig. 5.3 from 0 to fs/2

6.2 Effects of Zero Padding

As shown in previous section, using the basic FFT, without further adjustments, we only get very rough estimate of spectral resolution of the actual signal in Fig. 5.3. Detail of spectral segment of this signal is in Fig. 6.7a. Frequency step in this case is approx. only 3.9 Hz.

According to the equation (6.19) there are two ways to improve the Frequency step.

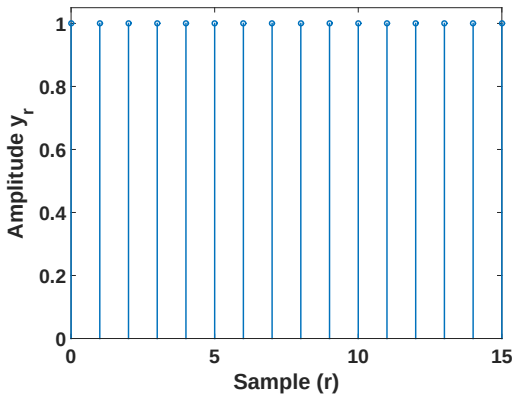

(a) Short rectangle with N = 16

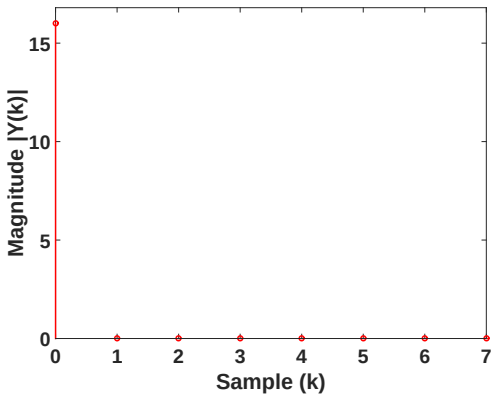

(b) Spectrum of short rectangle Fig. 6.6a

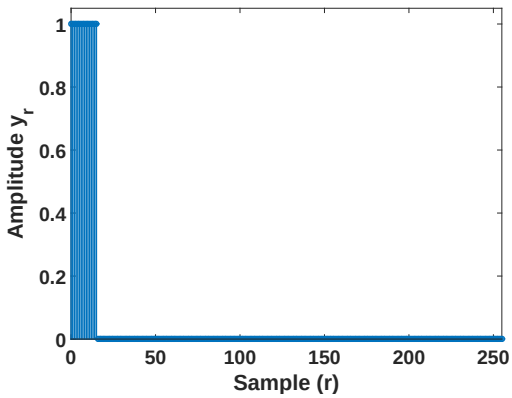

(c) Interpolated rectangle with N = 256

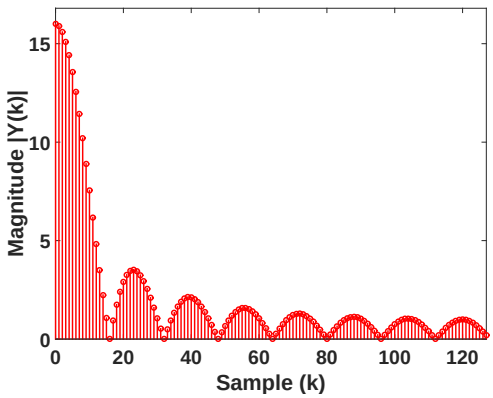

(d) Spectrum of rectangle in Fig. 6.6c

Fig. 6.6: Example of interpolation principle

First of them is to reduce the numerator of a fraction, thus the Sampling frequency. However, application of this approach is not advantageous with regard to

the waveform and quality of the signal recorded for further processing (e.g. attenuation calculation).

Next one is to increase the number of signal samples N. This method is called Interpolation and it is based on zero padding (Fig. 6.6). For spectral analysis, signal padding by zeros corresponds to oversampling original spectrum with several times greater Δf. If the length of padded zeros is defined as Q that are added behind a signal of length N, then new Frequency step is $(N+Q)/N$ times greater.

$$\Delta f = \frac{f_s}{N+Q} \tag{6.20}$$

With this method of adding zeros behind a signal, the number of signal samples N can be supplemented to the correct length to comply condition for symmetry of the FFT. It is the most common and simple way to adjust a signal in order to satisfy the condition of Length of signal= 2^M.

Code 6.2: Example of interpolated FFT

```
...
Ni      =       8192;                   %Q+N
iFFT    =       abs(fft(sig,Ni));       %Interpolated FFT
```

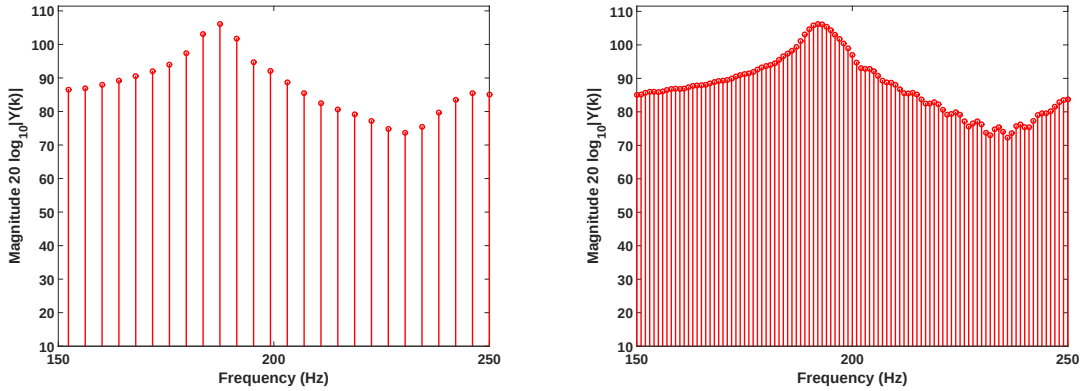

(a) Detail spectrum of the real signal in Fig. 5.3 before interpolation

(b) Detail spectrum of the signal in Fig. 5.3 after interpolation to N = 8192

Fig. 6.7: Comparison of the spectrum after using interpolation

Because used SRAM memory has a capacity 1 Mbit, which corresponds to 128 kB, then in order to respect the condition of symmetry, maximum used window size can be 64 kB, therefore N= 8192 samples. Comparing the spectra before and after the signal interpolation is shown in Fig. 6.7. New interpolated spectrum in Fig. 6.7b has Frequency step approx. Δf= 0.98 Hz, (equation 6.20).

6.3 Decimation

Final resolution of the signal from previous section get significantly more accurate result. However, the resolution based on the equation (6.20) does not provide sufficiently accurate results.

As previously mentioned, to improve the resolution of Δf , two basic principles can be used. The one with the addition of zeros after the signal has already been described and applied in the section 6.2 Effects of Zero Padding. Further improvement through scanning the signal with sensing lower sampling frequency f_s is unacceptable, as already mentioned.

But, fortunately, except limiting by HW there is the possibility of SW implementation solutions to reduce the sampling rate f_s. A system component that performs this reducing of the f_s is called a decimator.

Decimation principle such as Digital Signal Processing consists in selecting each D^{th} sample.

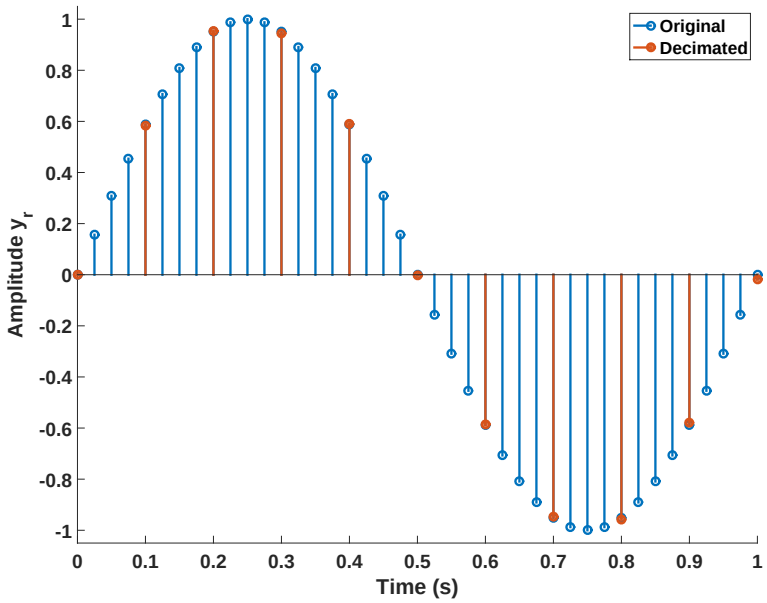

Fig. 6.8: Example of decimation principle

Code 6.3: Example of decimation

```
t = 0:.025:1;              % time axis
x = sin(2*pi*1*t);         % signal
y = decimate(x,4);         % decimated signal by D = 4
```

As shown in Fig. 6.8, decimated signal looks like a signal sampled by quarter-frequency. New Decimated sample frequency (f_s') is therefore

$$f_s' = \frac{f_s}{D} \tag{6.21}$$

where D is integer Decimation factor and f_s is original sample rate.

By this approach the original signal can be decimated to much lower Sampling frequency. The disadvantage of this process is that it still must comply with Nyquist-Shannon sampling theorem. That means that with the reduction of sample rate f_s, the ability to show the higher spectral lines decreases.

Under these circumstances, the highest spectral line can be displayed on position with maximum frequency, equals $f_s'/2$. Mirroring of spectrum occurs around f_s'.

If this method is used on the original signal in Fig. 5.3 sampled by f_s= 8 kHz and Length of signal equals to 2048 samples, where decimation is performed to the frequency of 500 Hz, then, while maintaining the same window as in the case in Fig. 6.5, accomplished Δf is 0.24 Hz.

This frequency f_s' was chosen with respect to the main beam resonance, which is about 190 Hz. Decimated sample frequency is in conformity with Nyquist-Shannon sampling theorem. This theorem provides a prescription for the nominal sampling interval required to avoid aliasing. It can be simply stated as follows:

The sampling frequency should be greater than
twice the highest frequency contained in the signal.

Minimum Sampling frequency for correct display of the signal at a frequency 185 Hz is

$$f_s > 2 \times 190 \tag{6.22}$$

Because the frequency can be changed and to sufficiently fulfill the conditions (6.22) with reserve, 500 Hz was determined as adequate Sampling frequency.

The Decimation factor is therefore

$$D = \frac{f_s}{f_s'} = \frac{8000}{500} = 16 \tag{6.23}$$

Code 6.4: Example of decimated FFT

```
...
dec_to   =    500;          % new sample frequency (decimate)
D        =    fs/dec_to;    % decimade koeficient;

dec_sig = zeros(floor((length(sig)/D)),1);
j=0;
for i=1:D:((length(sig)))
    j=j+1;
    dec_sig(j) = sig(i);
end
dFFT=abs(fft(dec_sig,2048));
```

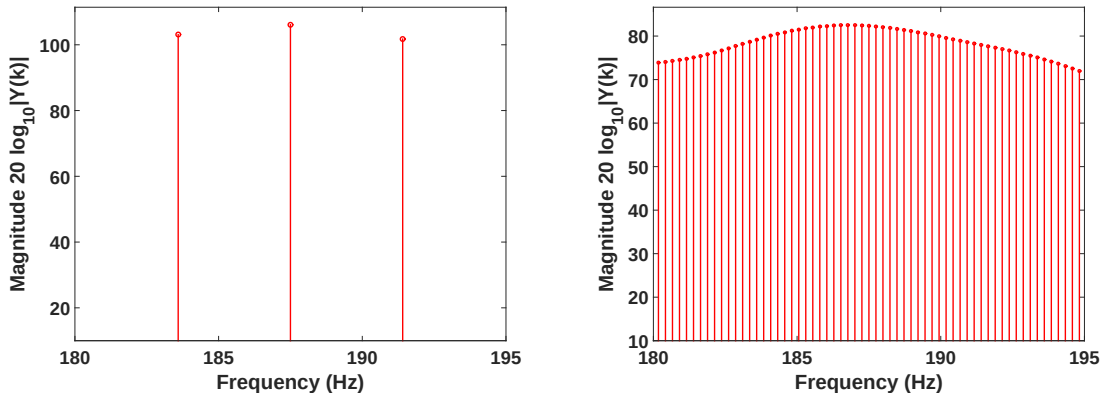

(a) Detail spectrum of the real signal in Fig. 5.3 before decimation

(b) Detail spectrum of the signal in Fig. 5.3 after decimation with the ame window

Fig. 6.9: Comparison of the spectrum after using decimation

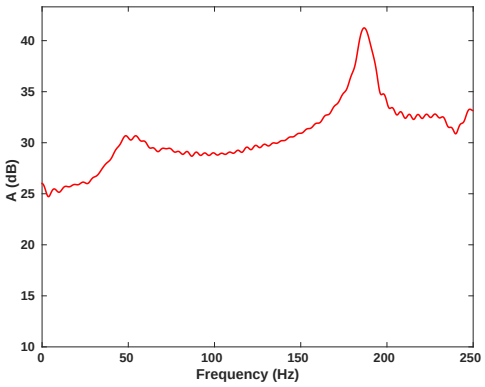

Fig. 6.10: Two-sided spectrum decimated f_s 8000 Hz $\rightarrow$ f'_s 500 Hz from 0 to $f'_s/2$

One of the adverse characteristics of the decimation is mirroring of spectral lines and hence possible change of the whole appearance of the spectral domain.

The standard spectrum is periodic with period $1/f_s$. General appearance of such a spectrum is shown in Fig. 6.11.

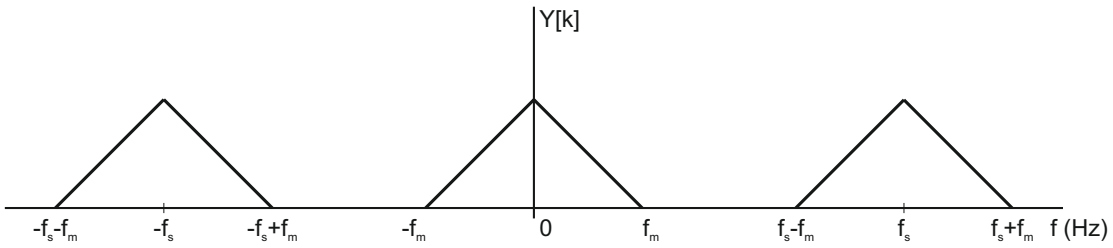

Fig. 6.11: Periodic spectrum with fulfilled sampling condition

Basically, three relation between f_s and f_m may occur where f_s is Sampling frequency and f_m is Maximum contained frequency in signal.

In case of Fig. 6.11 is

$$f_m < f_s - f_m \qquad \rightarrow \qquad f_m < \frac{f_s}{2} \tag{6.24}$$

This condition (6.24) ensures that there is no overlap of spectra.

When the signal is downsampling these curves move together until

$$f_m = f_s - f_m \qquad \rightarrow \qquad f_m = \frac{f_s}{2} \tag{6.25}$$

In this situation, the condition is on limit usability.

With further decrease of the Sampling frequency the condition (6.24), respectively (6.22) can not continue to be fulfilled.

If the situation arises where the f_s is correlated with the f_m

$$f_m > f_s - f_m \qquad \rightarrow \qquad f_m > \frac{f_s}{2} \tag{6.26}$$

then multiplexing of individual spectral components occurs, which decreases the usability and accuracy of the spectral diagram as shown in Fig. 6.12.

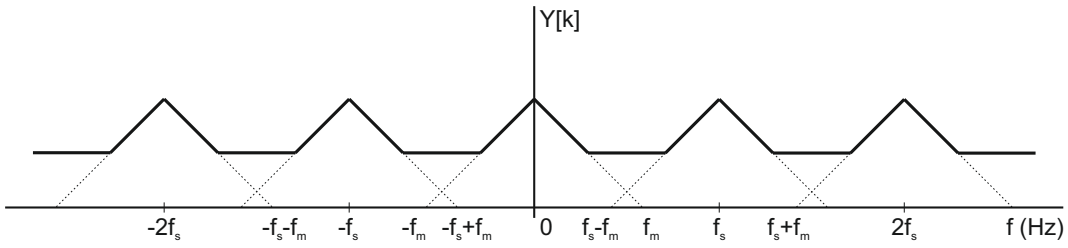

Fig. 6.12: Periodic spectrum with unfulfilled sampling condition

This handicap can be minimized by using a filtered input signal. There are several ways to do this.

The higher frequency components of the signal can be removed by using the analog Low-pass filter (LP filter) before the digitization of the signal by Analog to Digital Converter. However, this solution requires adjustments already in hardware design of Printed circuit board (PCB).

Another possibility is for example a digital Finite impulse response filter (FIR filter). This type of filter does not require any changes on PCB. This filter is purely issue of SW. FIR filter has no parallel in the analog wiring and enables simple design of steep filters of higher orders. It also has a linear phase characteristics, that means, it retains the shape of the signal in the passband and it is always stable. [15]

The difference between filtered and unfiltered decimated signal from Fig. 6.21 with new $f'_s = 1000\,\text{Hz}$ is shown in figure Fig. 6.13. In figure Fig. 6.13b is shown the spectral peak in the frequency range, around 80 Hz, where there is no power increase, in Fig. 6.13a is shown as a reference spectrum of the filtered signal to comparison. Shown peak is mirrored from the frequency 1030 Hz as can be seen in Fig. 6.23.

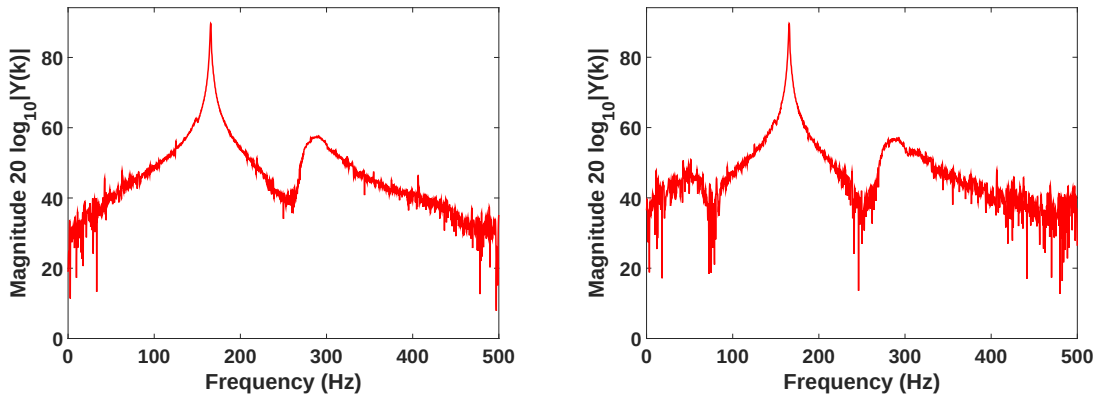

(a) Decimated spectrum after limitations by FIR filter

(b) Decimated spectrum without filter limitations

Fig. 6.13: Comparison of the spectrum after using filtration

6.4 Windowing

Amplitude ambiguity arises when window length is not an integer multiple of period of the signal. For aperiodic signal, the window length is theoretically equal to infinity, in practice it is required to have finite length of record. For processing either an aperiodic, random or signal with variable frequency, it is recommended to use windowing function. Most of these signals do not have a period and Fast Fourier Transform applied to such a signal's finite record length produces leakage in its spectrum [16].

This leakage is caused by the discontinuities near start and end of window (Fig. 6.15a). These artificial discontinuities show up in the FFT as high-frequency components not present in the original signal (Fig. 6.15b). These discontinuities may also arise with change of signal frequency which would not be integer multiple of the window length. The spectral power, which should have been concentrated on a single harmonic, has leaked to neighbouring harmonics [11]. This effect can be reduced by using a windowing application. This procedure effectively minimalizes the amplitude of signal near the discontinuities at the beginning and end of the signal. Example of using windows is in Fig. 6.20.

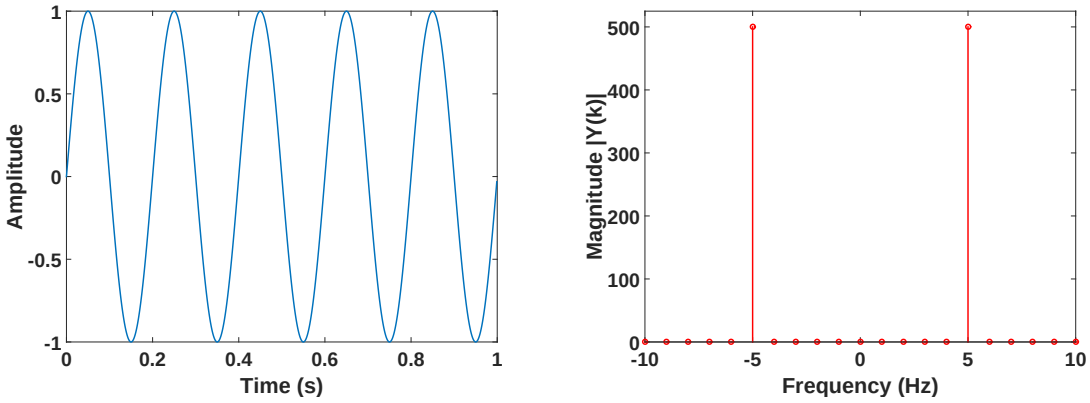

(a) Time domain (b) Spectral domain

Fig. 6.14: Sinusoidal waveform of the same length as the window.

The effect of windowing function in the time domain corresponds to multiplication of the signal with the selected window (Fig. 6.20a). In the spectrum it

corresponds to convolution of two FFT, one of the signal and other of the selected windowing function.

Before applying window function, it is necessary to consider the need for using it. Because the usage of different window type than basic rectangle, for signal where it is not essential, is disadvantageous. Under these circumstances the *picket-fence effect* occurs. This means that the main spectral peaks splits up into more frequencies. Thus, windowing function may help with leakage, but incorrect usage could cause the distortion of the spectrum such as amplitude ambiguity and frequency leakage.

This effect of distortion can be reduced either by increasing the window length over more periods of the signal by combinating of original signal with smooth transition window function. [11]

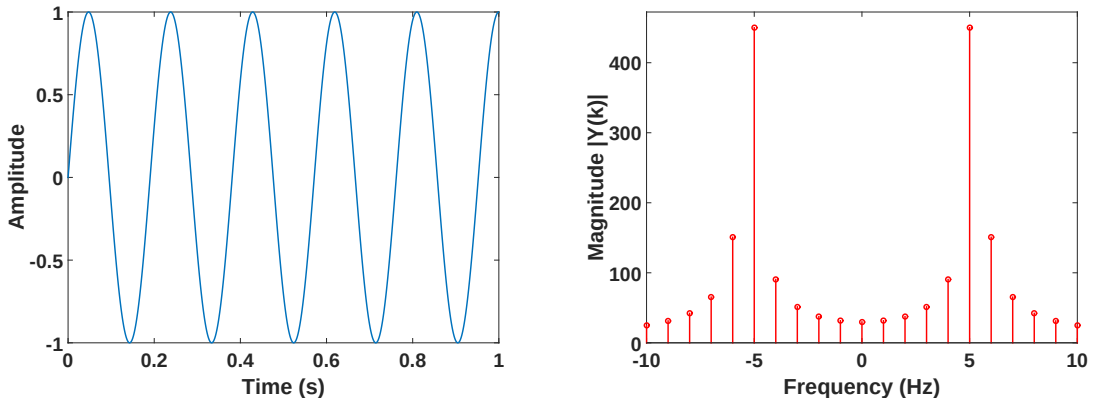

(a) Time domain (b) Spectral domain

Fig. 6.15: Sinusoid spectral leakage

6.4.1 Rectangle Window

It is not true that no window can be used. Always, when "no window" is used, then in fact basic rectangular window is applied to the signal. It is the simplest window sometimes known as the boxcar or Dirichlet window.

The table below shows some of the Boxcar properties (Tab. 6.1) and in Fig. 6.16 is shown waveform and spectrum of Rectangle window.

$$w[r] = 1 \qquad \text{for } r = 0, \ldots, N-1 \tag{6.27}$$

Tab. 6.1: Parameters of Rectangle window [13]

Property	Value
Width of the main lobe	$1 \cdot \Delta f$
The highest side lobe	-13 dB
Equivalent noise width	$1 \cdot \Delta f$

Width of the main lobe and equivalent noise width are related to Frequency step (Δf) according to equation (6.19).

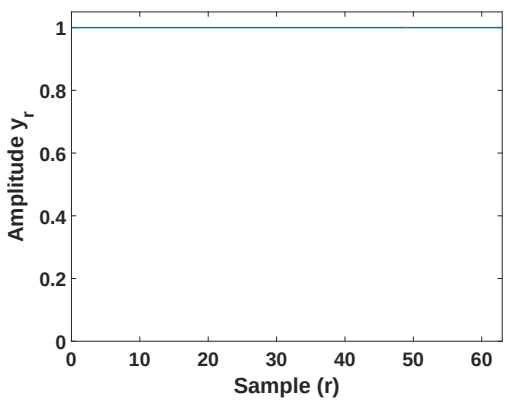

(a) Time domain

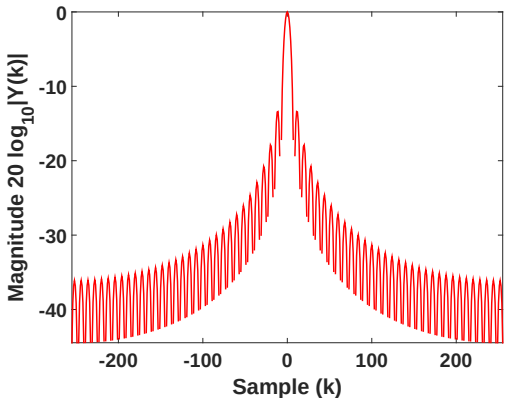

(b) Spectral domain

Fig. 6.16: Rectangular window

6.4.2 Hamming Window

In Fig. 6.17 is shown waveform and spectrum of the window.

This window type is optimized to minimize the first side lobe (Fig. 6.17b). This side lobe is usually maximum and nearest lobe to the main lobe for Rectangle Window (see 6.4.1) as is shown in Fig. 6.16b.

In the Fig. 6.17a is presented the progress of the window. Near beginning and end of signal can be noticed that although there is signal attenuation but not complete zeroing.

The Tab. 6.2 shows some of the Hamming window properties.

$$w[r] = 0.54 - 0.46 \cos \frac{2\pi r}{N} \qquad \text{for } r = 0, \ldots, N-1 \tag{6.28}$$

Tab. 6.2: Parameters of Hamming window [13]

Property	Value
Width of the main lobe	$2 \cdot \Delta f$
The highest side lobe	-43 dB
Equivalent noise width	$1.5 \cdot \Delta f$

Width of the main lobe and equivalent noise width are related to Frequency step (Δf) according to equation (6.19).

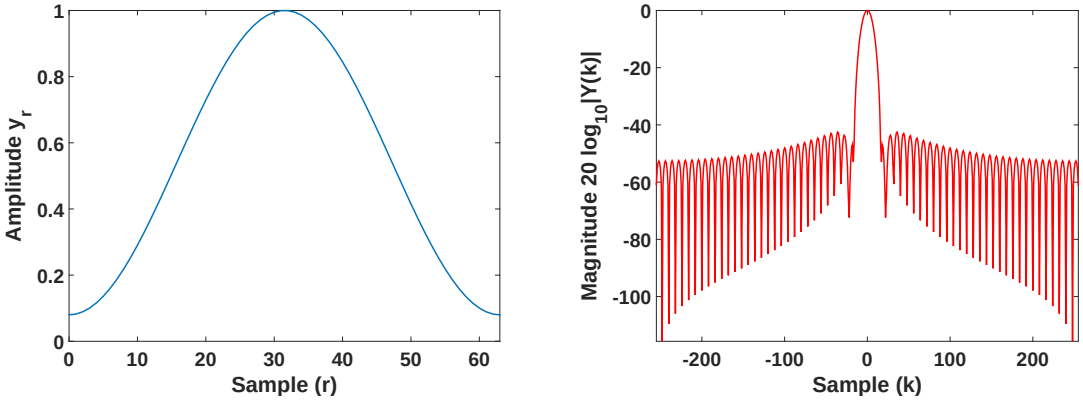

(a) Time domain (b) Spectral domain

Fig. 6.17: Hamming window

6.4.3 Hann Window

The Hann window also known as the Hanning's or the raised cosine window. Hanning window is not similar to Hamming Window (see 6.4.2) only by name but also by shape. One difference is the attenuation value at the beginning and the end of signal. This window reduces leakage and improve amplitude accuracy, however, frequency resolution is reduced.

In the Tab. 6.3 are listed some of the Hanning window properties and the waveform and spectrum of this window is shown in Fig. 6.18.

$$w[r] = \frac{1}{2}\left(1 - \cos\frac{2\pi r}{N}\right) \qquad \text{for } r = 0, \ldots, N-1 \tag{6.29}$$

Tab. 6.3: Parameters of Hanning window [13]

Property	Value
Width of the main lobe	$2 \cdot \Delta f$
The highest side lobe	-32 dB
Equivalent noise width	$1.36 \cdot \Delta f$

Width of the main lobe and equivalent noise width are related to Frequency step (Δf) according to equation (6.19).

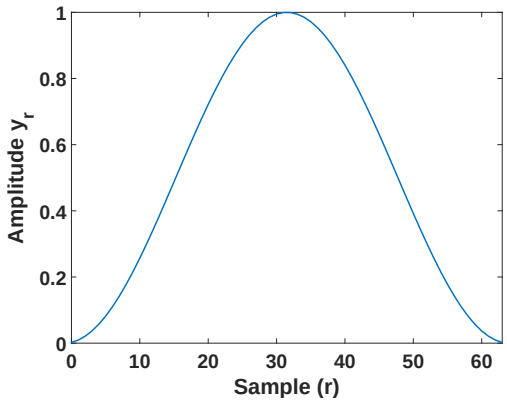

(a) Time domain

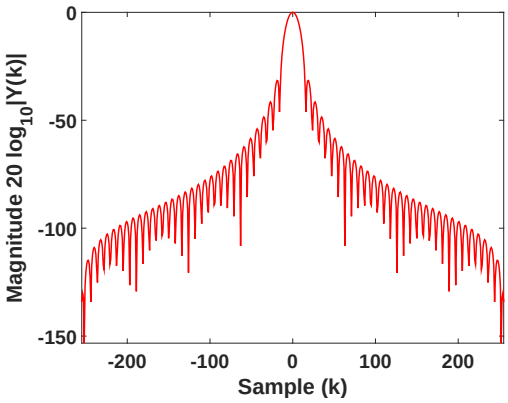

(b) Spectral domain

Fig. 6.18: Hanning window

6.4.4 Blackman Window

The Blackman window has a narrower waveform and therefore is useful for single tone measurement, because it has low maximum side lobe level.

Some of the Blackman window properties are shown in Tab. 6.4 and in Fig. 6.19 is shown waveform and spectrum of this window.

$$w[r] = 0.42 - 0.5\cos\frac{2\pi r}{N} - 0.8\cos\frac{4\pi r}{N} \qquad \text{for } r = 0, \ldots, N-1 \tag{6.30}$$

Tab. 6.4: Parameters of Blackman window [13]

Property	Value
Width of the main lobe	$3.5 \cdot \Delta f$
The highest side lobe	-58 dB
Equivalent noise width	$1.73 \cdot \Delta f$

Width of the main lobe and equivalent noise width are related to Frequency step (Δf) according to equation (6.19).

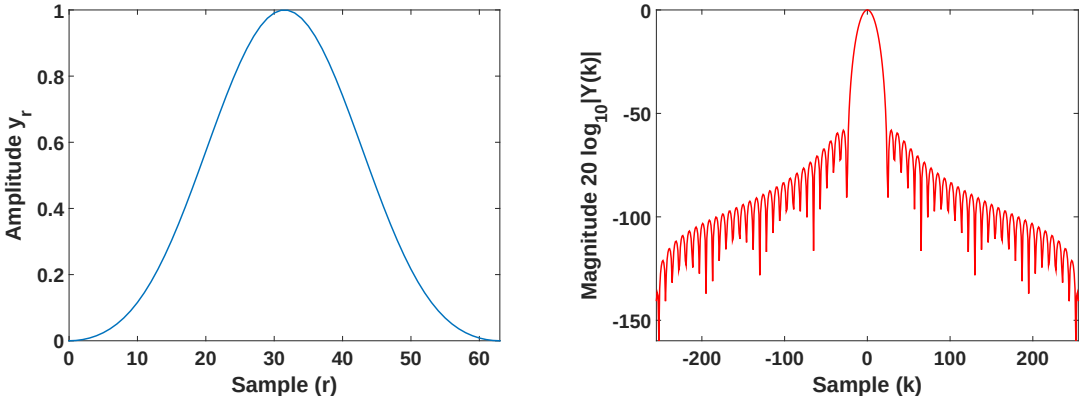

(a) Time domain

(b) Spectral domain

Fig. 6.19: Blackman window

6.4.5 Windowing Summary

There are many types of windows, each of them has different properties and is suitable for different application. Some of them are more effective for specific types of signal. Some improve frequency resolution and other improve amplitude accuracy.

Windows reduce the leakage effects, but can not eliminate leakage entirely. In fact, they only change the shape of the leakage. As already mentioned, the relationship between the signal and the used window in the time domain is multiplication and therefore in spectral domain it is a convolution. From this perspective, the significant sidelobes, which appear in the windows spectra, depending on the shape of the window in the time domain. Windows with narrower and "smooth" waveform have more significant attenuation of side lobes. However, with this feature also increases the width of the main lobe, which ultimately results in blurring of the spectral estimation Δf and splitting of spectral lines (*picket-fence effect*).

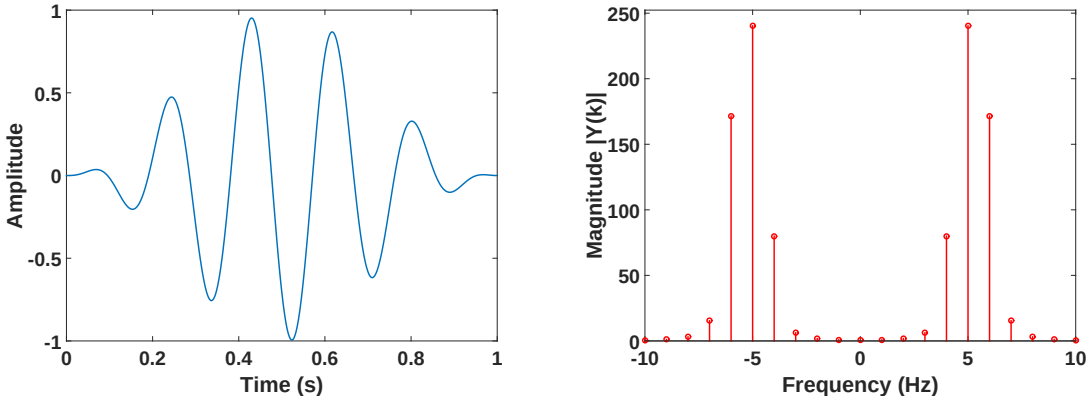

(a) Time domain (b) Spectral domain

Fig. 6.20: Windowing effect (Hanning with signal Fig. 6.15a)

It is clear that finding a suitable window is a compromise of more properties, which depends on the practical application.

In the case of CubeSat VZLUSat–1, when choosing a suitable window, there are several requirements that must be reflected. Among other things, such as computational complexity, SW and time requirements that restrict the application of satellite measurements.

6.5 Final Result

Digital Signal Processing is not a simple procedure, which could be solved according to a single universal process. Each signal type requires a slightly different approach and applied procedure.

During the Hardware and Software development for the measurement of mechanical material aging, there was a change in the mechanics of the measured HM panel. Consequently, this change led to a time extension signal as is shown in Fig. 6.21.

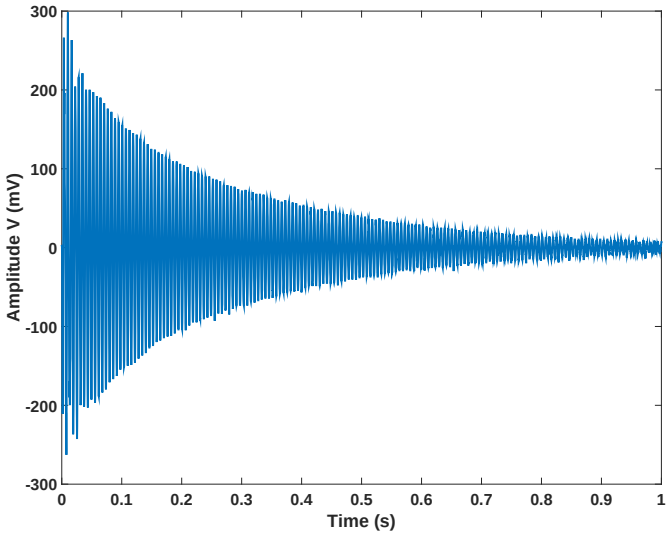

Fig. 6.21: Signal waveform in time domain with $f_s = 4\,\text{kHz}$

6.5.1 Frequency Resolution

Thanks to mentioned changes, Frequency resolution (B) in the spectral diagram was improved. Frequency resolution is an ability of a method to distinguish details in the spectrum. It can therefore be described as the ability to distinguish two nearby spectral lines in the spectrum belonging to the two close frequency harmonic signals f_1 and f_2.

If the calculation method has sufficient resolution, relative to the intervals of contained harmonics, narrow spectral lines belonging to these signals appears in the

spectrum. [14]

$$B = |f_1 - f_2| \tag{6.31}$$

Width of the resulting lines is inversely proportional to the Length of signal (T_0) and directly proportional to the type of window, respectively Window constant (c).

$$B = \frac{c}{T_0} \tag{6.32}$$

Therefore, with increasing length of the recorded signal T_0 is frequency resolution of B improves. Window constant c dependes on the type of used window and therefore on the extent signal distortion of its use. Overview of constants for above mentioned windows is in the Tab. 6.5.

Tab. 6.5: Window constants c

Type of window	Constant value
Ractangle	1
Hamming	2.5
Hanning	2.5
Blackman	3

It should be noted that, the Frequency resolution indicates something else than Frequency step. Frequency step Δf is determined by the number of used spectral lines N, the thickening of the spectrum is an effort to get minimal Δf.

Whereas, the frequency resolution B is the ability to distinguish individual details in the spectrum. [14]

If it is true that $B < \Delta f$ can be talk about the precise identification of the individual spectral lines. But if $B > \Delta f$ the determination is only approximate.

In this case of $T_0 = 1.024\,\mathrm{s}$, using a rectangular window appears, with regard to the Tab. 6.5, as the best decision.

$$B = \frac{1}{1.024} = 0.98\,\mathrm{Hz} \tag{6.33}$$

6.5.2 Used Window

As mentioned above, using of windowing has many advantages and disadvantages.

With compare the effect of the different windows on the signal spectrum, it is first necessary to use normalization on these signals, the maximum will be assigned a value of 1, and them bring then to a common graph, Fig. 6.22.

As shown in Fig. 6.22a, each window is reducing the spurious side lobes of spectrum differently. In this case of application, when only looking for the value of resonance frequency (respectively natural frequency of oscillation), spectrum leakage into neighborhood is not important but on the other hand the width of the main lobe (ramp slope) is. As is clear from Fig. 6.22b and tables in section 6.4 Windowing this property is best when using the Boxcar window.

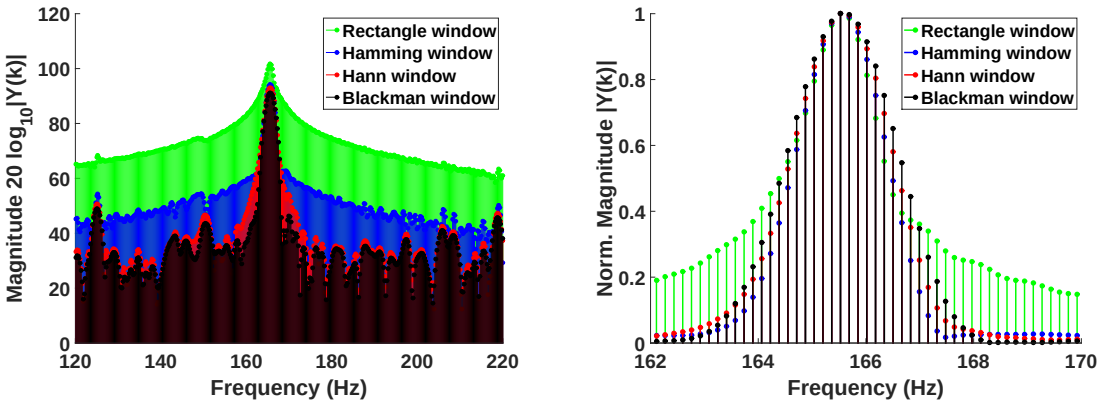

(a) Use of different windows

(b) Zoomed part of the normalized spectrum

Fig. 6.22: Comparison of the windows in the area of spectrum

This type of window, has in comparison with the others, minimum *picket-fence effect*. Which could distort the results. Another significant advantage is, as stated in subsection 6.5.1 Frequency Resolution, low Window constant c. Finally, computing requirements and memory allocation should be taken into consideration, with respect to the use of the 8-bits MCU. Rectangle has lower requirements compared with other windows.

6.5.3 Interpolation and Frequency Stepping

As previously mentioned, there have been several changes during the development on HW side as well as on SW side. One of them was change in the sampling frequency f_s. This change was made based on a compromise with my collaborator Ondřej Nentvich and his thesis about attenuation measurements [1]. Sampling frequency was reduced from 8 kHz to 4 kHz, which was classified as sufficient resolution for further processing of attenuation.

This change, besides reducing the amount of stored data, means a reduction (improvement) of the frequency step Δf.

By using $f_s = 4\,\text{kHz}$, $N = 4096$ samples is obtained from the signal about length of $T_0 = 1.024$ second. These samples in combination with the effect of zero padding, as is described in the section 6.2, lead, after substituting into the formula (6.20) to the final frequency step $\Delta f = 0.48\,\text{Hz}$.

$$\Delta f = \frac{f_s}{N+Q} = \frac{4000}{8192} = 0.48\text{Hz} \tag{6.34}$$

6.5.4 Decimation Effect

Decimation factors can have a positive effect in many applications to improve the Frequency step. Unfortunately, it also reduces the observed frequency range and without the use of a suitable filter, it increases spectrum distortion. Which is caused by superimpose of higher frequencies that cause spurious spectral peaks in lower frequency.

In this situation, the use of decimation only restricts readability of spectral results without any noticeable improvement. An adequate densification of spectral lines has already been accomplished by the combination of a lower sampling frequency and interpolating the signal at 8192 samples. Considering the additional requirement for measurement of at least two natural frequencies, decimation is directly inappropriate due to their values. (Tab. 4.2).

These values of natural frequencies will be used to more accurately describe the exact model of the measurement beam.

6.5.5 Summary

From the signal sensed from the oscillating beam, spectrum of oscillations was obtained by Fast Fourier Transform. By using Digital Signal Processing, which containes, besides actual FFT also application of a rectangular window and interpolation, everything of which was described above, a partial overview of natural oscillations of the beam but also resonances of the structure was obtained.

Overview of the measurement results is shown in Tab. 6.6.

Tab. 6.6: Properties of measured signal and spectrum

Property	Value
Sampling frequency (f_s)	4000 Hz
Length of signal (T_0)	1.024 seconds
Length of signal (N)	4096 samples
Number of interpolation samples (N+Q)	8192 samples
Frequency step (Δf)	0.49 Hz
Frequency resolution (B)	0.97 Hz

Due to spectrum frequency range, it will not be a problem to determine at least the first two natural frequencies of the beam. These frequencies are automatically searched by the program in the MCU on board of the satellite.

For time to time, on schedule stored in the Planner, or on demand, the whole raw signal will be sent to Earth. This will enable further analysis and potential changes in measurement parameters (e.g. Search limits, Sampling frequency).

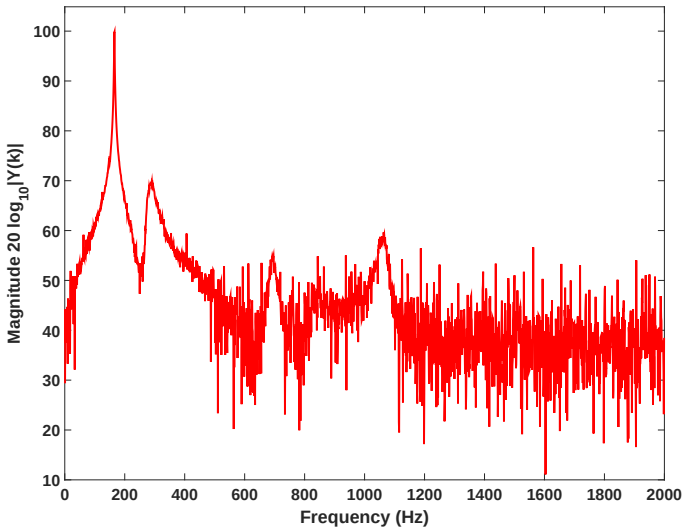

Fig. 6.23: Final two-sided spectrum of the real signal in Fig. 6.21 from 0 to fs/2

7 Evaporation

Part of properties verification of the new carbon fiber composite material is besides, the radiation resistance measurement [3], measurement of mechanical properties [1] and evaluation of changes (see chapters 4 – 6), also in addition evaporation measurement of water vapour and other gases from the material.

Water vapour in the air (or empty space, or any other gas) is generally called *humidity*, in liquid and solid materials it is usually designated as *moisture*.

Water and water vapour can be found everywhere. Water molecules has asymmetrical distribution of their electric charge, it means that, they are easily absorbed on almost any surface [11].

When water vapour starts to release from part of the satellite and vaporize in space it could be a problem. It is because these evaporated water molecules can condensate on other pieces of electronics. This humidity on contacts on PCB can cause short-circuit on board of the satellite and damage the whole device.

Molecules can also condense on optics lens or chips for image scanning. In this case it could be X-Ray Optics and Medipix board (see 3.2.1).

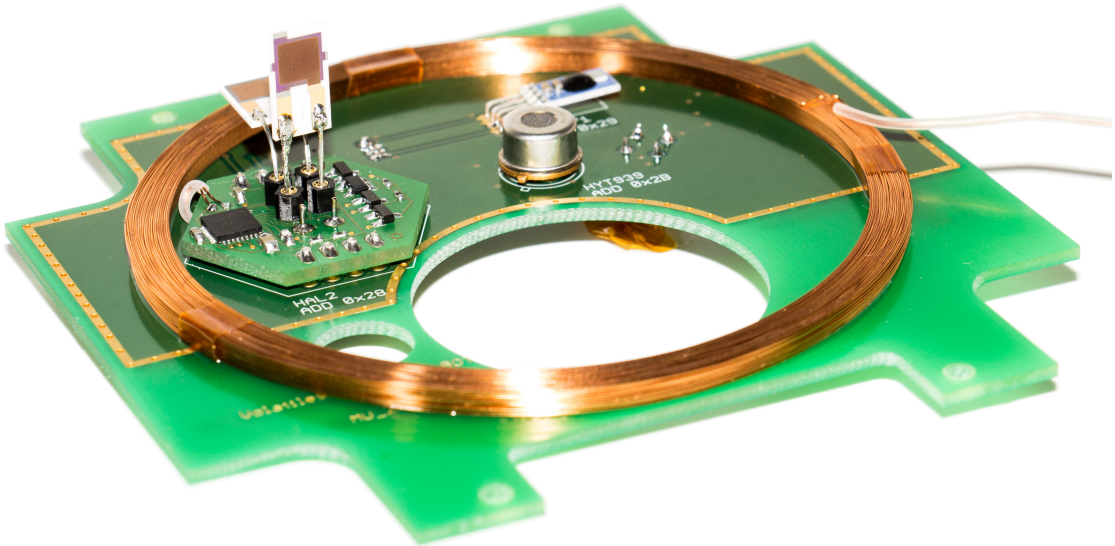

Fig. 7.1: Volatiles board

7.1 Water in Space

The Earth is one of extremely rare and special places in the Universe where water can stably exist as a liquid. Water and its vapour are also one of the main constituents gases of the Earth's atmosphere. It therefore has a large share of the total atmospheric pressure. This Pressure (P) can be expressed, according to Dalton's law, as the sum of partial pressures (7.1).

$$P_{\text{total}} = P_{N_2} + P_{O_2} + P_{H_2O} + P_{\text{other gases}} \tag{7.1}$$

If the total system pressure is changed by compression or expansion, each of partial components will changed the pressure by a similar factor to P_{total}. With increasing altitude the overall pressure decreases, and thus the partial pressure of the individual constituents. If there's not enough force for pressing the water into a liquid phase, then there's no force binding the water molecules together. If the pressure decrease further, water molecules will evaporate and diffuse away. This change of state from liquid to gas happens only as change in pressure, but not in the temperature, which is constant.

Laws of thermodynamics describes this issue which contends the phase diagram for any materials.

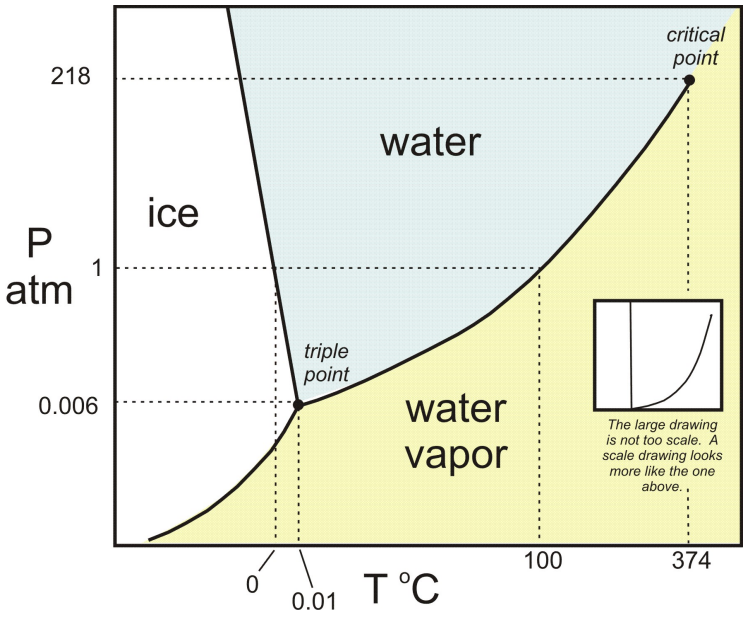

Fig. 7.2: Water phase diagram [21]

In the vacuum, the pressure is equal to basically zero. With regard to this diagram (Fig. 6.3), in a vacuum, most liquids have such a low boiling point that they vaporize almost instantly. But one of things what we know about space that it is the coldest which means that, water should to get frozen not evaporate. In reality, the effect of boiling is much faster than the effect of freezing. Water molecules from material will first evaporate and next the vapour passes immediately into the solid state. This type of change, directly from gas to solid material, is called *desublimation*. For that reason, most substances exist in space in either the gaseous or the solid state.

This cloud of very fine crystals of frozen water is very dangerous for the whole satellite.

8 Humidity Sensors

Humidity sensors have gained an increased number of applications in industrial processing and environmental control. There are many domestic applications, such as intelligent control of the living environment in buildings. In generally industry, humidity sensors are used for humidity control in dryers, ovens and in storage. Humidity control is also important in many industrial processes as is semiconductor industry, etc.

There are many possibilities for a measurement of humidity. Each of them has advantages and disadvantages, applications in each field require different operating conditions.

8.1 HYT Sensors

HYT sensors are a kind of Humidity and Temperatures modules from IST s.r.o. company. These sensors have a digital interface and they are calibrated already in the production. This kind of sensors is mechanically robust and has chemical and condensed water proof sensing area.

(a) HYT 271 (b) HYT 939

Fig. 8.1: Used type of HYT sensors

8.1.1 HYT 271 and HYT 939

HYT 271 and HYT 939 are capacitive polymer humidity sensors with digital interface. These sensor types have integrated signal processing in the module. Integrated electronics completely processes the measured data, corrects linearity error and temperature drift through "OnChip" computation and directly transmit the parameters of relative humidity and temperature as digital values.

For integration with a micro-controller, the humidity module uses an Inter-Integrated Circuit (I^2C) compatible interface which supports both standardised speeds 100 kHz and faster 400 kHz. Sensors also have low power consumption about 22 µA during operation [22].

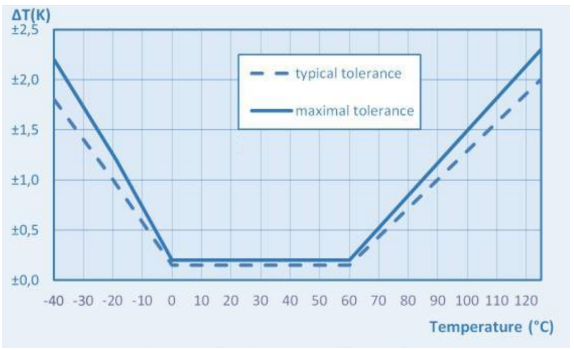

(a) Typical and maximal tolerance for temperature sensor

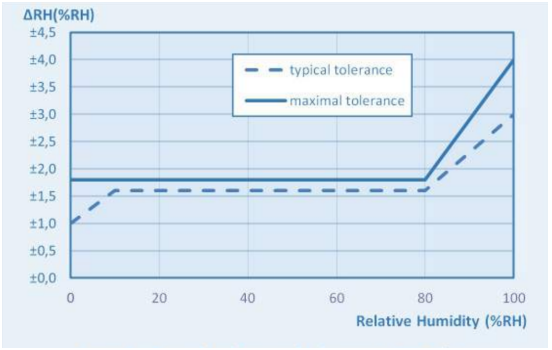

(b) Typical and maximal tolerance at 23°C for relative humidity

Fig. 8.2: HYT characteristics [22]

Tab. 8.1: HYT sensor's parameters [22]

Properties	HYT 271	HYT 939
Temperature measuring range	-40 ... 125 °C	-40 ... 125 °C
Temperature accuracy	± 0.2 °C	± 0.2 °C
Humidity measuring range	0 ... 100 %	0 ... 100 %
Humidity accuracy	± 1.8 %	± 1.8 %
Humidity resolution	± 0.03 %	± 0.2 %
Humidity response time	< 4 s	< 10 s
Resolution	14 bits	14 bits
Operating voltage	2.7 . . . 5.5 V	2.7 . . . 5.5 V
Normal operation	< 22 µA	< 22 µA
Sleep mode	< 1 µA	< 1 µA

8.1.2 Address Changing

All HYT sensors have been programmed with default slave address **0x28**. It is necessary to change this address if more of these sensors should work on the same bus. Address can be adjusted in the address range for 7 bits addresses (0x00 to 0x7F). The 8th bit is Read/Write bit. Therefore, up to 128 sensors can operate on the same bus.

For a change of address the module must be switched to *Command-Mode*. The switching is performed by sending the `start-command-mode` message **0xA0**. This command must be send within 10 ms after reset/power on. Each message in *command-mode* is 4 bytes long.

Code 8.1: Example of address changing

```
#include "Wire.h"
#define OldAddress 0x28
#define NewAddress 0x42
int power = 2;                              // Power port
void setup() {pinMode(power, OUTPUT);}      // I/O setting
void loop(){                                // Main loop
  digitalWrite(power, HIGH);                // Sensor power ON
  Wire.beginTransmission(OldAddress);       // Start Command mode
  Wire.write(0xA0);
  Wire.write(0x00);
  Wire.write(0x00);
  Wire.endTransmission();
  Wire.beginTransmission(OldAddress);       // Address changing
  Wire.write(0x5C);
  Wire.write(0x00);
  Wire.write(NewAddress);
  Wire.endTransmission();
  Wire.beginTransmission(OldAddress);       //Set Normal mode
  Wire.write(0x80);
  Wire.write(0x00);
  Wire.write(0x00);
  Wire.endTransmission();
  digitalWrite(power, LOW);                 // Sensor power OFF
  while (1){}
}
```

Change of address was conducted on the Arduino Duemilanove. Arduino Duemilanove is a microcontroller board based on the ATmega328. Code 8.1 is written for this development kit. Digital output 2, power port, switch power supply to the sensor. This step ensures the fulfillment of the 10 ms conditions for switching to the *Command-Mode*.

To verify a successful change of address or to check the attached sensors, it is recommend to use I^2C bus scanner (Code 8.2).

Code 8.2: Example of I^2C bus scanner

```
#include "Wire.h"
int power = 2;                                  // Power port
void setup()                                    // I/O setting
{
   pinMode(power, OUTPUT);
   Wire.begin();
   Serial.begin(57600);
}

void loop()                                                 // Main loop
{
   digitalWrite(power, HIGH);                               // Power ON
   Serial.println("Scanning in range 0x00 - 0x7F...");      // Scanning
   for (uint8_t add = 0X0; add < 0X80; add++) {
      Wire.requestFrom(add, (uint8_t)1);
         if (Wire.available()) {
               Serial.print("Device found at: ");
               Serial.println(add, HEX);
         }
   }
  digitalWrite(power, LOW);                                 // Power OFF
  Serial.println("Done...");
  while (1){}
}
```

8.1.3 Value Reading

The most of the time sensors are in sleep mode to minimise the current consumption. New measurement starts after command Measurement request (MR) is received. This MR command terminates the sleep mode and module starts the measurement cycle.

The measurement cycle begins with the temperature measurement and continues with humidity measurement. After that follows Digital Signal Processing such as linearising and temperature compensation. After the measurement cycle has been completely done, the measured and processed values are made available in outputs registers.

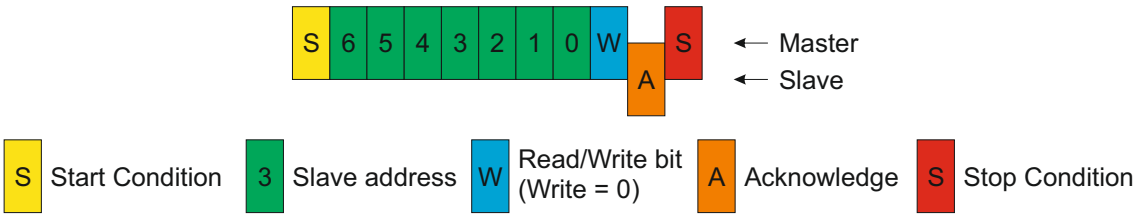

Fig. 8.3: Measuring request

The MR command begins by Start condition and the address of HYT module with last Read/Write bit set to 0 (Write). The sensor sends Acknowledge (ACK) as an answer to inform that the measurement has started. Master terminates the communication with Stop condition. This description is shown in Fig. 8.3.

Data values are read from output registers using Data Fetch (DF). This command is send with Read/Write bit as 1 (Read). Master can read up to four bytes of measured data after ACK. The first two data bytes contain the humidity value in 14 bit resolution and two status bits. These status bits are transferred in the first byte as Most significant bit (MSB). Second two bytes contain temperature in 14 bits resolution, the last two bits are not used and should be masked away. Master terminates the communication by No-Acknowledge (NACK). This data fetching is shown in Fig. 8.4.

This response can be send after each of bytes. Therefore, it is possible to read only humidity values or complete relative humidity with temperature in 8-bit resolution. [22]

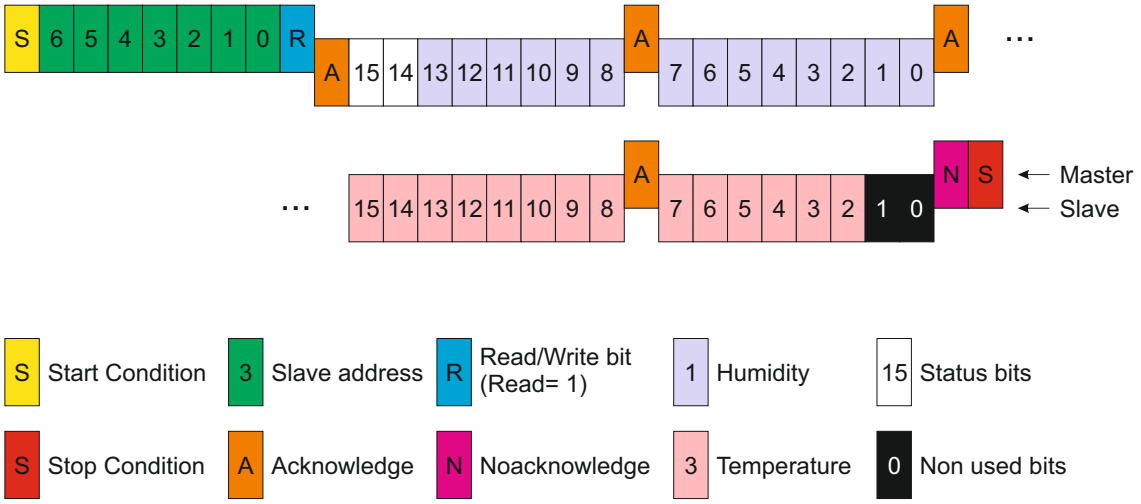

Fig. 8.4: Data fetch

8.1.4 Temperature

One of the most significant measurements on the probe is gaining of the temperature. Not only due to determine the temperature but also its influence to the surrounding sensors and other measured values.

As was mentioned above, temperature values are gained from HYT sensors as 3^{th} and 4^{th} read bytes. That is 16 bits value but real temperature has only 14 bits resolution. Which means, that this value has to be modified and recalculated to temperature in degrees of Celsius according to (8.1).

$$T(\text{°C}) = \frac{165}{2^{14}-1} T_{raw} - 40 \tag{8.1}$$

Example of temperature recalculation is in the Code 8.3. It is according to equation (8.1) and communication process in Fig. 8.4.

Code 8.3: HYT temperatures

```
...
Traw  =  (raw[2] << 6) | (raw[3] >> 2);
Temp  =  (165/(pow(2,14)-1))*Traw-40;
...
```

8.1.5 Relative Humidity

Relative humidity is generally defined as the ratio of the actual vapour pressure to saturation vapour pressure over a plane liquid water surface at the same temperature (8.2)

$$RH(\%) = \frac{P_v}{P_{sv}} 100\,\% \tag{8.2}$$

where P_{v} is Actual vapour pressure and P_{sv} is Saturation vapour pressure. [10]

The relative humidity is highly dependent on the temperature. It is because, the pressure could change with temperature and in the equation for calculating of Relative humidity (RH), it is actually twice (8.2). That is the reason, why the temperature must be measured in the same time. This temperature drift and linearity error are corrected directly on chip in sensor.

$$RH(\%) = \frac{100}{2^{14} - 1} H_{raw} \tag{8.3}$$

Relative humidity value is saved in first two read bytes from the sensor. This value is as well as in previous case in 14 bits resolution as is shown in Fig. 8.4.

First two MSBs are status bits. These bits are masked and resultant value is scaled into physical measurement units according to (8.3). This procedure is implemented in Code 8.4.

Code 8.4: HYT humidity

```
...
Hraw = (raw[0] << 8) | raw[1];
Hraw = (Hraw &= 0x3FFF);
Relative_humidity = (100/(pow(2,14)-1))*Hraw;
...
```

8.1.6 Dew Point

Dew point (DP) is the temperature at which the moisture in the air forms visible drops of water.

Technically, it is the temperature at which the water vapour in a sample of air at constant barometric pressure condenses into liquid water at the same rate at which it evaporates.

There are bonds among the conversion of Relative humidity, Temperature and Dew point temperature.

P_{sv} means Saturation vapour pressure and it computes pressure of vapour steam in the air. Constants A, B, C depend on measured Temperature (T). When T is less than zero degrees of Celsius, these constants are in Tab. 8.2.

$$P_{sv} = Ae^{\frac{B \cdot T}{C+T}} \tag{8.4}$$

Tab. 8.2: Constants for computing dew point [9]

Constants	$T < 0$	$T > 0$
A	610.714	610.78
B	22.44294	17.08085
C	272.44	234.175

By using equations (8.5,8.6) the Dew point of water vapour is computed. Equation (8.6) depends on value of LENKO! (PP) from (8.5). When PP is less than 610.714 (same value as A(T<0)), constants A, B, C match by first column in Tab. 8.2 (T<0), otherwise to the second. [9]

$$PP = \frac{Hum}{100} \cdot P_{sv} \tag{8.5}$$

$$DP = \frac{C \ln \frac{PP}{A}}{B - \ln \frac{PP}{A}} \tag{8.6}$$

This conversion can be implemented into the Matlab as a following Code 8.5.

Code 8.5: Calculation of the Dew point [9]

```
A = [610.714, 610.78];
B = [22.44294, 17.08085];
C = [272.44, 234.175];

for i=1:length(C10)
        if Temp(i) < 0
         Psv(i) = A(1) * exp(B(1) * Temp(i)/(C(1) + Temp(i)));
        else
         Psv(i) = A(2) * exp(B(2) * Temp(i)/(C(2) + Temp(i)));
        end
end
PP = 0.01 * Hum .* Psv';
for i=1:length(C10)
```

```
        if PP(i) < 610.78
                DP(i) = C(1) / (B(1) / log(PP(i) / A(1)) - 1);
        else
                DP(i) = C(2) / (B(2) / log(PP(i) / A(2)) - 1);
        end
end
```

8.2 HAL2 Sensors

HAL2 sensors are the type of Aluminium oxide (Al_2O_3) moisture sensors. The present Al_2O_3 sensors are usually fabricated through anodization. This process is easy and performed at low voltage (<100 V), thus it is also low cost. Low voltage anodization forms Al_2O_3 layer consisting of hexagonal cylindrical pores perpendicular to the surface (Fig. 8.5). That applies in case this process is preformed in acidic electrolyte in unchanging conditions. They are always characterized by long term period of anodization at a constant voltage. [29]

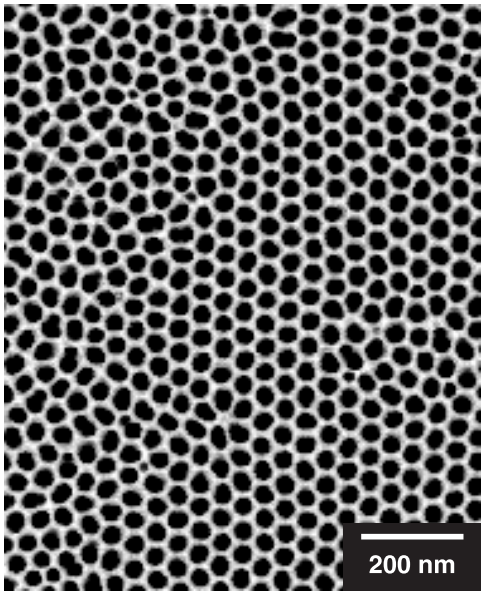

Fig. 8.5: Honeycomb structure of anodic aluminium oxide [29]

8.2.1 Construction

These sensors have three layer structure. The basic aluminium layer is applied on the small corundum ceramic plate. This plate is only supporting substrate. On the bottom aluminium electrode is porous Al_2O_3 film. A thin coating of gold is applied above the Aluminium oxide layer by means of sputter deposition like water permeable top electrode. Schematic view of HAL2 structure is shown in Fig. 8.6.

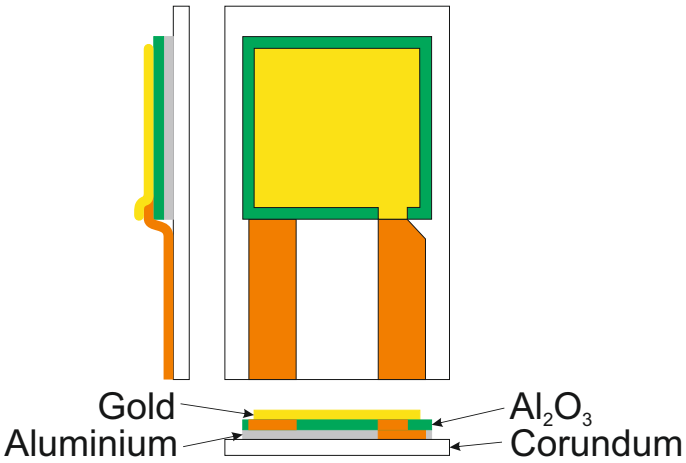

Fig. 8.6: Structure of HAL2 sensors

Basically it is like a capacitor. Structure of this capacitor consists of a aluminium bottom electrode, a dielectric from an anodized porous Al_2O_3 film and a thin water permeable gold top electrode.

When the water vapour is transported through the gold layer, a change of the Al_2O_3 permittivity occurs. Hence, the capacity of sensor is changed as well as its conductivity.

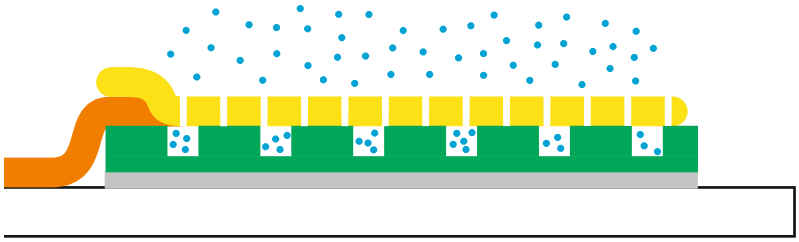

Fig. 8.7: Principle of HAL2 sensors

8.3 Capacitance Measuring by PCap02A

PCap02A is from PicoCap® family and is used to measuring especially of a small capacitances. To the chip is able to connect up to 8 capacitors in grounded mode or up to 4 capacitors in floating mode. One of them is usually used as reference. Device is using *discharge time measurement* to determinate capacitance which is called Capacitance to digital converter (CDC). In case of requirement of measurement temperature dependences of capacitance at same conditions, the chip has also temperature measurement unit called Resistance to digital converter (RDC). PCap02A has integrated DSP unit for processing of capacitances and temperature. The controller could be connected to the other device using Serial peripheral interface (SPI) or I^{2}C bus. In the following Tab. 8.3 are picked up some important properties of PCap02A.

Tab. 8.3: PCap02A parameters [23]

Properties	Values	Notes
Operating voltage	2.1 . . . 3.6 V	
Current consumption	$< 2.5\,\mu$A	At 2.5 Hz with 13.1 bit resolution
Output ration	0 . . . $\approx$ 8	Measurement value to reference
Resolution	24 bits	
Temperature range	−40 ... +125 °C	
I^{2}C bus frequency	100 kHz	
SPI bus frequency	20 MHz	

In the Fig. 8.8 is basic circuit of the PCap02A chip with voltage converter on I^{2}C bus. The power supply of the chip is up to 3.6 V, but input power has 5 V. So it is necessary to convert voltage down using low drop step down regulator.

In the Fig. 8.9 is shown PCB of previous mentioned circuit with PCap02A. At the top of picture is located communication connector with power supply. In the middle of board is placed six holes for three measured capacitors, two holes for each.

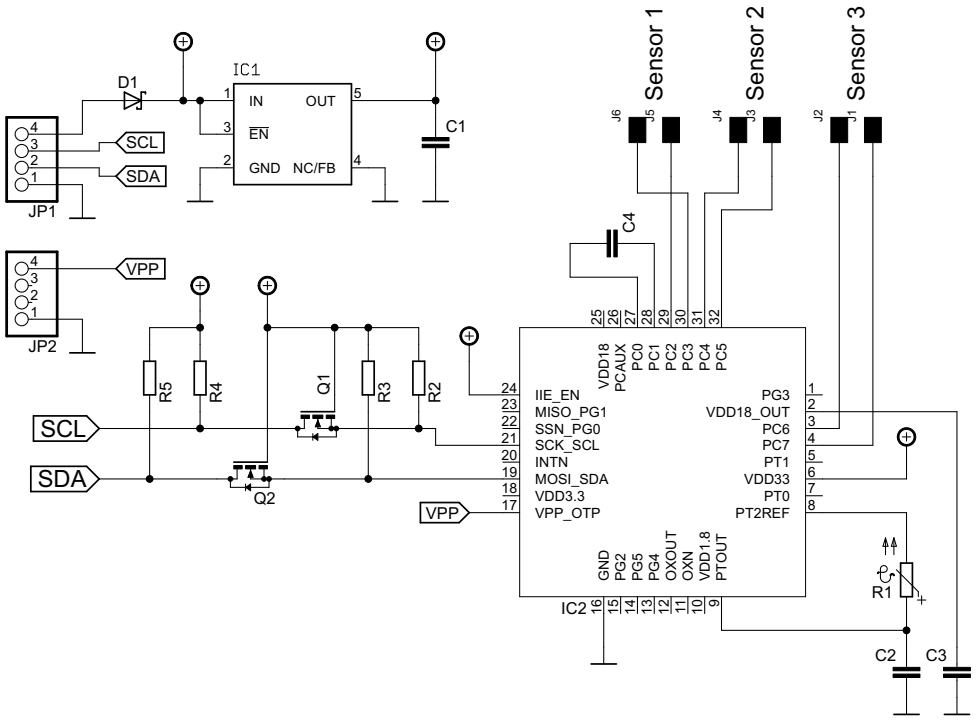

Fig. 8.8: Schematic of board for HAL2 sensors

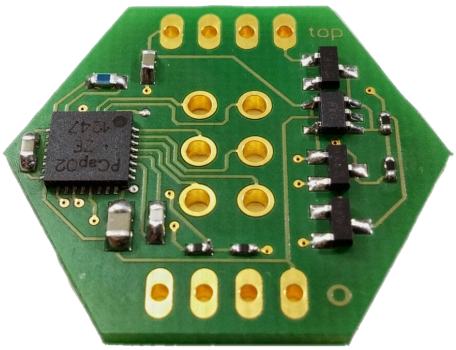

Fig. 8.9: Board for HAL2 sensors

8.3.1 Capacitance Measurement

The capacitors can be connected in four different circuits and with different maximum number of capacitors. These circuits can be seen in Fig. 8.10.

The basic connection *single grounded mode* can have up to 7 capacitors and one

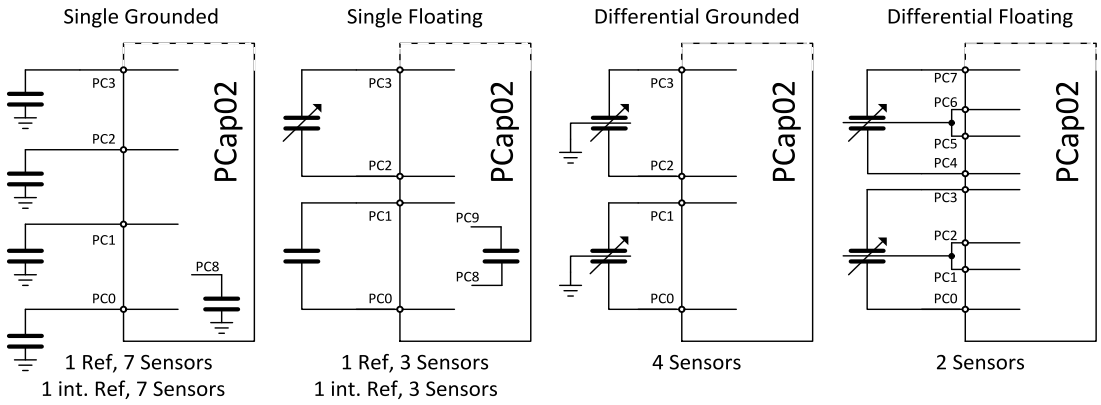

Fig. 8.10: Capacitors connection

reference, where one side of them is connected to the ground and second one is to the chip, port PCx.

Next is *single floating mode*, can has up to four capacitors connected, which one of them is reference. Using this method has advantageous, that current do not flow through the ground and resultant capacitance is not affected by interference from other devices over ground as in previous case.

The *differential methods* are using to gain ratio of capacitances, for example in accelerometers which has interdigital structure (two capacitors with one common electrode) to determinate acceleration.

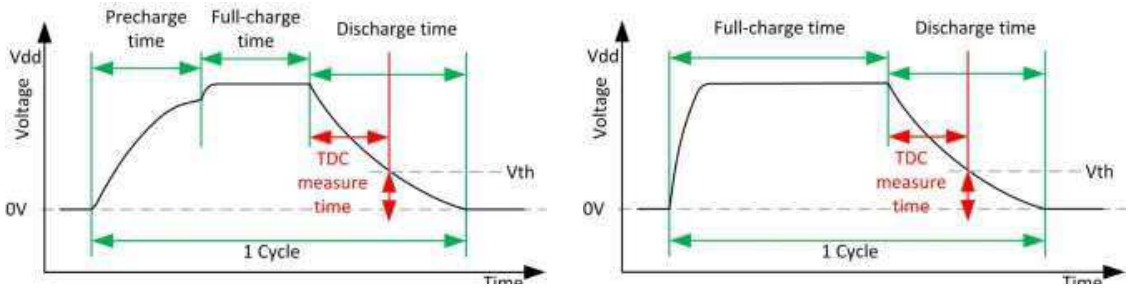

(a) Pre-charge cycle

(b) Fast-charge cycle

Fig. 8.11: Cycles of measuring capacity in PCap02A

Capacitance measurement is based on Time to digital converter (TDC) and is divided into two or three steps. First step is pre-charge where capacitor is charged through the serial resistor to reduce current where this condition is necessary. The required is for example in MEMS devices.

Second step is full-charge where measured capacitor is charged to the power supply without serial resistor to reduce current.

Last step is discharge of the capacitor. During this step is measured discharge time as in Fig. 8.11, where can seen difference between pre-charge mode and fast-charge mode. The fast-charge mode has omitted pre-charge step and has only full-charge and discharge step.

Measurement time is counted from fully charged capacitor to the predefined threshold voltage.

Resultant ratio is computed from this time and time of reference capacitor. When is known reference capacitance, it is possible calculate measured capacity. Requirements for reference capacity should has high temperature stability, that do not affect measurements.

8.3.2 Temperature Measurement

Temperature measurement is similar to the capacitance measurement. Different measured parameter is resistance instead of capacitance. It is required to add externally one 10 nF capacitor.

For measuring temperature could be used internal aluminium thermistor or up to three external sensors (PT0 – PT2), for example PT1000. Input PT0 could be used as reference alternately. Also as reference can be used internal Poly-Si with temperature dependence close to zero.

Resultant ratio can be determinate from internal Poly-Si reference or external. During operation could be switched. Also can be mixed external and internal thermometers.

8.3.3 Value Reading

Measured values are stored in many registers. Every result has three resultant bytes with own ratio in range from 0 to 7.9999995, where first three bits are digit part and last 21 bits is decimal part of number. From this point of view is enough to read first byte or two, but for more precision is possible to transfer all three bytes. To read data from PCap02A is used I^2C bus altogether with HYT sensors.

8.3.4 Communication with PCap02A

Communication with PCap02A has a few commands. Namely: *Initialize*, *CDC Start Measurement*, *Write Data to SRAM* and next.

First what is needed to send to the chip is *Initialize*. It has operation code `0x8A`

in hexadecimal form. When PCap02A do not have programmed internal one time programmable memory with program, it is necessary to send it. Communication of writing program to internal SRAM is according to following diagram Fig. 8.12 and analysed signal Fig. 8.16.

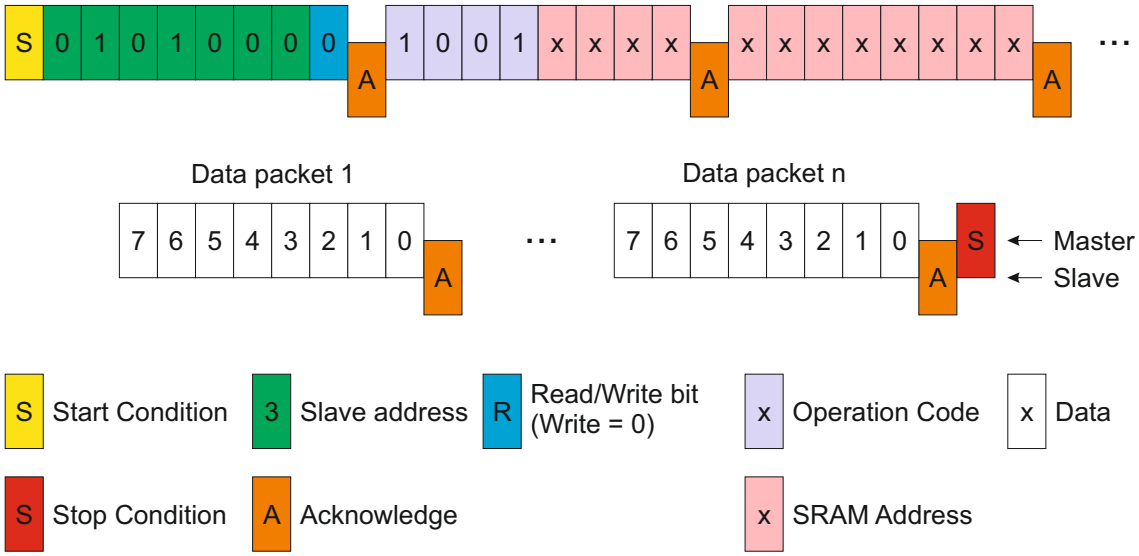

Fig. 8.12: Write program to SRAM to the PCap02A

After slave address follows four bits (light blue boxes) which according to operation code. Next 12 bits (pink boxes) represents address position of internal SRAM which is automatically incremented with incoming data.

Third thing is necessary to send configurations parameters. These are saved in 78 registers. For simplification and right configuration are sent all registers except the last one, where is stored run bit. Operation code of write configuration has 9 bits and it begins by `0xC0` then follows one more zero and 7 bits which represents configuration register.

To start measurement chip has start CDC command with operation code `0x8C`. When results are ready to read it, here are 45 output registers for all measured data including status. Reading process is illustrated in the following diagram Fig. 8.14.

Read results command has 7 bits (up to 128) to set beginning position of register. Usually are read all 45 bytes, but it is not necessary when is important only for example one value. Internal pointer of result is automatically incremented as in previous case, write to SRAM.

For simplification in our case are read all registers and then picked up only important ones.

8.3.5 Connection Testing

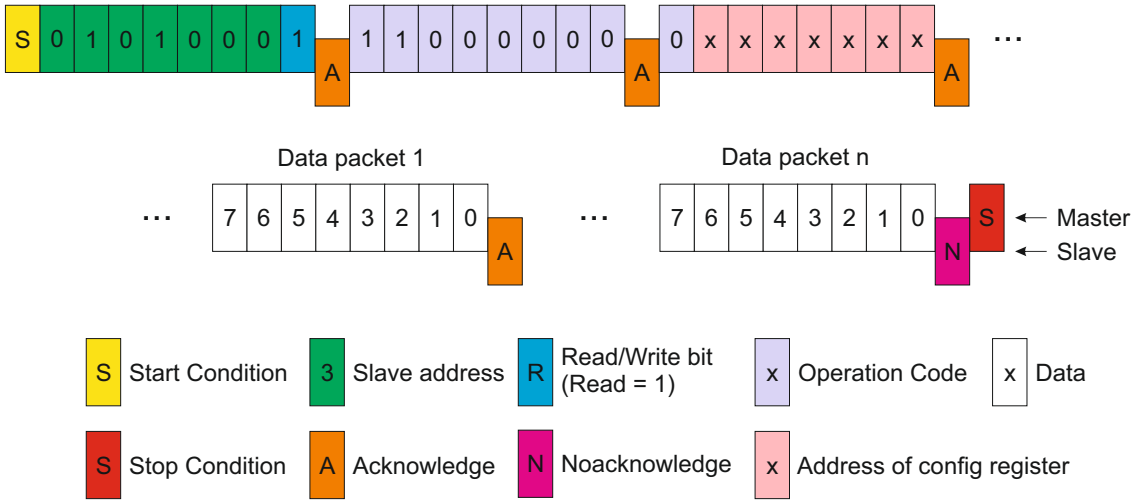

Fig. 8.13: Write configuration to the PCap02A

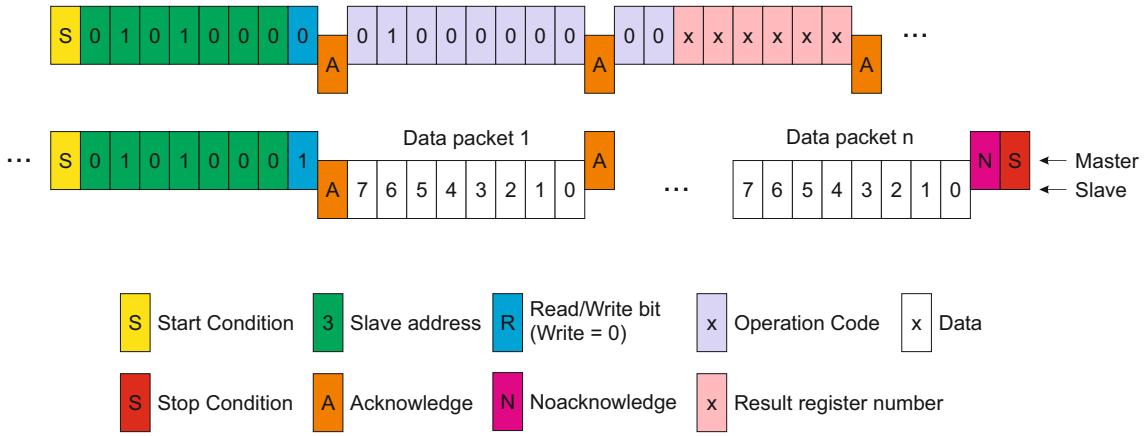

Fig. 8.14: Read results from PCap02A

Communication with PCap02A was tested very first with MBED development kit. It is an easy programmable kit with powerful core. To verify connection was used digital analyser, because at beginning implementing were problems with communication and right configuration of the chip. Finally problem was solved and PCap02A communicate very well. In the following screenshots of the analyser could be seen initialization sequence in Fig. 8.15 and on the second one is write program to the internal SRAM in Fig. 8.16.

jss

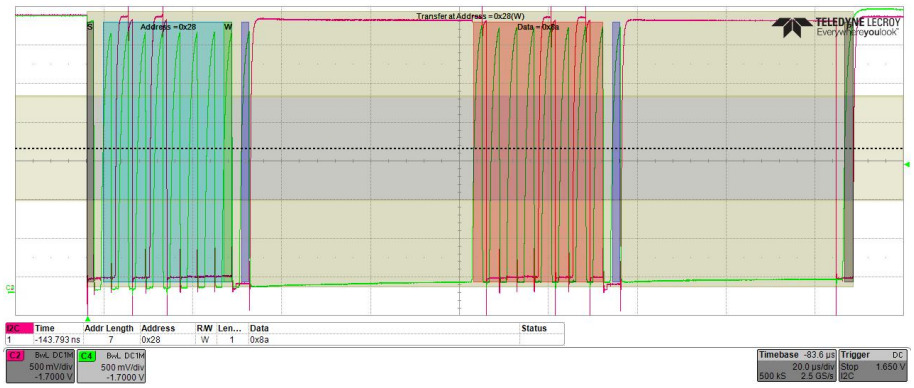

Fig. 8.15: Analysed communication with PCap02A - Initialize

Fig. 8.16: Analysed communication with PCap02A - Write to SRAM

9 Volatiles board

Sensors for humidity and temperature measurement are being on Volatiles board. Volatiles measurement is not standardized for CubeSat, therefore was PCB designed and made directly for use on VZLUSat–1. Drawings of the board is on the following Fig. 9.1.

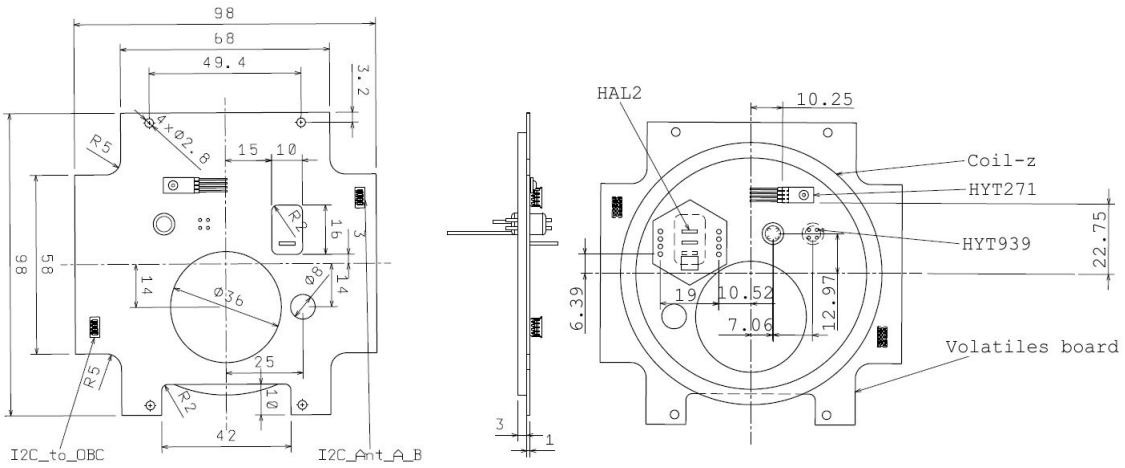

Fig. 9.1: Drawings of Volatiles board

9.1 I²C Interface

Communication on Volatiles board is ensured by Inter-Integrated Circuit (I^2C) interface. This bus was chosen with regards to common communication interface for all sensors on board.

This second I^2C bus is running from On Board Computer through the board with humidity sensors to the radio and the second magnetometer. The first one goes from OBC through others payloads as main communication bus.

Generally, the I^2C bus is consists of two wires Serial data (SDA) and Serial clock (SCL) with common ground. These wires are shared for all devices as shown in Fig. 9.2.

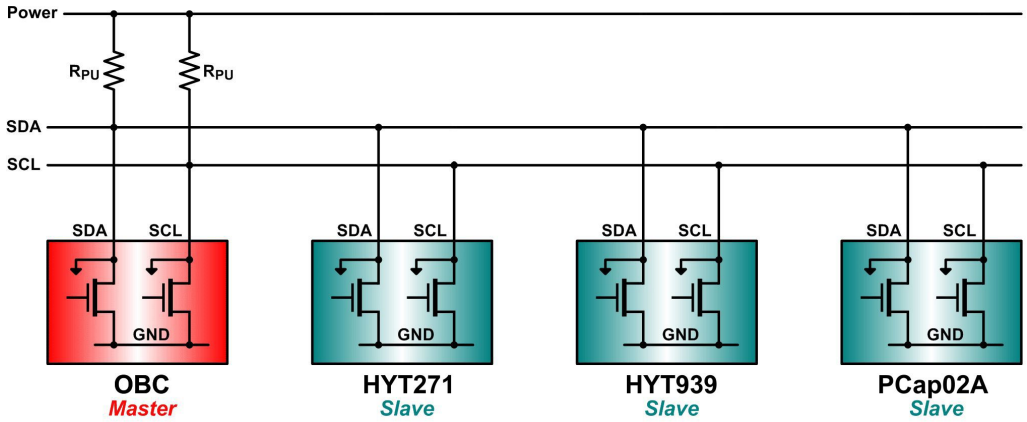

Fig. 9.2: Schematic of I^{2}C connection - edit from [30]

This bus can works as singlemaster or multimaster. This bus is connected as singlemaster and has only one master device. The multimaster type can connect several devices of master or slave type. Master devices control communication, create start and stop condition and generate a clock signal and must listen to the bus before starting of communication to prevent collision with other masters.

When bus is idle, positive voltages are on SDA and SCL wires. Communications starts with start condition by master, a falling edge on the SDA line when SCL is still in logic 1. Generally, follows 7-bits address, this means, that on one bus can be theoretically connected up tu 128 devices. The address has to be unique for each device. The last eight bit of this byte is *Read/Write bit*, which determinates following action, reading (high) or writing (low). Each byte is acknowledged by ACK. After this initialisation procedure can starts data transfer. The direction of the following byte or bytes transmitted, from master to slave or conversely, depends on the *Read/Write bit*. Right value of bits are transferred with the rising edge of SCL. When transmission is ending, master sends NACK bit instead of ACK and after that communication is terminated by stop condition, a rising edge on the SDA while SCL is in high.

Data bytes are transmitted on SDA line, for the conditions, that the change of the Serial data line can be realize with consider on Serial clock which has to be in logical 0. Communication via I^{2}C is illustrated in Fig. 9.3.

Because the SCL is always made as open collector, can be set on low level even if other device tries to set high level. This property is used, when some device is slow and do not managed the communication.

Open collector requires pull-up resistors connected between power supply and wires SDA and SCL. These resistor ensure high level on bus also in the time when

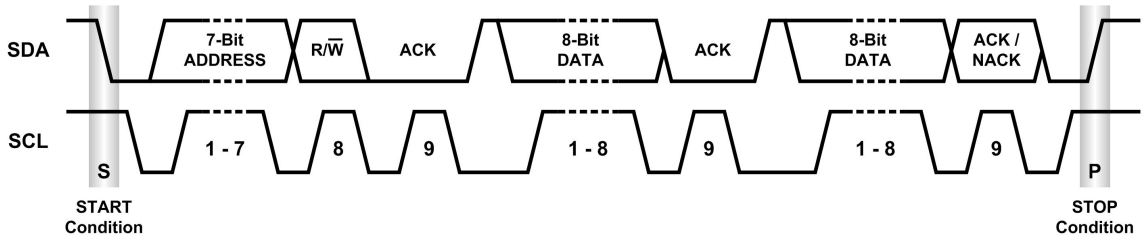

Fig. 9.3: Chart with communication via I^2C [30]

bus is idle. In this case, resistors are not located directly on Volatiles board but they are placed on OBC board where is also the same bus connected.

9.2 PCB Design

Of course, sensors and other devices require power supply as well. This mean that although for I^2C are needed only two wires (SDA and SCL) for correct function of the whole system are required at least four conductors. This minimum of wires is enough for every used components, therefore is wired four conductors bus over the Volatiles board.

With regard to Volatiles board location is needed to consider EMC radiation. This radiation can interfere to others payloads. On neighbouring board is, for example, very sensitive analogue cascade amplifier which can be as victim.

This disruption can be minimized by correct principles and rules of PCB design. In the following sections are listed some of them.

9.2.1 Spilled Copper

Before starts to design the PCB it is necessary to choose how many layers should the board have. In this case it is the simple circuit, thus there are not a large demandingness for space.

On this board is only one I^2C bus and some sensors, for all of that is enough dimensions of one side of board. But according the Fig. 9.1 are some sensors from top and others from bottom side of the board. With regarding to crosstalk and radiation from board is this solution of design not advantageous.

One of the factors which affect the radiation is size of current loop. It is recommend to make it a small is possible to reduce the radiation, voltage peaks, current peaks ...

In Fig. 9.4a is shown area of loop for case where is ground and signal wired as

single conductor on one side of the board. This area of loop is remarkable larger than in Fig. 9.4b, where is used spilled copper layer for common ground at one side of PCB. Loop area is in this case remarkable smaller because is made up only of Height of PCB (H) and length of signal wire.

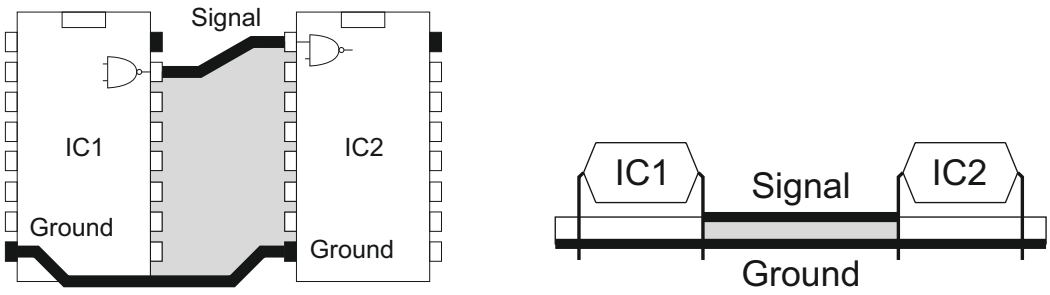

(a) Ground as a wire (b) Ground as a layer

Fig. 9.4: Area of current loop

9.2.2 Longitudinal Radiation

For minimize longitudinal radiation is important to have crossover of power or signal layer over the ground layer.

In the case, that the both layer have the same dimension , the longitudinal radiation is maximum as in Fig. 9.5a. To reduce of radiation close loop of electric field to the ground layer (spilled copper). Enough crossover for this situation has to be at least twenty-times higher than the H. This case is shown in the Fig. 9.5b. Standard double sided PCB with $H = 1.5\,\text{mm}$ the crossover should be at least 3 cm, which is too much. With regarding to this property is used adjustment which is represented in Fig. 9.5c. There is whole board encircled by 1 mm width wire ring with regular vias placement to ground. [33]

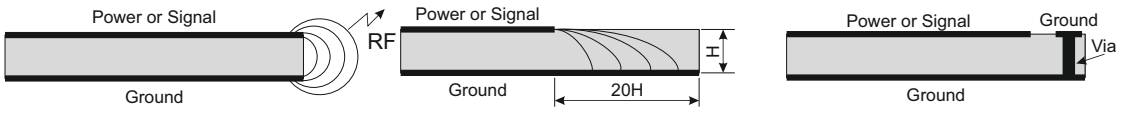

(a) Board without crossover (b) Rule of 20H (c) Board with ring

Fig. 9.5: Longitudinal radiation

9.2.3 Radiation Emission

In case of parallel conductors leading, when one is closer to the other, appears crosstalk. This mean, that signal from one wire can be measured on the other which is not connected to the same path.

These crosstalks and interferences are caused by parasitic capacity C_p of the signal way. Because the $\mathrm{I}^2\mathrm{C}$ bus is a voltage bus, thus the information is transmitted by voltage level change. Combination of this Parasitic capacity (C_p) between wires and speed of time change of voltage generates parasitic noisy current I_n (9.1).

$$I_n = C_p \frac{dU}{dt} \tag{9.1}$$

Due to this equation (9.1) is I_n raising in depends on raising C_p or slew rate of signal. This disturbing can be minimized by decreasing of slew rate, which is set by communication speed. Other way is decreasing C_p or if is possible to decrease bus voltage.

Parasitic capacity depends on Permittivity of vacuum (ε_0), Relative permittivity (ε_r), cross section of longitudinal cut and distance of wires. It is similar to capacitance of plain capacitor (9.2).

$$C_p = \epsilon_0 \cdot \epsilon_r \cdot \frac{S}{l} \tag{9.2}$$

where S is Dimension of capacitor boards and l is Distance of capacitor boards. For standard PCB core of type FR4 is $\varepsilon_r = 4.7$.

In this case, the capacitance can be reduced only by distance between wires. For sufficient attenuation of crosstalk is length l too high. Hence, there are added protective parallel wires. These wires enclose each of the critical signal wire and they are connected to ground layer at many places by vias. This way is created conductor which is behaves slight like coaxial cable, it decrease the radiation level of wires and risk of crosstalk [33].

9.2.4 Final Design

For final design of the Volatiles board is considering all features which are mentioned above. On the top side of board is spilled copper as power layer with signal paths. Each signal path is enclosed by parallel grounded wires which create coaxial cable. This edit allow decrease the crosstalk. Whole circuit design is encircuited by ground ring with vias, which minimize longitudinal radiation. This ring is connected to bottom spilled ground layer.

All these improvements contribute to the better electromagnetic susceptibility and the lower electromagnetic interference.

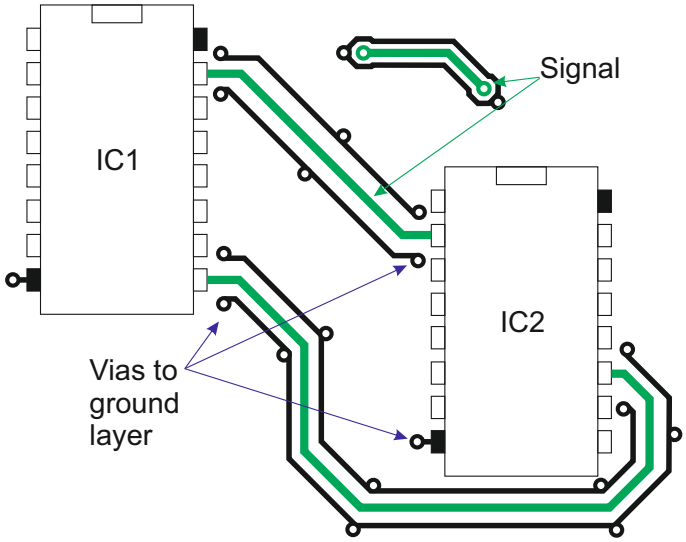

Fig. 9.6: Example of coaxial cable on PCB

According to Fig. 9.1 are sensors located at both side of board. After first probe composing has to been made some changes in placement of other components. Final component placement is in the Fig. 9.7.

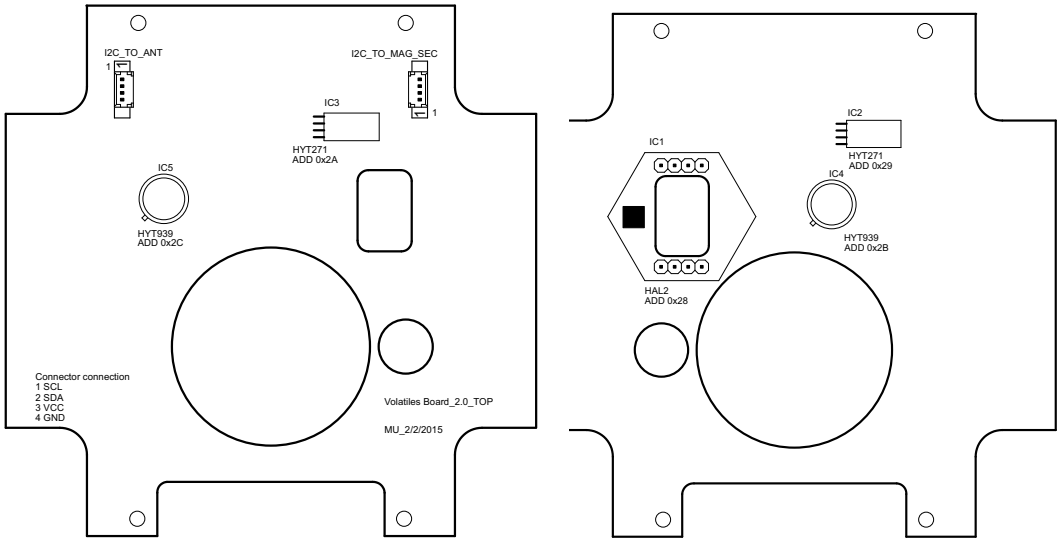

(a) Top side (b) Bottom side

Fig. 9.7: Component placement of Volatiles board

From each side of board is placed one from pair of HYT modules and one from three of HAL2 sensors. The active layer of third HAL2 is takeout from probe.

On the board are located two four-pins connectors as well. First *I2C_TO_ANT* is input connector from radio board respective from OBC. Second connector with name *I2C_TO_MAG_SEC* is plugged in to the second magnetometer on the same I^{2}C bus, first one is on OBC board.

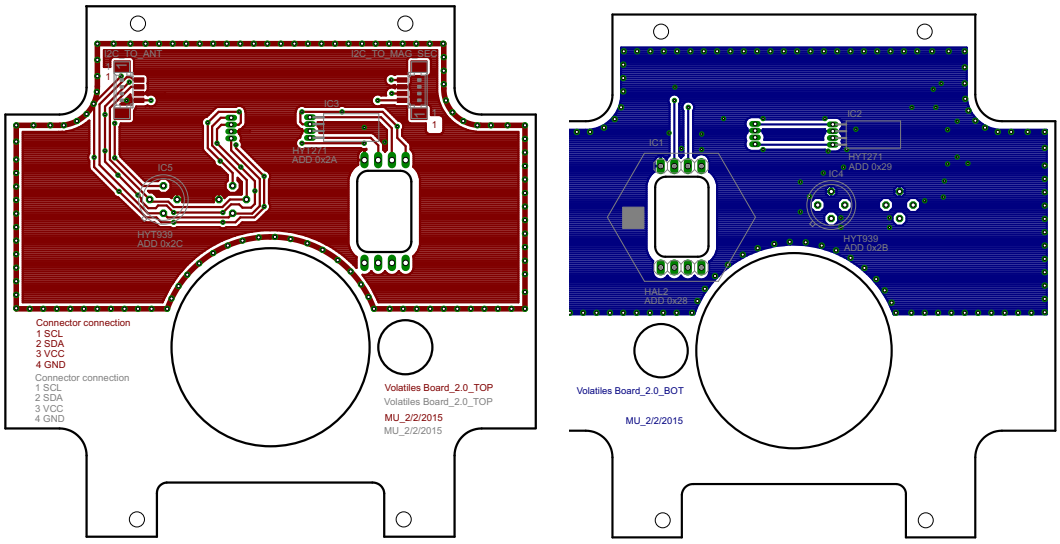

(a) Top side (b) Bottom side

Fig. 9.8: Complete design of Volatiles board

Each of HAL2 sensors has a thermometer PT1000. One of them is evaluated by PCap02A (more information about it is in the section 8.3.2 Temperature Measurement) and others around Measure board (see 3.2 Experiments).

Pull-up resistors (R_{PU}) for I^{2}C bus are not located on Volatiles board, they are placed on OBC board and connected between power supply and SDA respective SCL line. There are not placed addition blocking capacitor as well. This capacitors are integrated directly in HYT sensors, board for HAL2 sensors has own additional power converter with these capacitors (Fig. 8.8).

Volatiles board has also glued coil. This coil is one of six others coils in the probe, which are ensuring stabilization of the nanosatellite, with help of Earth's magnetic field, because the CubeSat has not allowed to use an active engines.

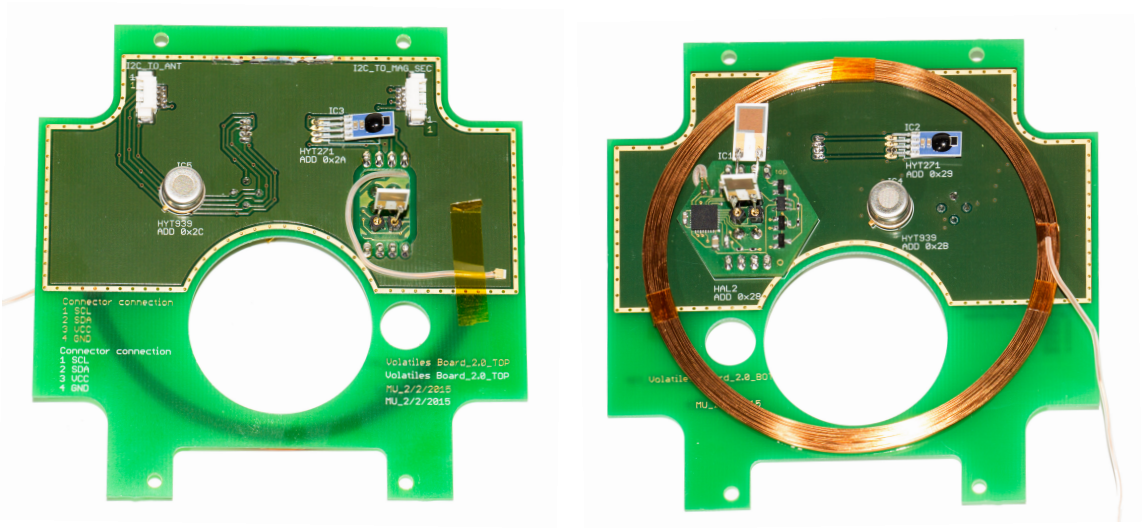

(a) Top side

(b) Bottom side

Fig. 9.9: Photo of Volatiles board

10 Calibration

Every sensors, which are on probe board have to be calibrated before using in space. All sensors with the aim of measurement the outgassing of part of the VZLUSat–1 satellite in space. There are two HYT 939, two HYT 271 and three HAL2 sensors on Volatiles board, in this case. As was mentioned, HYT sensors communicate via I^2C and HAL2 sensors are connected to board with PCap02A (see 8.3). This board is communicate via I^2C as well.

Calibration has to be done before complementation of probe and definitely before launching probe to the space.

Without this procedure it would be measured some data but it will be not possible to exactly determinate what they mean.

10.1 Preparing

It is required to change the addresses on almost all sensors, because all of them has as default factory address **0x28**. PCap02A has defined this address in hardware.

Process of address changing is described in section 8.1.2 Address Changing for HYT sensors.

Tab. 10.1: Used address on Volatiles board

Device	Address	Position on board
PCap02A	0x28	IC1
HYT 271	0x29	IC2
HYT 271	0x2A	IC3
HYT 939	0x2B	IC4
HYT 939	0x2C	IC5

10.1.1 Mbed

During calibration and testing procedures, except situation when was Volatiles board connected directly to OBC on VZLUSat–1, was board connected by I^2C line to Mbed development kit and read out data were further transferred to computer via USB.

Mbed is developing platform based on ARM processor designed for rapid prototyping. This platform is based on the 32-bit ARM Cortex-M3 core running at 96MHz. Whole developing kit has include 512 kB FLASH, 32 kB RAM. On board is lots of interfaces like Ethernet, SPI, I^2C and more as well. There are also analog-to-digital and digital-to-analog converters. Can be used lot of digital I/O interfaces.

Developing board is powered from USB but can be connected to external power source as well.

Programs for this developing kit is required in C/C++ languages. [31]

In this case is Mbed used only to writing configuration to PCap02A and next to reading values from Volatiles board via I^2C.

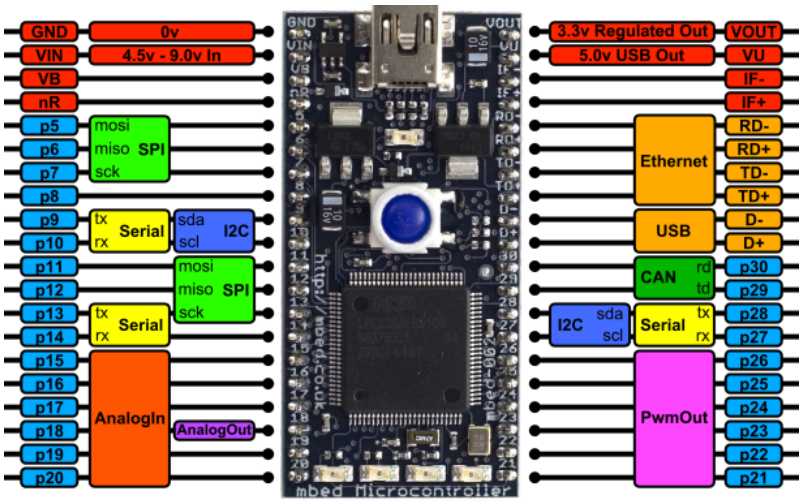

Fig. 10.1: Mbed developing board [31]

10.2 Function Test

As a first step for calibration is connecting and verifying of function each sensor. If are all sensors still alive and communicate with program.

Functional test of these sensors consist of measurement the response of humidity sensors on Volatiles Board in closed box with dry air inlet (the air brings to the box is desiccate by molecular sieve). As can be seen in Fig. 10.2a Volatiles Board is, in this case, placed in a plastic box in a way that none of its sides touched the box and sensors on each side of the board had enough space around them.

Dry air inlet was installed so that the flow of dry air would be approximately the same on both sides of the board. In the wall of the box opposite to dry air inlet is a small hole through which I^2C line entered to the box that also served as a vent. Whole arrangement of full functional test can be seen in Fig. 10.2b.

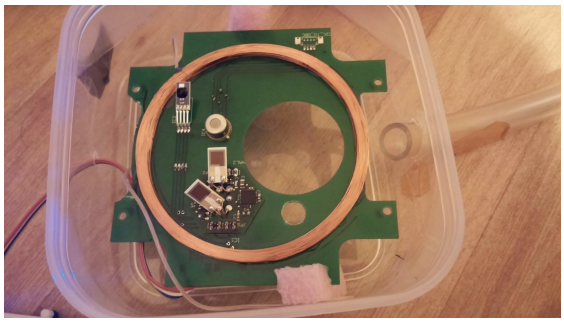

(a) Volatiles board in box

(b) Arrangement of Functional test

Fig. 10.2: Construction of Function tests

This test was intended to show functionality of the sensors after environmental tests, not to calibrate them. Initial temperature and relative humidity was not controlled and depended on ambient conditions.

(a) Results form HYTs

(b) Results form HALs

Fig. 10.3: Sample of function test measurement

Initial values of sensors are slightly differed, which could be caused by their different position in measuring chamber, but other results shown that the response of the sensor to the humidity change is correct. Small differences in measured values was most probably caused by their position on different sides of Volatiles board.

10.3 Atmospheric Pressure

As a first step, sensors had to be calibrated at atmospheric pressure for lower

humidity. Sensors were placed to the calibration chamber and their response to lower humidity in various temperatures was tested.

Special calibration chamber that allows controlled changes of temperature in the range of 20 °C to 70 °C was made for the measurement and can be seen in Fig. 10.4. All sensors are placed on aluminium block heated by Peltier plate. There are two HYT 271 sensors, two HYT 939 sensors, three HAL2 and one Pt1000. Detailed view on the placement of the sensors can be seen in Fig. 10.5.

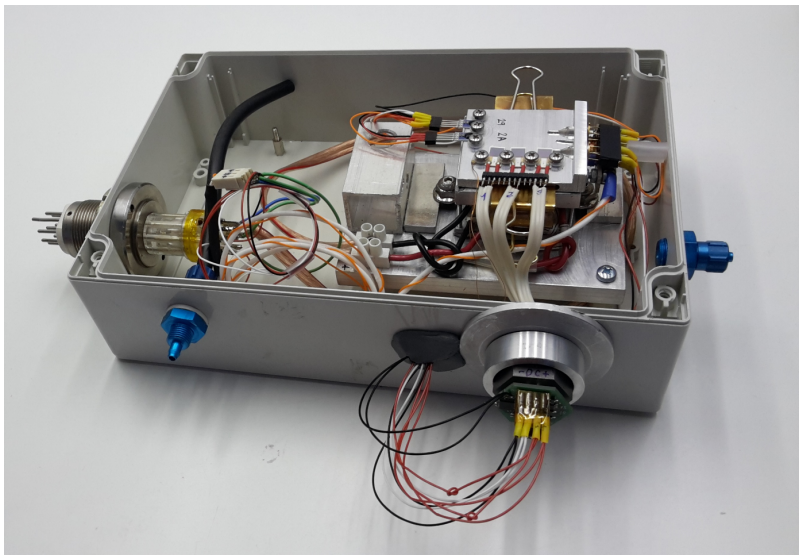

Fig. 10.4: Calibration chamber

Measurement of HAL2 sensors and Pt1000 ensures board with PCapO2A. This board is connected through I^2C together with HYT sensors to Mbed development kit and read out data were further transferred to computer via USB. Data from all humidity sensors were read out simultaneously. HAL2 sensors were read out as capacitances relative to reference capacitance 2.2 nF.

The sensors were calibrated at set Dew point 10, 0, -10,-20, -30, -40 and -70°C. Because of outgassing of components inside the calibration chamber and possible leaks we were not able to achieve lowest possible dew point generated by dew point generator (-70°C). The lowest dew point measured in the outlet was -49 °C.

At first, the sensors were calibrated at room temperature (Peltier plate turned off). Next step of a calibration consisted of measuring their dependence on temperature. After stabilisation of the atmosphere inside calibration chamber, temperature was consecutively set to 20, 30, 40, 50, 60 and 70 °C. Calibration at increased temperature wasn't done at lowest humidity level (-70 °C DP).

Each measurement was the average of 10 consecutively read out values, recorded after stabilisation of conditions inside the calibration chamber. Signal of the sensors

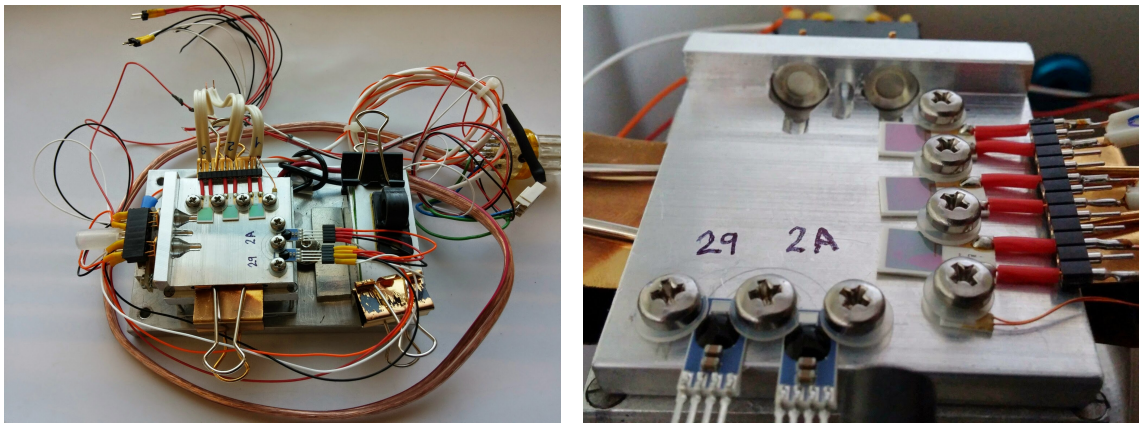

(a) Whole system (b) Detail on placement

Fig. 10.5: Heating block with sensors

was related to output values of dew point.

The values of measured temperature and Dew point at calibration points are summarized in Tab. 10.2 and Tab. 10.3. Temperature from two HYT 271 is averaging and taken as a reference, because they had similar position as HAL2 sensors and Pt1000 sensor connected to HAL2 board was not calibrated before.

Tab. 10.2: Temperature measured at calibration points

	Set temperature							**Set dew**
	Room	**20 °C**	**30 °C**	**40 °C**	**50 °C**	**60 °C**	**70 °C**	**point**
	21.253	20.176	29.237	38.936	48.155	57.485	66.738	**10 °C**
	21.052	20.245	29.557	38.879	47.902	57.534	67.09	**0 °C**
	20.813	20.083	29.517	38.721	48.368	57.461	66.992	**-10 °C**
	20.648	20.135	29.208	38.515	48.073	57.607	66.816	**-20 °C**
	20.552	20.246	29.371	38.584	48.047	57.475	66.896	**-30 °C**
	20.449	19.949	29.351	38.786	48.194	57.562	66.739	**-40 °C**
	20.431	20.111						**-70 °C**
$\bar{x}$	20.74	20.14	29.37	38.74	48.12	57.52	66.88	
δx	0.29	0.1	0.13	0.15	0.14	0.05	0.13	

Results from atmospheric calibration are also in following graphs.

Tab. 10.3: Dew point measured at calibration points

	Set dew point							Set
	10 °C	**0 °C**	**-10 °C**	**-20 °C**	**-30 °C**	**-40 °C**	**-70 °C**	**temperature**
	8	0	-6.1	-17.1	-27.7	-34.9	-43	**Room**
	7.9	0.4	-9.4	-19	-30.3	-38	-47.8	**20 °C**
	8.2	0.2	-9.4	-19.1	-30.8	-37.7	-48	**30 °C**
	8.3	0	-9.7	-19	-31.1	-37.6	-48.7	**40 °C**
	8.4	0	-9.6	-19	-31.3	-37.5	-49	**50 °C**
	8.6	0	-9.6	-18.9	-31.4	-37.4	-49.1	**60 °C**
	8.7	0.1	-9.4	-18.8	-31.2	-37	-49	**70 °C**
$\bar{x}$	8.35	0.12	-9.52	-18.97	-31.02	-37.53	-48.6	
δx	0.26	0.15	0.12	0.09	0.37	0.3	0.51	

(a) Measurement of HYT sensors at various temperatures 1.part

(b) Measurement of HYT sensors at various temperatures 2.part

(c) Measurement of HAL sensors at various temperatures 1.part

(d) Measurement of HAL sensors at various temperatures 1.part

Fig. 10.6: Calibration on Atmospheric pressure

10.4 Vacuum Chamber

After calibration in atmospheric pressure follows testing in vacuum chamber. This part of calibration procedure should help to get an image of sensor's behaviour on orbit. In this case sensors were tested in wide temperature range from -25 °C to 80 °C at low pressure.

For this measuring was necessary to make and adjust measurement vacuum equipment. It was required uniform heating for all sensors which is fundamental for comparison characteristics of sensors. This arrangement is shown in Fig. 10.7

All sensors were again placed on aluminium block. This block was temperature connected with Peltier plate. Aluminium block with sensors and plate were placed into vacuum chamber. I^2C bus was connected through bushing out from the chamber

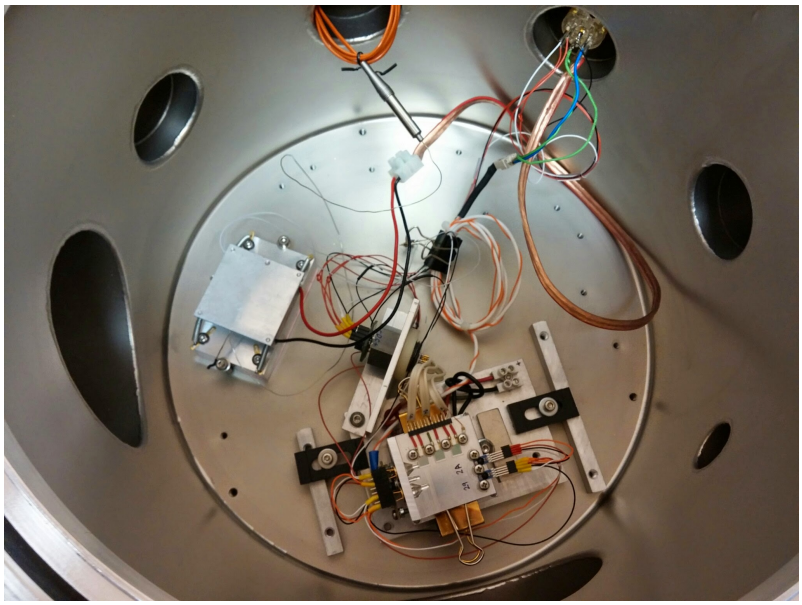

Fig. 10.7: Sensors in vacuum chamber

same as power supply for Peltier plate.

As first time vacuum chamber was pumped out to low pressure approx. $\cdot 10^{-4}$ mbar with tested block of sensors inside. Then Peltier plate was connected to power supply and sensors were heated. During pumping out and after pressure stabilization values from sensors were read as well.

After sensors had been tempering to maximum allowed temperature than temperature had been slowly decreasing to room temperature. This temperature cycle was repeated several times without venting of the vacuum chamber. After these measurements cycles vacuum chamber was venting and whole test was repeated with enough time delay.

After this part of measurement was necessary to change Peltier plate for testing at low temperature below zero degree of Celsius. For this temperature range were also used above mentioned procedures.

10.4.1 Results from Vacuum Measurement

Reading and measurement values are pre-processed and processed on several levels. The value of digital sensors HYT is after reading the raw data from the sensor, computing converted into digital format relative humidity and temperature directly by development kit Mbed. Data from measurement in vacuum chamber were read through bushing on chamber. Next step is data processing in MatlabR2015a. During pumping out the chamber was register pressure inside as well. These data

Fig. 10.8: Arrangement of Vacuum test

have to be write down by hand because there is not output from pressure meter.

Fig. 10.9: Decreasing pressure during pumping

Points of pressure were spline to curve by MatlabR2015a as well. For this processes was used following Code 10.1.

Code 10.1: Spline by pressure

```
close all
clear all
clc

Presures = [          %Pressure (sample_mbar; ...)
4 4.6e2;
6 2.2e2;
7 1.2e2;
8 7.4e1;
9 2.2e1;
10 6.3e0;
11 2e0;
12 1e-1;
13 1.2e-3;
```

```
];

line=Press(1,1):0.1:Press(length(Press),1);      % New axis
Presspline=spline(Press(:,1),Press(:,2),line);   % Spline
```

Sensor response of HYT type slowly decreases during evacuating the chamber. Response from HAL sensors shows changes but signal was still strong enough. Data from HALs are very noisy and it is recommended to make Digital Signal Processing on them.

One possibility how to make the shape smooth is moving average. This method is very simple and used for smooth out short-term fluctuations. Disadvantage of this process is that, it is make the slower response of signal. Principle of this based on equation (10.1).

$$x_i = \frac{1}{k}\sum_{n=i}^{k+i}|x_n| \qquad i \in \mathbb{Z}, \quad i \in \langle 0; N-k) \tag{10.1}$$

Where x is Point of signal, N is Number points of signal and k is Number points of moving averages.

11 Pre-flight Preparations and Testing

Testing of VZLUSat–1 was made in several phases and different approaches were applied. The payloads were replaced by dummy, like any sensors, by qualification engineering models or proto-flight models. Every board have to pass the line of test before can be used for space mission. Some of these tests are used only once but for opposite side the boards have to pass multiple times of others.

11.1 Engineering Qualification Model

Before then the final version of satellite will be set up is necessary to make Engineering qualification model (EQM) testing. In this part of testing procedure is test of boards mechanical and electrical compatibility.

After that, is whole probe underwent environmental testing — vibration, shock and thermal vacuum tests.

After these tests were made the mentioned changes on PCB design of Volatiles.

11.1.1 Vibration and Shock Test

VZLUSat–1 was fully assembled, adjusted and inspected. Verification consisted of different vibration tests — the device was exposed to sinusoidal and random vibrations in mounted axes. Next test block were shock tests, when shocks in tests axis were applied. After each of these test was done complete resonance search in all axis. [32]

11.1.2 Thermal Vacuum Test

Because the experiments will process on orbit, there were also thermal vacuum tests. The probe placed in vacuum chamber, functional tested there, next baked out and thermal vacuum tests became cycling. It consisted of four test for low and for high temperature. Then were made again the functional tests, at first at minimum, then at maximum operational temperature. Then was done a perform bake out test,

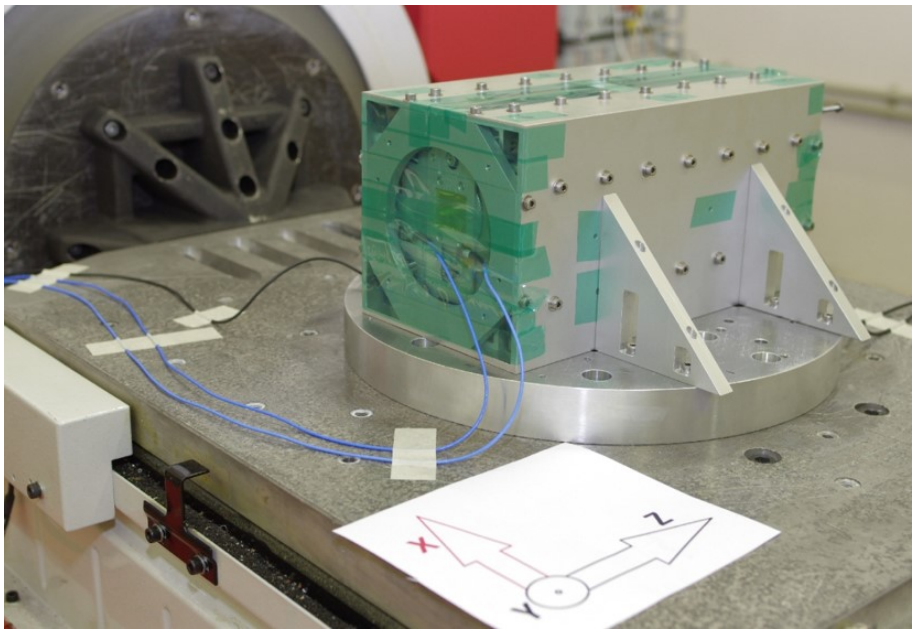

Fig. 11.1: Vibration and shock testing [32]

the device put out from the vacuum chamber and final functional tests executed. [32]

11.1.3 Other Tests

After all these invasive assays, more subtile EMC test followed. In this phase were examined bonding and isolation tests to find out, if something did not break during the vibrations and baking out. EMC was studied for radiated emissions in E and H field. The spacecraft had to be in tolerance band all time.

Also so called end to end situations were simulated. That means, situations when any part does not work completely, for example when a switch or connector does not work or extendible part did not tilt.

In the end of each of test or of a subtest, functional test and visual inspection were examined, in the end full functional tests were done. These tests were prepared in standard environment – room temperature, ambient pressure and humidity and cleanroom class 100 000 and verify the functionality and parameters of each board. It verifies interaction between individual boards as well as their behaviour as integrated complex. [32]

11.2 Function test after EQM

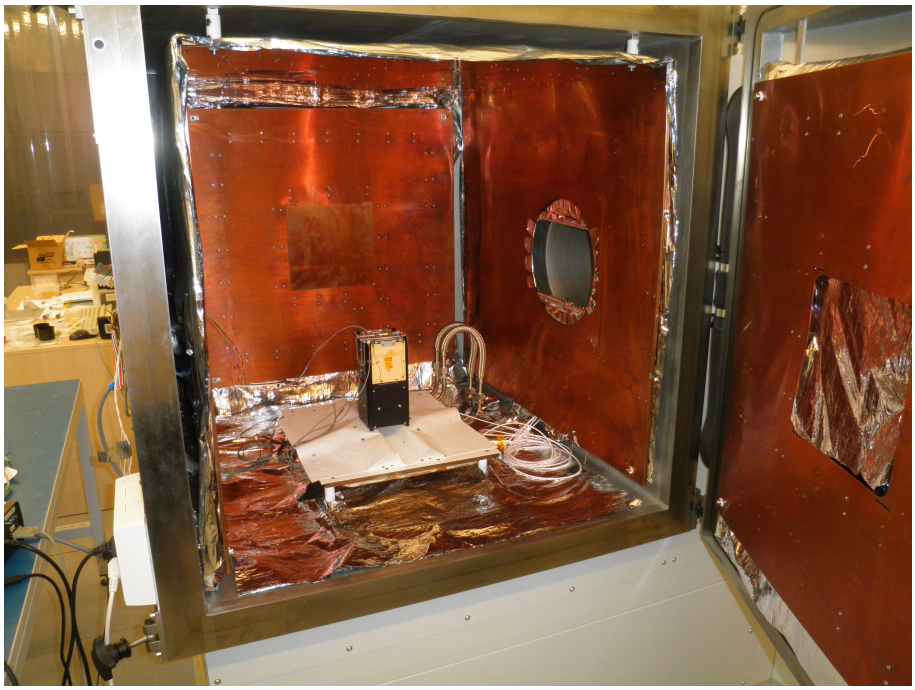

Fig. 11.2: Thermal vacuum testing [32]

As was mentioned, after EQM testing in thermal vacuum chamber, vibration and shock testing is necessary to make function test. This type of test is described in 10.2 Function Test.

(a) Before EQM testing (b) After EQM testing

Fig. 11.3: Results form HYT sensors

From these results can be seen that from electrical point of view all sensor survived. All HW parts of whole board survived as well. But when Fig. 11.3a and Fig. 11.3b are compared, there can be seen a difference between charts of one sensor. Although this HYT sensor with address `0x29` measures but was probably mechanical damaged. This damage may have occurred during manipulation with the Volatiles board when the probe was assembled.

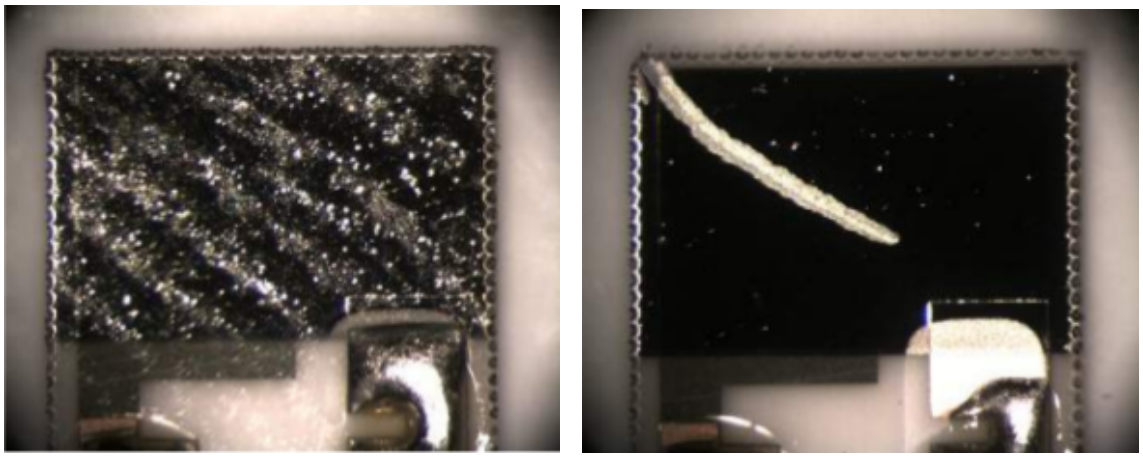

(a) Sensor with contaminations

(b) Sensor with a scratch

Fig. 11.4: Examples of damage [22]

12 Conclusion

Shrnutí, co už to přineslo, potenciál, ...
Článek, poster, konference ..

References

[1] NENTVICH, Ondřej. *Measurement of changing mechanical properties of carbon composite on nanosatellite miniCube mission QB50*: master's thesis. Prague: Czech Technical University in Prague, Faculty of Electrical Engineering, Department of Microelectronics, 2015. 25 p. Supervised by Ing. Ladislav Sieger, CSc.

[2] URBAN, M., NENTVICH, O., STEHLÍKOVÁ, V., SIEGER, L., YANA, K. Measuring carbon fiber aging on orbit. *Hosei science collection report*, 2014, vol. 26, no. 50, p. 1–6. ISSN 2188-8507.

[3] STEHLÍKOVÁ, Veronika. *Radiation resistance measurement on nanosatellite miniCube mission QB50*: master's thesis. Prague: Czech Technical University in Prague, Faculty of Electrical Engineering, Department of Microelectronics, 2015. 25 p. Supervised by Ing. Ladislav Sieger, CSc.

[4] Project QB50. [online]. 2015 [cited 2015-04-20]. Available from <`https://www.qb50.eu/index.php/project-description-obj`>.

[5] GomSpace [online]. 2007-2015 [cited 2015-04-20]. Available from <`http://gomspace.com/`>.

[6] NASA - CubeSat Launch initiative [online]. [cited 2015-06-12]. Available from <`https://www.nasa.gov/directorates/heo/home/CubeSats_initiative.html`>.

[7] KAZUO Yana, Ph.D., *Consultations*, Summer 2014, Hosei University, Tokyo, Japan

[8] HÁNA, Petr, *Consultations*, Technical University of Liberec

[9] MIKULIČKOVÁ, Lenka, *Consultations*, Thin-film Technology Service s.r.o.

[10] *A guide to the measurement of humidity*. 1996, 68 p. ISBN 09-044-5724-9.

[11] WEBSTER, John G a Halit EREN. *Measurement, instrumentation, and sensors handbook: electromagnetic, optical, radiation, chemical, and biomedical measurement*. Second edition. ISBN 978-1-4398-4891-3.

[12] HÁNA, P., INNEMAN, A., DÁNIEL, V., et al. *Mechanical properties of Carbon Fiber Composites for applications in space*. Proc. SPIE 9442, *Optics and Measurement Conference 2014*. 2015, no. 1. DOI: 10.1117/12.2175925.

[13] SOVKA, Pavel. *Vybrané metody číslicového zpracování signálů*. Vyd. 2. Praha: ČVUT, 2003, 258 s. ISBN 80-010-2821-6.

[14] UHLÍŘ, Jan a Pavel SOVKA. *Číslicové zpracování signálů*. Vyd. 2. přeprac. Praha: Vydavatelství ČVUT, 2002, vii, 327 s. ISBN 80-010-2613-2.

[15] SOVKA, Pavel. *Study materials for the course Číslicové zpracování signálů A2M99CZS* during the winter semester 2013/2014 at the Faculty of Electrical Engineering, Czech Technical University in Prague.

[16] DUNN, Patrick F. *Measurement and data analysis for engineering and science*. 2nd ed. Boca Raton, FL: CRC Press/Taylor, 2010, xiii, 490 p. ISBN 14-398-2568-8.

[17] Decimation-in-time (DIT) Radix-2 FFT [online]. [cited 2015-06-21]. Available from <http://cnx.org/contents/ce67266a-1851-47e4-8bfc-82eb447212b4@7/Decimation-in-time_(DIT)_Radix>.

[18] QB50 FIPEX Science Unit – Interface Control Document [online]. [cited 2015-02-14]. Available from <https://www.qb50.eu/index.php/tech-docs/category/19-up-to-date-docs?download=78:fipex-icd>.

[19] QB50 INMS User Manual [online]. [cited 2015-06-16]. Available from <https://www.qb50.eu/index.php/tech-docs/category/21-up-to-date-docs?download=61:inms-user-manual-issue-1>.

[20] MNLP User Manual [online]. [cited 2015-04-08]. Available from <https://www.qb50.eu/index.php/tech-docs/category/23-up-to-date-docs?download=95:mnlp-user-manual>.

[21] Teaching Phase Equilibria [online]. [cited 2015-07-15]. Available from <http://serc.carleton.edu/research_education/equilibria/phaserule.html/>.

[22] Data Sheet HYT module - Application Note - Humidity Module.

[23] Data Sheet PCapØ2A, Document-No: DB_PCapØ2A_Vol1_en.pdf from May 29, 2014, Version 1.6

[24] JAN, J. *Číslicová filtrace, analýza a restaurace signálů*. 2.nd ed. Brno: VUTIUM, 2002. 427 p. ISBN 80-214-2911-9.

[25] TŮMA, J. *Zpracování signálů získaných z mechanických systémů užitím FFT*. Praha: Sdělovací technika, 2000. 168 p. ISBN 80-901936-1-7.

[26] Datasheet PT1000. [online]. 2011 [cited 2015-04-02]. Available from <http://www.fel.zcu.cz/uredni-desky/UD_Formulare/BPDP_prace/1983.pdf>.

[27] PODUŠKA, J. *Experimentální analýza dynamického chování vetknutého nosníku*. Brno: Vysoké učení technické v Brně, Fakulta strojního inženýrství, 2011. 36 s. Vedoucí bakalářské práce Ing. Lukáš Březina, Ph.D.

[28] BREPTA, Rudolf, Ladislav PŮST a František TUREK. *Mechanické kmitání*. Vyd. 1. Praha: Sobotáles, 1994, 589 s. Česká matice technická (Sobotáles). ISBN 80-901684-8-5.

[29] CHEN, Zhi a Chi LU. *Humidity Sensors: A Review of Materials and Mechanisms.* Sensor Letters. 2005, 3(4): 274-295. DOI: 10.1166/sl.2005.045. ISSN 1546198x.

[30] SIGNAL CHAIN BASICS (Part 32): Digital interfaces (con't) – The I2C Bus. [online]. 2009-06-08 [cited 2015-04-23]. Available from http://www.planetanalog.com/document.asp?doc_id=527900.

[31] mbed LPC1768 [online]. [cited 2015-06-20]. Available from https://developer.mbed.org/platforms/mbed-LPC1768/.

[32] Aerospace Research and Test Establishment, Beranovych 130, Prague – Czech Republic.

[33] ZÁHLAVA, Vít. *Návrh a konstrukce desek plošných spojů: principy a pravidla praktického návrhu*. 1. vyd. Praha: BEN - technická literatura, 2010, 123 s. ISBN 978-80-7300-266-4.

List of appendices

A List of CubeSats of the current mission QB50

The list of the current CubeSats in the QB50 project. Last update 1st April 2015.

QB50 ID	Lead Institute	CubeSat Name	Country
AT03	U of App. Sci., Wiener Neustadt	Pegasus	Austria
AU01	The University of Adelaide	SUSat	Australia
AU02	University of New South Wales	UNSW-EC0	Australia
AU03	University of Syndey	i-INSPIRE II	Australia
AZ01	Stellenbosch University	ZA-AeroSat	South Africa
BE05	von Karman Institute	QARMAN	Belgium
BR01	Instituto Federal Fluminense	14-BISAT	Brazil
CA01	York University, Toronto	YUsend-QB50	Canada
CA03	University of Alberta	ExAlta-1	Canada
CN01	Beihang University	BUSAT-1	China
CN02	Harbin Institute of Technology	LilacSat-1	China
CN03	Nanjing University of Science and Technology	NJUST-1	China
CN04	Northwestern Polytechnic University	Aoxiang 1	China
CN05	Zhejiang University	ZJU CubeSat	China
CN06	National University of Defense Technology	NUDTSat	China
CN07	ShanghaiTech University	STU-1	China
CZ02	VZLU	VZLUsat-1	Czech Republic
DE04	FH Aachen, University of Applied Science	DragSail-CubeSat	Germany
ES01	Universidad Politécnica de Madrid	QBITO	Spain
FI01	Aalto University	Aalto-2	Finland
FR01	École Polytechnique	X-CubeSat	France
FR02	Institut Supérieur de l'Aéronautique et de l'Espace ISAE	EntrySat	France
FR03	Institut Supérieur Des Sciences Et Technique (INSSET)	SAT_IP2	France
FR04	UPEC	OGMS-SA	France
FR05	MinesParisTech	SpaceCube	France
GB03	MSSL, University College London	UCLSat	United Kingdom
GB06	University of Surrey	InflateSail	United Kingdom
GR01	Democritus University of Thrace / Space Research Lab	DUTH	Greece
GR02	University of Patras	UPSat	Greece
IL01	The Space laboratory of the Herzliya Science Center	Hoopoe	Israel
IN01	Anna University	ANUSAT-2	India
IT02	University of Rome "LA SAPIENZA"	URSA MAIOR	Italy
KR01	Korea Advanced Institute of Science and Technology	LINK	Korea
KR02	Seoul National University	SNUSAT-1	Korea
LT01	Vilnius University	LituanicaSAT-2	Lithuania
NL01	Delft University of Technology	DELFFI-1	Netherlands
NL02	Delft University of Technology	DELFFI-2	Netherlands
PT01	University of Porto	GAMASAT	Portugal
RO01	Institute of Space Science and the Romanian Space Agency Research Center	RoBiSAT-1	Romania
RO02	Institute of Space Science and the Romanian Space Agency Research Center	RoBiSAT-2	Romania
RU01	Samara State Aerospace University	SamSat	Russia
TR01	Istanbul Technical University / Air Force Academy	BeEagleSat	Turkey
TR02	HAVELSAN	HAVELSAT	Turkey
TW01	National Cheng Kung University	PHOENIX	Taiwan
UA01	National Technical University of Ukraine / Shenyang Aerospace University	PolyITAN-2-SAU	Ukraine
US01	University of Colorado Boulder	Challenger	USA
US02	University of Michigan	Atlantis	USA
US03	Stanford University	Discovery	USA
US04	Universidad del Turabo	Columbia	USA

Fig. A.1: List of CubeSats [4]

B Odkladová plocha

- **INMS** – Ion-Neutral Mass Spectrometer
- **FIPEX** – Flux-Φ-Probe Experiment
- **m-NLP** – multi-Needle Langmuir Probe

before considering accomplished circumstances leakage

either observation such distorted comprising superimpose spurious restricts tapered

C The content of enclosed CD/DVD

Nezapomeňte uvést, co čtenář najde na přiloženém médiu. Je vhodné okomentovat obsah každého adresáře, specifikovat, který soubor obsahuje důležitá nastavení, který soubor je určen ke spuštění atd. Také je dobře napsat, v jaké verzi software byl kód testován (např. Matlab 2010b).